HHS Public Access

Author manuscript

*Chem Rev*. Author manuscript; available in PMC 2021 April 22.

Published in final edited form as:

*Chem Rev*. 2020 April 22; 120(8): 3749–3786. doi:10.1021/acs.chemrev.9b00717.

# Mediated Fuel Cells: Soluble Redox Mediators and their Applications to Electrochemical Reduction of $O_2$ and Oxidation of $H_2$, Alcohols, Biomass, and Complex Fuels

**Colin W. Anson**, **Shannon S. Stahl***

Department of Chemistry, University of Wisconsin–Madison, 1101 University Avenue, Madison, Wisconsin 53706, United States

## Abstract

Mediated fuel cells are electrochemical devices that produce power in a manner similar to that of conventional proton exchange membrane fuel cells (PEMFCs). They differ from PEMFCs in their use of redox mediators dissolved in liquid electrolyte to conduct oxidation of the fuel or reduction of the oxidant, typically $O_2$, in bulk solution. The mediators transport electrons (and often protons) between the electrode and the catalysts or chemical reagents in solution. This strategy can help overcome many of the challenges associated with conventional fuel cells, including managing complex multi-phase reactions (as in $O_2$ reduction) or the use of challenging or heterogeneous fuels, such as hydrocarbons, polyols and biomass. Mediators are also commonly used in enzymatic fuel cells, where direct electron transfer from the electrode to the enzymatic active site can be slow. This review provides a comprehensive survey of historical and recent mediated fuel cell efforts, including applications using chemical and enzymatic catalysts.

## Graphical Abstract

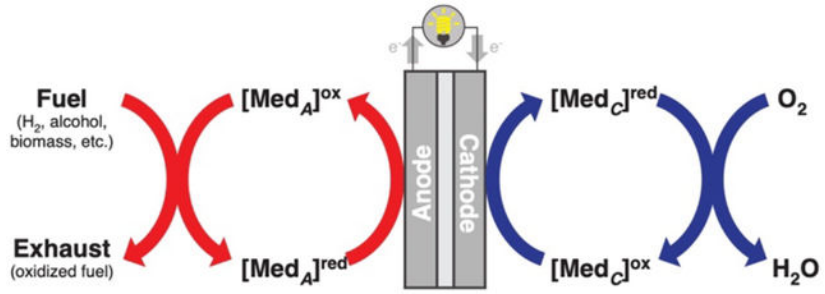


## 1. Introduction

### 1.1. Proton-exchange-membrane fuel cells (PEMFCs) and redox flow batteries (RFBs): Context for mediated fuel cells (MedFCs).

Growing worldwide energy demands continue to motivate the exploration and development of diverse energy storage[1] and conversion[2] technologies that could support broader use of

*corresponding author: stahl@chem.wisc.edu.

renewable energy sources, such as solar, wind, hydroelectric, and biomass.[3] Electrochemical technologies are a major focus of these efforts, with prominent examples including solid-state[4–7] and redox flow batteries,[8,9] supercapacitors,[10,11] and (photo)electrochemical production of chemicals, ranging from hydrogen ($H_2$) to carbon-based molecules (formic acid, syn gas, MeOH, among others).[12,13] Chemicals produced from the latter processes may be stored or transported to other locations for power generation, ideally with fuel cells to leverage their higher energy efficiency relative to conventional combustion-based power generation.[14] This review article surveys historical and recent advances in mediated (or "indirect") electrochemical processes for power generation. These processes are conceptually related to proton exchange membrane fuel cells (PEMFCs) and redox flow batteries (RFBs) (Figure 1), while incorporating features distinct from these established technologies.

PEMFCs are the most common class of fuel cells for low-temperature power generation.[15] These devices convert energy from chemical bonds into electricity by oxidizing a chemical fuel at the anode and reducing an oxidant at the cathode. Conventional PEMFCs use $H_2$ as the fuel[16] and $O_2$ as the oxidant. The electrons from $H_2$ are transported from the electrode through the electrical circuit, while the protons are transported through a membrane electrolyte, consisting of a sulfonated fluoropolymer (e.g., Nafion®), to the cathode where they combine with $O_2$ and the electrons to produce water (Figure 1A). A related class of fuel cells, anion exchange membrane fuel cells (AEMFCs), utilize membrane electrolytes that conduct anions, such as $Cl^-$ or $OH^-$, and have been the focus of growing interest.[17]

Water management is a key challenge in conventional PEMFCs.[18] Water must be present within the ionic polymer membrane to support efficient proton transport from the anode to the cathode,[19] and this requirement is met by using humidified sources of $H_2$ and $O_2$ gases. Meanwhile, the water generated at the cathode from $O_2$ reduction must be removed to avoid flooding of the catalyst. The issues related to water management limit the temperature range available for effective operation of PEMFCs (typical operation ≤ 100 °C). Membrane-electrode assemblies[20] and bipolar plates[21] have been engineered to address these challenges, while ensuring effective delivery of gases to the catalyst surface, efficient coupling of the catalytic reactions of $H_2$ and $O_2$ with the proton- and electron-transport processes, and precise management of water. Fuel cell technologies continue to improve, with recent advances enabling access to current and power densities of ≥ 2.5 A/cm$^2$ and 1.2 W/cm$^2$, respectively.[22]

The requirement for high loadings of Pt catalyst at the cathode to achieve optimal performance represents one of the most significant impediments to conventional PEMFCs.[23] Pt catalysts are also used at the anode, but the higher catalytic rates for $H_2$ oxidation relative to $O_2$ reduction mean that much less catalyst is required at the anode. Advances have been made in the development of non-platinum group metal (non-PGM) catalysts for $O_2$ reduction;[24–26] however, these catalysts typically have lower intrinsic activity than Pt and, therefore, require higher catalyst loadings to achieve the similar current densities. The higher catalyst loading introduces additional limitations associated with the increased electrical resistance from the thicker catalyst layer and restricted mass transport of $O_2$ and water through the electrode. Consequently, commercial applications of non-PGM cathode catalysts

have thus far been restricted to low power-density applications, in which the complications arising from higher catalyst loadings are less problematic.[27,28]

Alongside the development of PEMFCs that use $H_2$ as a fuel, considerable effort has been directed toward the development of fuel cells capable of using liquid fuels. Such devices avoid challenges associated with the storage, transport, and distribution of $H_2$. Direct methanol fuel cells (DMFCs),[29] which oxidize MeOH (supplied as a concentrated aqueous solution) to $CO_2$ at the anode, are among the most prominent applications of liquid fuel cells. The lower rates of MeOH oxidation relative to $H_2$ oxidation, however, leads to considerably lower power densities in DMFCs (< 120 mW/cm$^2$).[30] The use of fuels more complex than MeOH, such as sugars or other biomass-derived molecules, and limitations on the practical concentrations of these fuels in the aqueous solutions delivered to the anode, can further constrain catalytic rates and power densities in liquid fuel cells.[31] Liquid fuel cells must be operated under conditions that avoid cathode flooding, which can arise from transport of water from the fuel solution through the membrane as protons are transported from the anode to the cathode. Complications of the type described here account for the limited commercial application of PEMFCs with fuels other than hydrogen.

Redox flow batteries (RFBs) represent the second class of electrochemical devices directly relevant to the subject matter of this review article. RFBs store electrical energy by transferring electrons to and from molecules or ions dissolved in solution (Figure 1B). Typical systems feature two tanks of redox couples, one containing a cathodic species that has a high reduction potential and the other with an anodic, low-potential species. Electrical energy is stored and generated by flowing the redox couple solutions through the cathode and anode compartments, which are separated by a semi-permeable membrane that enables selective transfer of protons or other ions while preventing mixing of the mediators. The underlying concepts of redox flow batteries were first demonstrated in the late 1800s,[32] with significant technological development beginning in the 1960s.[33] Commercial installations have emerged in recent years.[34] Examples of the redox couples at the anode/cathode used in commercial systems include Cr/Fe, Zn/Br, and V/V.[8] The systems using Fe, Cr, Zn and Br species benefit from the low cost of the chemicals, but the all-vanadium redox flow batteries exhibit the longest lifetimes and are the most widely used. Challenges associated with these technologies include the high toxicity and corrosivity of the electrolyte (particularly for V- and Br-based systems), the limited number of redox couples that operate near the limiting potentials for $H^+/H_2O$ reduction and $H_2O/OH^-$ oxidation for aqueous electrolytes, and the limited material supply and high cost of V. All-organic redox species have been the focus of much recent attention as a means to address these limitations. Examples include derivatives of quinones, nitroxyls, and viologens (Figure 2).[9,35] The synthetic modularity of these molecules, which allows their redox potentials and other physical properties (e.g., solubility, stability) to be tuned, greatly expands the scope of possible compounds that may be considered. Water-soluble redox couples are especially appealing because water is low-cost solvent with inherently low solvent resistivity;[36–38] however, non-aqueous RFBs have also been the focus of major research efforts.[39]

### 1.2. Mediated fuel cells (MedFCs): Overview and opportunities.

The above discussion of PEMFC and RFB technologies provides the relevant context for the introduction of mediated fuel cells (MedFCs, Figure 1C), which are the focus of this review article. The latter devices feature dissolved mediators analogous to the mediators used in RFBs; however, catalytic regeneration of the mediators in an off-electrode compartment enables sustained production of electricity analogous to the operation of PEMFCs. Mediator regeneration is achieved by supplying a fuel to reduce the low-potential mediator and $O_2$ to oxidize the high potential mediator, typically employing a catalyst for both processes. Mediated fuel cell systems are distinct from RFBs because they can operate continuously, as long as the supplies of fuel and oxidant are maintained.

Several factors impact the utility of redox mediators for use in mediated fuel cells. First, the redox potential of the mediator should be as close as possible to the formal potential of the fuel or the oxidant. For a “conventional” system using $H_2$ as the fuel and $O_2$ as the oxidant, the anode mediator should have a redox potential near 0.0 V vs. RHE (Reversible Hydrogen Electrode; i.e., adjusting for the pH of the system), and the cathodic mediator a redox potential near 1.23 V vs. RHE. Additionally, the redox mediator should display fast electron transfer kinetics, to minimize any overpotentials caused by kinetic losses in the system, it needs to be stable in both oxidized and reduced states to enable long-term performance, and it must be highly soluble in aqueous solution for the cell to maximize the current densities.

MedFCs have several potential advantages over conventional fuel cells that warrant their consideration for further development. These features include the following:

**1) Enabling the use of “challenging” fuels.—**By moving fuel oxidation away from the anode, a greater number of fuel options could become available, and more diverse catalysts may be considered. For example, the use of $H_2$ feeds containing carbon monoxide, sulfur-, or nitrogen-based contaminants has been demonstrated,[40] and this advantage was one of the original motivations for investigating MedFCs.[41] Another advantage is that fuels that are too complicated to oxidize at an electrode under mild conditions (<150 °C) may be considered. Examples of these alternatives include alcohols more complicated than MeOH and heterogeneous fuel sources, such coal or biomass-derived cellulose or lignin, which are challenging fuels for direct activation at an electrode.

**2) Overcoming challenges with the oxygen reduction reaction (ORR).—**A major motivation in previous studies of mediated fuel cells has been the replacement of Pt, which is required in relatively high loading in conventional PEM cathodes, with non-PGM alternatives.[42] The high loadings of Pt are necessary to achieve sufficiently high activity within the narrow spatial dimension at the gas-diffusion electrodes. By moving the catalytic $O_2$ reduction process into an off-electrode compartment, the ORR may be optimized independently of the electrochemistry. The lower intrinsic activity of non-PGM catalysts relative to Pt is less problematic in this configuration. For example, mass-transport restrictions are significantly reduced when the catalyst does not need to be in direct contact with the electrode and membrane, and higher mass loadings of the non-PGM catalyst may be integrated in an off-electrode reactor in a manner that does not impede system

performance. The electrochemical reaction of the mediator features a simpler two-phase (liquid/solid) system at the electrode, rather than the more complicated three-phase (gas/liquid/solid) system present in conventional fuel cells. While there is still a three-phase reaction occurring at the off-electrode catalyst, many of the engineering and materials constraints are relaxed. For example, it is not essential to use a conductive catalyst support, and there are fewer limitations on the amount of catalyst that can be used, allowing higher loadings of less active and less expensive catalysts than Pt to be used.

**3) Opportunities to improve overall system performance.—**At first glance, mediated fuel cells appear to increase the complexity of a fuel cell stack, due to the requirement for extra plumbing and pumps to operate the mediator-regeneration loop. In fact, however, they can simplify the balance of plant accessories. PEMFCs are typically limited to operating at or below 100 °C and require humidification of the gases to avoid dehydration of the membrane. Since mediated fuel cells use aqueous mediator solutions, the membrane remains well-hydrated and gas humidification is unnecessary. Additional benefits arise from using aqueous solutions, which can absorb heat generated from the oxidation and reduction reactions, thereby facilitating temperature control of the fuel cell stack. Finally, mediated cathode systems are ideally suited for pairing with liquid fuels, including both conventional and mediated anode processes, because they are not susceptible to the flooding from water convection that can occur with gas-diffusion cathodes in PEMFCs.

**4) Reduced performance losses from activation polarization.—**Activation polarization is the loss in cell voltage at low current densities due to the kinetic barriers for electron transfer to the species to be oxidized or reduced. The particularly high kinetic barriers associated with catalytic reduction of $O_2$ leads to substantial losses in the cell potential when $O_2$ is directly reduced at an electrode. Similar issues arise at the anode, when using fuels more complex than $H_2$, such as methanol. Redox mediators, on the other hand, may be selected to have fast electrochemical kinetics and thereby minimize activation polarization losses.

### 1.3. Scope of coverage and notes on nomenclature and symbolic notation used in this review.

Redox mediators have been employed in a wide range of electrochemical devices and applications, many of which have been the subject of previous review. Important examples include electrochemical synthesis of organic and inorganic chemicals,[43–46] in addition to diverse energy-based technologies beyond flow batteries,[8,9] including dye-sensitized solar cells,[47,48] solid-state batteries (e.g., “redox targeting”),[49,50] decoupled water splitting,[51] electrochemical capacitors,[52] and solar flow batteries.[53] This review covers mediated fuel cells (MedFCs) that feature a mediated cathode for $O_2$ reduction, a mediated anode for $H_2$, alcohol, or biomass oxidation, or a doubly mediated system, wherein mediators are used for both half-reactions of the fuel cell. Some aspects of these reactions have been reviewed previously;[41,42,54] however, significant advances in recent years, together with the partial coverage of these previous reviews, provided motivation to prepare this comprehensive survey. Only systems that are designed or intended to produce power (galvanic cells) are covered in depth, though reference is occasionally made to relevant electrolysis systems.

Most of the examples consist of full fuel cells, but relevant half-cell studies are also discussed. Enzymatic fuel cells[55–57] using soluble mediators are included, but microbial fuel cells[58,59] are not presented. While microbial fuel cells feature certain advantages, including the capability to produce their own mediators and potential for genetic engineeringfor enhanced performance,[60] their added complexity makes it is difficult to compare them directly to the other systems.

Historically, mediated fuel cells have been given the name “chemically regenerable redox fuel cells”, or CRRFCs,[41,42,54,61–64] to distinguish them from “redox fuel cells”, which are now typically called redox flow batteries (RFBs). With the shift in the flow battery nomenclature, we have chosen to adopt the simplified term “mediated fuel cell” or “MedFC” for these systems (avoiding the term “MFC”, which is commonly employed for microbial fuel cells).

To simplify the notation used to describe mediated fuel cell systems, we have adopted the following notation: fuel|anode catalyst|anode mediator||cathode mediator|cathode catalyst|oxidant, whereby the double bar (||) refers to the membrane separating the anode and anode compartments and the single bar (|) separates the different components within the mediated anode or cathode systems. Certain studies only investigated one of the half-cell systems, or a system was conducted in the absence of a mediator or catalyst. In such cases, certain components are omitted from the symbolic notation. The distinction between a “mediator” and a “catalyst” is not always well defined in multi-component electrochemical mediator systems. We have attempted to be consistent in use of the term “mediator” for the major redox-active species that undergoes electron-transfer at the electrode, and the term “catalyst” for the species that undergoes the redox reaction with the fuel or oxidant in a redox cascade. Ambiguities can arise, for example, in single-component mediator systems in which the “mediator” also serves as the “catalyst”. A table containing information for all reported mediated fuel cells using chemical catalysts is given in Appendix I. All reports of mediated fuel cells using enzymatic catalysts is provided in Section 3.2.

## 2. The Cathode: Oxygen Reduction

The reduction of $O_2$ is the predominant cathodic reaction for fuel cell technology, owing to the availability of $O_2$ and formation of water as a benign product. State-of-the-art catalysts in PEMFCs and DMFCs are composed of Pt or Pt alloys that exhibit the best combination of high activity, low overpotential, long-term stability, and selectivity for 4 $e^-$ reduction of $O_2$ to $H_2O$.[65,66] While optimal performance is achieved with these Pt-based catalysts, their high costs continues to be a limiting factor in PEMFC commercialization. The cost of Pt has been forecasted to account for over 40% of the stack cost.[67] Eliminating or decreasing the loading of Pt or Pt-group metals is a high priority, and heterogeneous electrocatalysts such as Pt-alloys and non-PGM electrocatalysts, including metal-free carbon-based materials, have been developed.[68,69] The first commercial PEMFC system utilizing non-PGM catalysts was announced in 2017.[28] Nonetheless, no catalysts have thus far achieved the activity and stability metrics of Pt or Pt alloys, and alternate solutions continue to be the focus of active study. Mediated $O_2$ reduction was the focus of considerable historical investigation, and new advances have emerged in recent years. The following sections survey the different

mediators that have been reported for mediated ORR, including historical and recent examples, and systems implemented in fuel cell devices and fundamental studies.

### 2.1. $Br^-/Br_2$ mediator

The bromide/bromine redox couple has been widely used in flow battery research due to its high redox potential (1.06 V vs. NHE), fast electrode kinetics, and high solubility of the relevant species in different redox states. The potential is within 200 mV of the thermodynamic potential for $O_2$ reduction to $H_2O$ and, therefore, could provide a low-overpotential strategy for mediated ORR. Fuel cells reported with bromine-based mediators for the ORR are shown in Table 1.

The first report of a MedFC utilizing bromine-based cathode mediators was published in 1955 by Posner.[70] In this work, other cathodic mediators were examined, but they exhibited low cell potentials. A variety of catalysts and mediators were screened, and the use of bromine in combination with $NO_2$ showed promise (Figure 3). The anode contained chars, coke, or coal as the fuel and a variety of metal ions were tested as anodic mediators. Tests were also performed without $NO_x/O_2$-based regeneration, and the results showed that $Br_2$ at the cathode shows minimal polarization (<0.05 V) up to a cell current density of >50 $A/ft^2$ (i.e., ~54 $mA/cm^2$) with 1.2 N $Br_2$ and 0.7 N HBr in 3 N HCl. Challenges with long-term stability of the cathode system was acknowledged, but >8 h of sustained activity was demonstrated.

In the same year, Posner and Merton-Bingham studied the mechanism of $NO_x$-catalyzed autoxidation of HBr.[71] The authors proposed a 6-step sequence (Figure 4A), with the slow step involving the reaction of NOBr in solution with an unknown, gas-phase species resulting from the reaction of $HNO_2$ and HBr (species “X” in Figure 4A). Later studies by Reneke noted reproducibility problems with the analytical techniques for bromine quantification employed by Posner and Merton-Bingham.[72] Reneke also suggested that the mechanism of Posner and Merton-Bingham was unnecessarily complex and proposed an alternative 3-step mechanism (Figure 4B). Calculations from Reneke’s report propose that a 10-kW fuel cell using this system to regenerate $Br_2$ would require a regeneration tower over 130 ft in height and 1.5 ft in diameter. These dimensions likely prevent large-scale implementation of this technology; however, the report from Posner, as well as subsequent studies, show that fuel cell operation is possible.

In 1959, Carson and Feldman from the General Electric Company described a 100 W fuel cell stack, using seven cells connected in series.[40] The cathodic mediator was $Br_2/Br^-$, again using nitric oxide to promote aerobic regeneration of $Br_2$. The fuel was $H_2$, which reduced a $Ti^{IV}$ mediator to $Ti^{III}$ (i.e., $TiO^{2+}/Ti^{3+}$) using Pd-black as an off-electrode catalyst ($H_2|Pt|TiO^{2+}||Br_2|NO_x|O_2$) (see Section 3.1.2 for discussion of the anode performance). The cells were operated at 80 °C, and an open-circuit potential of around 0.95 V was obtained. Continuous operation of the system was demonstrated for over 16 days, but the regeneration of the mediators was not sufficient to operate the system at its peak activity for longer than a few minutes. Additionally, the overall efficiency was low, due to high internal resistance of the cell, and the overall device was quite large, due to a complicated liquid delivery system to each cell. Carson and Feldman noted that, while this system demonstrated technical

feasibility, several improvements would be necessary for commercialization, including the use of non-volatile mediators/catalysts on the cathode.

In 1964, Juda, at Ionics, Inc., patented a fuel cell using bromine-based mediators.[73] $H_2$ oxidation at a heterogeneous Pt electrode was used as the anodic reaction. The cathode compartment contained a solution of KBr, HBr and $Br_2$ with $NO_2$ as the catalyst. An open circuit potential of 0.98 V and an operating potential of 0.7 V at 10 mA/cm$^2$ at room temperature were obtained. Juda compared these results to a system using similar loadings of KI, HI, and $I_2$ without a catalyst, which generated an open circuit potential of 0.5 V and an operating potential of 0.3 V at a current density of 10 mA/cm$^2$. No sustained operation of these cells was reported.

### 2.2. Vanadyl and vanadium-containing polyoxometalate cathodic mediators

The $VO^{2+}/VO_2^+$ redox couple is the most widely studied cathodic mediator in mediated fuel cells. Some major advantages of this system include the high redox potential (~1.0 V vs. NHE), its non-volatile nature, good stability, and reasonably high solubility (> 2 M). These features underlie the widespread implementation of the same mediator system for redox flow battery applications.[74] A catalyst is required to increase the rate of $VO^{2+}$ reoxidation by $O_2$. Both $NO_x$-based catalysts and heteropolyacids (HPAs; also called polyoxometalates, POMs) have been used for this purpose. Table 2 lists the various implementations reported for cathodic vanadium mediators.

The first example of $VO^{2+}/VO_2^+$ mediators for electrocatalytic $O_2$ reduction was patented by Schaefer and Kordesch at Union Carbide Corporation in 1966.[75] While details of the invention are somewhat limited, they described a cell using an $H_2$ gas anode and $NaVO_3$ dissolved in a strong HCl electrolyte (19–39% by weight). When the cathode was supplied with $O_2$, it was operated for over 24 h at 80 °C and sustained a potential between 1.5 and 1.7 V vs. cadmium (conversion to a standardized reference was not given) at a current density of 50 mA/cm$^2$. An HCl electrolyte was necessary for regeneration; when $H_2SO_4$ was used as the electrolyte, addition of HBr and $HNO_3$ was necessary to achieve sustained activity.

Oei, working at Ford, reported the use of a $VO^{2+}/VO_2^+$ mediated cathode. The initial report investigated the performance of various electrolytes in a RFB context (i.e., no regeneration of either redox couple by $O_2$ or a fuel): $VO^{2+}/VO_2^+$ as the cathodic redox couple and $Sn^{2+}/Sn^{4+}$, $Fe^{2+}/Fe^{3+}$, or $Cu/Cu^{2+}$ as the anodic redox couples.[63] Initial tests optimized the flow-field configuration and electrode materials. The different electrode materials displayed similar performance for the vanadium redox process, but substantially different activity for the $Sn^{2+}/Sn^{4+}$ redox couple. Later in the same year, Kummer and Oei reported a mediated cathode system with $VO^{2+}$ and POMs as the mediator/catalyst composition (POM = $H_3PMo_{12}O_{40}$ or $H_5PMo_{10}V_2O_{40}$). A silicon-containing POM was used as the anodic mediator ($H_2|Pt|Si\text{-}POM||VO^{2+}|POM|O_2$; see Section 3.1.4 for discussion of anodic performance).[76–78] Polarization curves were obtained using 0.8 M $VOSO_4$ and 0.28 M $H_3PMo_{12}O_{40}$ at a pH 0.75 (Figure 5). The highest power density obtained was ~38 mW/cm$^2$. Reasonable iR-free voltages were obtained, but the internal resistance of the cell contributed to significant losses in cell potential (0.83 V with iR-correction vs. 0.55 V without iR-correction at ~80 mA/cm$^2$). Slow regeneration of the cathode mediator system

caused the potential of the cathode compartment to drop from 468 mV to 330 mV over 900 minutes of operation. A pH change was observed in the cathode compartment, which was attributed to vanadium migration through the membrane. The authors commented that long-term performance would be determined by the size of the regenerators, and to achieve reasonable rates, the regenerator would be too large for commercial vehicle use. For example, a 20-kW engine would weigh over 5,000 pounds.

In 1985, Kummer and Oei reported further optimization of their mediated fuel cell design.[79] To avoid the substantial performance decreases observed in $VO^{2+}$ oxidation catalyzed by POMs, they shifted to the use of $NO_x$ gases as a catalyst (Figure 6A). Over a 12 h experiment, the cathodic performance remained nearly constant (Figure 6B), showing more stable performance than previous reports.[63] To prevent loss of $NO_x$ species, a static pressure of $O_2$ was used without bubbling gas into the cathode solution. When using a $V^{2+}/V^{3+}$ anode solution, power densities of 73.5 mW/cm$^2$ were achievable.

The $VO^{2+}/VO_2^+$ redox couple has been adopted by other groups in various fuel cell studies focused on anodic reaction chemistry. Folkesson constructed a cell using a $VO^{2+}/VO_2^+$ redox mediator regenerated aerobically using $NO_x$ as a catalyst with a variety of anode redox mediators for $H_2$ oxidation (see Sections 3.1.2, 3.1.3, and 3.1.7 for further discussion of the anodic chemistry).[80] Folkesson demonstrated reasonably stable cell performance generating around 15 mW/cm$^2$ using the $VO^{2+}/VO_2^+$ and $Ti^{3+}/TiO^{2+}$ redox couples. A later report mentions the aerobic oxidation of $VO^{2+}$ catalyzed by Pt for a fuel cell using a $V^{3+}/VO^{2+}$ anode for the oxidation of sugars in a fuel cell stack capable of producing 10 kW of power; however, no evidence for the aerobic oxidation of $VO^{2+}$ was presented.[81] Whitesides and coworkers have used vanadyl-based mediators paired with $NO_x$ catalysts in a variety of applications (c.f. Figure 6A). Their initial report focused on the use of methane as a fuel, mediated by $Fe^{2+}/Fe^{3+}$ and catalyzed by Pt black ($CH_4|Pt|Fe^{2+}||VO^{2+}|NO_x|O_2$; see Section 3.1.3 for further discussion of the anode).[82] Methane oxidation occurred under forcing conditions in a high-pressure reactor (120 °C, 54 atm $CH_4$), and the $Fe^{2+}$ in the resulting aqueous reaction mixture was oxidized at the anode (Figure 7). Polarization curves were obtained, but the performance of the overall system was low, due to engineering difficulties in cell construction and the large potential losses associated with use of the $Fe^{2+}/Fe^{3+}$ redox couple as the anodic redox mediator (~600 mV difference between thermodynamic potential of methane oxidation to $CO_2$ and the $Fe^{2+}/Fe^{3+}$ redox potential). This approach was later extended by Whitesides and coworkers to the use of ethylene glycol as a fuel, generating a power density of 9.9 mW/cm$^3$,[83] and to the use of solid carbonaceous fuels, including coal (see Section 3.1.3 for further discussion).[84]

Deng and coworkers reported a fuel cell using $VO^{2+}/VO_2^+$-based mediators and an $HNO_3$ catalyst to mediate $O_2$ reduction on the cathode paired with an $Fe^{2+}/Fe^{3+}$ anodic mediator for biomass (wheat straw) oxidation.[85] Power densities of over 100 mW/cm$^2$ were achieved with 10 g of wheat straw in 100 mL of electrolyte (10 mL HCl and 30 g $FeCl_3$ in $H_2O$), and a stable current density of 320 mA/cm$^2$ was achieved at a voltage of 0.3 V for over 12 h (see Section 3.1.3 for discussion of the anode). Further studies by Deng and coworkers compared the performance of a mediated cathode utilizing a $VO^{2+}/VO_2^+$ mediator with $HNO_3$ as a catalyst with the performance of a mediated cathode using an $H_{12}P_3Mo_{18}V_7O_{85}$ POM

mediator (see section 3.1.4 for discussion of the relevant anode).[86] Glucose and other biomass sources were used as the fuel with an $FeCl_3$ anodic mediator (glucose|$Fe^{3+}$||$VO^{2+}$|$NO_x$|$O_2$ vs. glucose|$Fe^{3+}$||POM|$O_2$). The cell utilizing the vanadium/$NO_x$ system achieved a maximum power density of approximately 90 mW/$cm^2$, whereas the POM-mediated cell only achieved a maximum power density of approximately 35 mW/$cm^2$. This difference was attributed to the higher open circuit potential achieved by the vanadium-based system compared to the POM-based system.

As discussed above, Oei demonstrated that mixtures of POMs and $VO^{2+}$ undergo aerobic oxidation. POM/$VO^{2+}$ reactions with $O_2$ have been intensely studied for decades, particularly for Mo/V-containing POMs.[87–94] These reactions are quite complex, due to the complicated speciation of POMs in acidic solutions. This complexity can be observed in the $^{31}P$ and $^{51}V$ NMR spectra of $H_{12}P_3Mo_{18}V_7O_{85}$, in which a multitude of different POM isomers and structures are observed (Figure 8).

Starting in the mid-2000s, Acal Energy Ltd., a company based in the UK, filed numerous patents describing the use of POMs as combined mediator/catalysts for the electrocatalytic ORR for fuel cells. In contrast to the Oei work discussed above, Acal used a conventional Pt/C $H_2$ anode. POMs have a variety of promising characteristics, including their inexpensive components, ability to operate at high potentials, and thermodynamic stability.[95,96] Several POM species with promising activities were identified. Higher vanadium incorporation into the vanadium-substituted phosphomolybdate ($H_{3+x}PMo_{12-x}V_xO_{40}$, $0<x<6$) led to enhanced activity, as did the inclusion of sodium ions ($Na_xH_3PMo_{12-x}V_xO_{40}$, $0<x,6$).[97] Addition of 0.15 M $VO^{2+}$ (as $V_2O_4$) as an additional mediator to a solution of 0.3 M $H_3Na_3PMo_9V_3O_{40}$ gave higher sustained voltages when the fuel cell was run at 400 mA/$cm^2$. A cell voltage of ~0.5 V was observed with no added $V_2O_4$ and ~0.58 V with added $V_2O_4$.[98] In a later patent application, Acal disclosed that a mediated fuel cell with 0.3 M $Na_4H_3PMo_8V_4O_{40}$, operated at 80 °C and an ambient pressure, achieved sustained performance over 40 min at approximately 0.4 V and 1.5 A/$cm^2$.[99] In 2019, Knuckey, Creeth, and coworkers disclosed the role of elevated temperatures and air pressures on POM reoxidation.[100] Using $H_7PMo_8V_4O_{40}$, they tested the rate of open-circuit potential (OCP) recovery after cell discharge at 0.8 V. At a regenerator temperature of 80 °C and atmospheric pressure using air, it took over 4000 s for the OCP to increase to 0.88 V. In contrast, at 120 °C and 2 $bar_g$ (air), the same OCP was reached in under within 300 s.

Building on the work of Acal, Matsui, Eguchi, and coworkers published a systematic study of three POMs as fuel cell cathode mediators: $H_3PMo_{12}O_{40}$, $H_5PMo_{10}V_2O_{40}$, and $H_6PMo_9V_3O_{40}$.[101] Polarization curves examining the influence of POM identity, concentration (0.01–0.3 M), and cell temperature (20, 40, or 80 °C) were reported using a conventional Pt/C $H_2$ anode (Figure 9). The vanadium-containing POMs displayed higher activity than the all-molybdenum POM, and increased performance was observed at higher mediator concentrations and higher temperatures. The aerobic regeneration activity of the three POMs during fuel cell operation was examined. Using 0.01 M solutions at either 25 °C or 80 °C and purged with either Ar or $O_2$, the voltage of the cell was monitored as a function of time at a current density of 5.36 mA/$cm^2$. The voltage using the all-Mo $H_3PMo_{12}O_{40}$ mediator decayed identically under $O_2$ or Ar, indicating that the aerobic oxidation of the

reduced mediator was slow. $H_5PV_2Mo_{10}O_{40}$ showed similar behavior under $O_2$ and Ar at 25 °C, indicating slow aerobic reoxidation; however, steady currents under $O_2$ at 80 °C indicated that the POM was oxidized at a sufficient rate for sustained activity at elevated temperature. $H_6PV_3Mo_9O_{40}$ is oxidized at both temperatures, yielding stable voltages over the course of the experiment. The maximum power density obtained (measured by polarization curves) was approximately 40 mW/cm$^2$, obtained with 0.3 M $H_6PV_3Mo_9O_{40}$ at 20 °C or with 0.1 M $H_6PV_3Mo_9O_{40}$ at 80 °C.

Davies and coworkers published a separate study of the use of a $H_6PV_3Mo_9O_{40}$ POM (HV3) solution as the cathodic mediator, again utilizing a conventional Pt/C $H_2$ anode (Figure 10).[63] Many of the reaction parameters of the cathode were examined. A primary focus in this report was the influence of the concentration of reduced vanadium ($VO^{2+}$) on the performance of the cell and examination of the “regenerator efficiency” to probe how well the reduced mediator undergoes oxidation by $O_2$. The authors reported the performance of the cell at various $VO^{2+}$ fractions (i.e., the amount of reduced vanadium relative to total vanadium): 0.05 (almost fully oxidized), 0.25, 0.45, 0.65, and 0.85 (mostly reduced). As expected, the highest OCP values were obtained with the most oxidized solution (0.05 $VO^{2+}$), and a maximum power density of nearly 1 W/cm$^2$ was achieved with 95% oxidized 0.3 M $H_6PV_3Mo_9O_{40}$ at 80 °C. Regeneration experiments, however, indicated that only approximately half of the $V^{IV}$ can be aerobically oxidized to $V^V$, which will limit overall performance. Based on their regeneration data and the polarization curves, the authors predicted the steady-state performance of the combined system, and the results indicated that the steady-state performance will be similar to the results observed with the 0.85 $VO^{2+}$ (mostly reduced) fraction. This result indicated that the regeneration ability of their system was too low to reach optimal power densities. The authors compared their calculated steady state results, as well as their data at 0.05 and 0.65 $VO^{2+}$ fractions, to state-of-the-art conventional PEMFCs and to other mediated cathode fuel cells (Table 3). Their result at 0.05 $VO^{2+}$ fraction was above that for state-of-art PEMFCs and far above those reported for other cathode-mediated systems, while the 0.65 $VO^{2+}$ fraction and the calculated steady state performance were below that of traditional PEMFCs, with a maximum sustainable power density estimated to be 0.38 W/cm$^2$.

In a follow up report, Davies and coworkers examined four different POM species in the same manner described above,[102] with the four POM solutions labeled HV3 (empirical formula $H_6PV_3Mo_9O_{40}$), HV4 (empirical formula $H_7PV_4Mo_8O_{40}$), NaV3 (empirical formula $Na_3H_3PV_3Mo_9O_{40}$), and NaV4 (empirical formula $Na_4H_3PV_4Mo_8O_{40}$). The “protonic” HV3 and HV4 POMs displayed higher open circuit voltages at all $V^{IV}$ fractions relative to the sodiumcontaining solutions, due to the lower pH of the protonic solutions. Polarization curves using almost fully oxidized HV3 or HV4 (5% $V^{IV}$) displayed power densities of over 1 W/cm$^2$. However, the HV3 composition underwent oxidative regeneration much more slowly than the other POM compositions, leading to poor extrapolated steady-state performance. The authors predicted the steady-state performance for each POM identity based on the polarization curves at different $V^{IV}$ fractions and the regeneration data, and they then projected the expected steady-state polarization curves for each POM (Figure 11). Due to its poor reoxidation, HV3 had the lowest estimated performance at steady-state. The two V4 POMs had nearly identical performance, with

NaV4 displaying slightly higher maximum power density (578 mW/cm$^2$; see also, last entry in Table 3). The authors pointed out that the regenerator performance continued to be a limiting factor in achieving maximal power densities and cite an Acal patent describing the formation of “microbubbles” to enhance POM oxidation.[103] A steady-state durability test was performed using the NaV4 POM at a current density of 0.4 A/cm$^2$, and no loss in activity was detected over a 200 h run.

In 2018, Ward and Davies published a study investigating the role of temperature and catholyte concentration of a POM-mediated cathode.[104] Using both HV4 and NaV4 POM compositions, the temperatures tested ranged from 40–90 °C and catholyte concentrations ranged from 0.2–0.45 M. Increases in temperature led to a slight decrease in the redox potential of the catholyte, while an increase in concentration led to larger increases in the catholyte redox potential. The authors also examined the role of temperature and concentration on the pH and conductivity of the catholyte and observed that increasing temperature and concentration both led to decreases in the pH and increases to the conductivity. Polarization curves with different concentrations of HV4 (95% oxidized) showed a 25% increase in maximum power density when shifting from 0.2 M POM to 0.3 M POM at 80 °C, but only a 6% increase when shifting from 0.3 M POM to 0.45 M POM. The minimal improvement at high concentrations was attributed to an increase in cell ohmic resistance as the catholyte concentration increased, perhaps due to $VO_2^+$ and $VO^{2+}$ incorporation into the membrane. For NaV4 catholyte solutions, the best results at 80 °C were obtained using a 0.3 M concentration of the POM, which also corresponded to the lowest observed ohmic cell resistance. Increasing the temperature of both 0.3 M HV4 and NaV4 solutions resulted in enhanced performance at low current densities due to decreased activation losses, as expected; however, detrimental effects were observed at 90 °C at high current densities. The authors suggested that the poorer performance arose from anode effects, e.g., a decrease in electrochemical Pt surface area and decreased exchange current densities. POM regeneration data, collected using the same procedure as in previous reports, indicated that NaV4 has an increased rate of reoxidation relative to HV4. Concentration had only a minor impact on the rate of regeneration. Increasing the temperature typically led to higher reoxidation rates, with an exception observed upon increasing from 80 °C to 90 °C with highly reduced (>60 % reduced) NaV4 samples. The authors attributed a decreased reoxidation rate in this case to decreased $O_2$ solubility and mass transport constraints. Steady-state experiments for each condition were performed at 1 A/cm$^2$, and the highest voltage (0.47 V) was obtained with 0.45 M NaV4 at 90 °C. Very similar performance, however, was obtained using 0.3 M NaV4 at 80 °C, with only a 10 mV drop in cell voltage relative to the more forcing conditions. The authors concluded that the optimal conditions for fuel cell performance are 80 °C with 0.3 M NaV4 and estimated that a steady state peak power density of approximately 510 mW/cm$^2$ could be achieved.

Stahl and coworkers reported a double MedFC using $Na_4H_3PMo_8V_4O_{40}$ as a cathodic mediator paired with a mediated anode consisting of a Pt/C catalyst and anthraquinone mediator to mediate $H_2$ oxidation.[105] In initial tests using the mediated anode with a conventional cathode consisting of a Pt/C electrocatalyst, low power densities were obtained due to flooding of the cathode. Significantly higher power densities (up to 528 mW/cm2

with *iR*-correction) were obtained when a POM-mediated cathode was used instead (see Section 3.1.6 for further discussion of the mediated anode).

Recently, analogous vanadium-containing POMs have been used as cathodic mediators for ORR in various biomass-based fuel cells. A different set of lower-potential POMs were used as mediators for anodic biomass oxidation.[106] The relevant anodic chemistry is discussed in Section 3.1.4. The selection of POMs used in the cathode was expanded beyond the Keggin-type POMs typically used by Acal and others described above, inspired by the fundamental POM/$O_2$ reactivity reported by Zhizhina and Odyakov.[91]

The first example was reported by Deng and coworkers in 2014,[107] describing a cell capable of using fresh grass, switchgrass, starch, or cellulose as the anodic fuels (Figure 12). A 0.3 M solution of $H_{12}P_3Mo_{18}V_7O_{85}$ (or the di- or tri-sodium salt thereof) was used as the cathodic mediator solution, and $H_3PW_{11}MoO_{40}$ was used as the anodic mediator. Stable power densities of 30 mW/cm$^2$ were obtained for 10 h of operation at 80 °C. Consistent with the high loading of vanadium in the cathodic POM mediator, a very high potential (> 1.0 V vs. NHE) was achieved, even with multiple reduced vanadium centers in the POM. The influence of concentration and degree of reduction on the rate of aerobic oxidation was investigated. The degree of reduction was defined as the average number of electrons each POM complex had collected, and the highest rate of oxidation was reached at a high degree of reduction (>1.8 $e^-$/POM) and at intermediate concentrations (~0.15 M). Analyses of anodic reactions are presented in Section 3.1.4.

Several additional studies have employed cathodes with V-containing POM mediators or mediated systems using both $VO^{2+}$ and POMs in efforts primarily focused on processes at the anode (i.e., thorough analysis of the cathode performance was not conducted). These studies will be elaborated in Section 3, but are briefly noted here. Deng and coworkers described a fuel cell using alcohol-based fuels, such as methanol, glycerol, or glucose, using $H_{12}P_3Mo_{18}V_7O_{85}$ as a cathodic POM mediator. Maximum power densities of over 30 mW/cm$^2$ with sorbitol as the alcohol, based on single-scan polarization curves with a fully oxidized mediator at the cathode (i.e., without steady-state POM regeneration by $O_2$).[108] The same group later reported a fuel cell system utilizing the same POM mediator in the cathode and using low-rank coal as the fuel.[109] The same cathodic POM mediator was subsequently utilized by Li and coworkers in a fuel cell utilizing glucose, cellulose, or starch as a fuel.[110] Deng and coworkers utilized sewage sludge as the fuel in their system using $H_3PMo_{12}O_{40}$ as the anodic mediator and $H_{12}P_3Mo_{18}V_7O_{85}$ as the cathodic mediator.[111] Chao, Deng, and coworkers reported a biomass fuel cell using sugars treated photochemically and thermally with $H_3PMo_{12}O_{40}$ at the anode and $H_{12}P_3Mo_{18}V_7O_{85}$ at the cathode.[112]

A fuel cell using lignin as a fuel and $H_3PMo_{12}O_{40}$ as the anodic mediator was reported by Zhao and Zhu,[113] with several cathode variations. Examples included (a) a traditional Pt/C gas-diffusion cathode with $O_2$ as the oxidant, (b) carbon electrodes with $PMo_{12}O_{40}$ or $K_5PV_2Mo_{10}O_{40}$ as POM mediators with $O_2$, and (c) a carbon electrode with $KMnO_4$ as a stoichiometric oxidant. Open circuit potentials and maximum power densities were measured at 90 °C and are summarized in Table 4. In general, the power densities were

higher with solution-phase oxidants versus a conventional $O_2$ cathode. Continuous operation of the cell at 90 °C with each oxidant was examined. The cathodes using $O_2$ at Pt/C (current density ~ 0.4 mA/cm$^2$) and the mediated $H_3PMo_{12}O_{40}|O_2$ system (current density ~ 0.5 mA/cm$^2$) displayed reasonably stable behavior, while the current density decreased substantially for cathodes utilizing $KMnO_4$ or $K_5PV_2Mo_{10}O_{40}|O_2$.

### 2.3. $Fe^{2+}/Fe^{3+}$ mediator

The $Fe^{2+}/Fe^{3+}$ redox couples, including those from aqueous Fe salts, $[Fe(CN)_6]^{4/3-}$, and ferrocene derivatives, have been the subject of substantial interest from the flow battery community.[8] The electrode kinetics can be rapid, and these mediators have low cost and toxicity. On the other hand, the redox potential of free $Fe^{2+}/Fe^{3+}$ (~0.7 V) is relatively low compared to the thermodynamic potential for $O_2$, even while ancillary ligands may be used to access higher potentials. The various mediated cathode systems using this mediator for $O_2$ reduction are summarized in Table 5.

In 1931, Lamb and Elder studied the aerobic oxidation of $FeSO_4$ in acidic solutions catalyzed by various substances, with the goal of utilizing this redox mediator in a fuel cell application.[114] The rate of oxidation of $Fe^{2+}$ was monitored by measuring the potential of the solution during the oxidation. The reaction rate was found to be first order in $pO_2$, second order in $[FeSO_4]$, and independent of $[H_2SO_4]$ above 0.23 M, but the reaction rate increased rapidly below this $H_2SO_4$ concentration. $CuSO_4$ was found to accelerate the oxidation, and it was noted that in the presence of $CuSO_4$ the oxidation of $FeSO_4$ accelerated with increasing acid concentration. Additionally, charcoal accelerated the reaction rate with a roughly first order dependence, and Pt black accelerated the reaction rate in a non-linear fashion, which the authors attributed to catalyst poisoning. The authors then constructed a working cathode solution with a $Zn/ZnSO_4$ anode to study the behavior of the mediated cathode under electrochemical conditions. Comparison of $O_2$ consumption in their kinetic studies with data obtained from the electrochemical studies show good agreement. In the electrochemical studies, the authors measured a current density of 21.5 mA/cm$^2$ while operating at a potential of 0.606 V.

In 1953, Posner published a pair of papers examining the oxidation of $Fe^{2+}$ in concentrated HCl solutions with no catalyst and in dilute HCl solutions catalyzed by charcoal.[115,116] At high concentrations of HCl (> 4.0 N), $Fe^{2+}$ was rapidly autoxidized, while below this value, the reaction was slow, consistent with the previous observations of Lamb and Elder. At the high concentrations of acid, the rate of $Fe^{2+}$ oxidation was first order in $[Fe^{2+}]$, approximately first order in [HCl] between 6–8 N, and first order in $pO_2$. Posner proposed that the rate of oxidation increases at high [HCl] due to the formation of an $Fe^{2+}$-HCl complex, the oxidation of which bypasses formation of superoxide and proceeds directly to $HO_2^{\bullet}$. When $H_2SO_4$ is used as the acid, no acceleration of the autoxidation rate is observed at high concentrations, suggesting that the active complex is not formed with this acid. At lower acid loadings, with charcoal as a catalyst, the autoxidation rate was first order in the catalyst loading, $pO_2$, and $[H^+]$, and proportional to $[Fe^{2+}]/([Fe^{2+}]+[Fe^{3+}])$. The use of iron as a mediator for the ORR was not pursued further, however, due to its low potential.[70] Efforts were made to identify ligands that could increase the $Fe^{2+/}Fe^{3+}$ potential.[117] No

suitable ligands were identified, however, and use of $Fe^{2+/}Fe^{3+}$ as ORR cathode mediators were abandoned for many years.

Iron-based mediators reemerged in the mid- to late-2000s, when Acal Energy Ltd. published a series of patents using various iron-based mediators in fuel cell cathodes. A patent application[118] described a MedFC using a conventional Pt/C $H_2$ anode paired with a mediated cathode system containing $K_3Fe(CN)_6$ and KOH. The use of both a cationic- and anionic-selective membrane was required for optimal performance. In a separate experiment, they disclosed the aerobic regeneration of $K_3Fe(CN)_6$ from $K_4Fe(CN)_6$ using a solution containing 0.02 M EDTA and 0.01 M $MnSO_4$. However, there was no integration between the aerobic regeneration studies and the fuel cell experiments. In subsequent patents, ferrocene (Fc) species were described as mediators using iron complexes to catalyze aerobic oxidation of the reduced mediator.[119–122] Examples include the use of $Fc(CH_2SO_3H)_2$ as a cathodic mediator and $[Fe(trilen\text{-}(SO_3Na)_3)]^{2+}$ as the catalyst at pH 2 (Figure 13). A fuel cell was constructed incorporating a conventional Pt/C $H_2$ anode (i.e., $H_2|Pt/C||Fc(CH_2SO_3H)_2|[Fe(trilen\text{-}SO_3Na)_3)]^{2+}|O_2$), and the mediator was partially oxidized by bubbling $O_2$ through a solution of the mediator and catalyst (10 mM mediator and 1.0 mM catalyst). A polarization curve was measured with this cell. This system exhibited an open-circuit potential of approximately 0.78 V, but the potential decreased rapidly with increasing current, resulting in a current density of only 16 $mA/cm^2$ at a cell voltage of 0.2 V. The authors confirmed that the mediator undergoes regeneration during fuel cell operation by monitoring the open-circuit potential vs. time. Fc derivatives with the cyclopentadienyl rings linked together by an alkyl tether exhibit increased stability relative to unlinked derivatives at pH 2.5.[123] In spite of these improvements, subsequent efforts by Acal emphasized polyoxometalate mediators (cf. Section 2.2).

In 2016, Park and coworkers reported the use of iron phthalocyanine, Fe(pc), as a catalyst for the aerobic oxidation of $Fe^{2+}$ in the context of a MedFC.[61] They studied the kinetics of $Fe^{2+}$ [as $Fe(SO_4)$] oxidation by $O_2$ (1 atm) in 1 M $H_2SO_4$ catalyzed by 0.25 mM Fe(pc) or $[Fe^{III}$(tetra(4-OMephenyl)porphyrin)]Cl. Fe(pc) was a more effective catalyst with >90% conversion of $Fe^{2+}$ to $Fe^{3+}$ after 5 h. This reaction was proposed to proceed *via* $O_2$ binding to the iron macrocycle in the $Fe^{II}$ oxidation state and subsequent reduction of $O_2$ to water with $H_2SO_4$ and aqueous $Fe^{2+}$ ions as the source of protons and electrons (Figure 14A). The authors then measured polarization curves for the three oxidized solutions (0.5 M $FeSO_4$ plus 1.0 M $H_2SO_4$ and (i) no catalyst, (ii) Fe(pc), or (iii) $[Fe^{III}$(tetra(4-MeOphenyl)porphyrin)]Cl). They found the best performance for the solution containing Fe(pc), stemming from the much higher conversion of $Fe^{2+}$ to $Fe^{3+}$ (Figure 14B). In this study, the cell was held at 80 °C and $H_2$ was supplied as the fuel to a Pt/C anode ($H_2|Pt/C||Fe^{2+}|Fe(pc)|O_2$). The solution containing Fe(pc) as the catalyst led to a peak power density of ~250 $mW/cm^2$, which was over three-fold higher than the other two solutions (65 $mW/cm^2$ for the uncatalyzed solution and 76.8 $mW/cm^2$ for the solution containing the Fe-porphyrin catalyst). However, no sustained electrolysis data was included to provide evidence for efficient on-stream regeneration of the mediator during fuel cell operation. The authors noted that further adoption of mediated cathode systems would require higher potential mediators, as well as more active catalysts for the mediator oxidation.

In order to study Fe complexes similar to those reported by Acal, Metz and coworkers used computational methods to calculate the reduction potential of a variety of different Fe complexes bearing chelating nitrogen ligands (Figure 15).[62] Using experimental $E_{1/2}$ values for [Fe(II)trilen (R = H/Cl/$SO_3$Na)-$OH_2$]$^{2+}$ and Fe(II)N4Py(R = H/$CH_3$)-$OH_2$]$^{2+}$, the authors calculated the difference between potential energy surfaces by the self-consistent field method, $\Delta E$(SCF), and found good agreement between these values. The authors used these benchmarks to estimate the redox potential of [Fe(II)trilen (R = $CH_3$/$CF_3$/CN)-$OH_2$]$^{2+}$ and [Fe(II)TFM-trilen(R = H/$SO_3$Na)-$OH_2$]$^{2+}$. The complex [Fe(II)TFM-trilen(R = $SO_3$Na)-$OH_2$]$^{2+}$ was expected to have a redox potential of nearly 1 V, which would increase the open-circuit potential by ~25% relative to the highest previous Fe complex studied experimentally. A synthetic route to this complex was proposed, but it wasn't prepared. Thus, experimental validation of these results, including assessment of mediator stability and aerobic regeneration, awaits further study.

### 2.4. $NO_x$ mediators

In previous sections, $NO_x$ species have been utilized as catalysts for aerobic oxidation of a mediator. $HNO_3$ has also been utilized as a single-component mediator/catalyst system. Both $HNO_3$ and $HNO_2$ have high reduction potentials to NO, 0.957 V and 1.028 V vs. NHE, respectively. These values are close to the formal reduction potential of $O_2$ to $H_2O$, 1.23 V, and it is possible to access high concentrations of $HNO_3$ that support high current densities. The systems using $NO_x$ species derived from $HNO_3$ as cathode mediator/catalysts for $O_2$ reduction are given in Table 6.

In the early 1960s, research into the use of $HNO_3$-mediated ORR was conducted by researchers at Esso Research and Engineering Company in New Jersey.[124] Alcohols, such as methanol or ethylene glycol, were targeted as the fuels for this system. In the initial report, low concentrations of $HNO_3$ (approximately 1 wt% in $H_2SO_4$) gave substantially higher currents than $O_2$ alone. The researchers studied the mechanism of electroreduction of $HNO_3$ and proposed an autocatalytic mechanism with a rate-limiting step involving the reaction of $HNO_3$ with nitric oxide (NO) to form nitrous acid ($HNO_2$).[125] The latter was proposed as the electroactive species. Engineering of the external regenerator allowed up to 30 cycles of $HNO_3$ turnover, measured by comparing the total charge passed to stoichiometric redox equivalents available from $HNO_3$.[126] A challenge with this system was the loss of NO or other $NO_x$ species to the gas phase, but further development of the MeOH-$HNO_3$/$O_2$ fuel cell enabled power densities of 44 mW/cm$^2$ at 0.34 V using a new Pt/C-based catalyst at the cathode. A maximum power density of 19 mW/cm$^2$ was obtained during continuous operation for over 180 h using a standard Pt mesh cathode.[127]

The use of $NO_x$-based mediators for fuel cell cathodes was revisited in 2011, when Park and coworkers reported a fuel cell using the $NO_2^-$/$NO_3^-$ as a cathodic redox mediator using a nitrogen-doped carbon-felt electrode.[128] The reduction of $NO_3^-$ to $NO_2^-$ has a formal potential of 0.94 V, and aerobic oxidation of $NO_2^-$ is facile. The authors prepared an Fe-N/C catalyst by treatment of iron nitrate and melamine with carbon black and annealing of the resultant powder at 700 °C under $N_2$. This electrode showed enhanced activity for nitrate reduction relative to commercial Pt/C catalysts. Specifically, polarization curves using a

conventional Pt/C $H_2$ anode and 5 M $HNO_3$ as the oxidant in the cathode compartment showed higher current densities with Fe-N/C than with Pt/C cathodes (325 mA/cm$^2$ vs. 250 mA/cm$^2$, respectively) at 0.9 V. To monitor the stability of the cathode materials, the power density at 0.8 V was measured over the course of 100 h with an operating temperature of 80 °C. The Fe-N/C electrode showed minimal drop in activity, while the performance of the Pt/C cathode dropped dramatically. This decrease in activity was attributed to Pt dissolution. The selectivity of $NO_3^-$ reduction using the Fe-N/C electrode was measured, and a 98.3% selectivity for formation of $NO_2^-$ was observed, with the remainder forming $N_2$ and NO. No data describing aerobic regeneration of $NO_3^-$ was presented, though the authors suggested that this should be achievable.

In 2017, Park and coworkers reported an $H_2/O_2$ fuel cell using a Pt/C anode and a heteroatom-doped cathode with an $HNO_3$/NO mediator (Figure 16).[129] Nitrogen-doped carbon felt, prepared by treatment of commercial carbon felt at 700 °C under an atmosphere of $NH_3$, proved to be an efficient electrode material to facilitate the reduction of $NO_3^-$ to NO. Polarization curves using 5 M $HNO_3$ were collected at a variety of temperatures, and at 80 °C a power density of over 0.5 W/cm$^2$ was achieved at a potential of 0.8 V. To examine the long-term activity of this system, the fuel cell performance was monitored by holding the cell at a potential of 0.8 V for 30 days with circulation of the 5 M $HNO_3$ solution supplied with 1 atm $O_2$ ($H_2$|Pt/C||$HNO_3$|$O_2$). A slow linear decline in performance was observed during the experiment, falling to approximately 0.3 W/cm$^2$ after 30 days of operation (Figure 17); however, replacement of the cathode solution with fresh $HNO_3$ caused the cell performance to return to its original values. The authors calculated a “regeneration efficiency” of approximately 93%. With no $O_2$ supply, the system was capable of producing power for only 4 days, reflecting the redox capacity of the $HNO_3$ in the cathode solution.

A direct ethanol fuel cell utilizing a PtSn alloy anodic catalyst and a $HNO_3$-based catholyte mediator was reported in 2018 by Park and coworkers (Figure 18).[130] The system achieved a maximum power density of 68 mW/cm$^2$ and an open-circuit potential of ~0.85 V. In contrast, a system using direct $O_2$ reduction on a commercial Pt/C catalyst on the cathode achieved a maximum power density of 34 mW/cm$^2$ and an open-circuit potential of ~0.65 V. No $NO_2$ regeneration data was presented in this work.

### 2.5. Nitroxyl/Oxoammonium mediators

Organic aminoxyls, such as TEMPO (2,2,6,6-tetramethylpiperidine *N*-oxyl), are organic radicals that can undergo 1 e$^-$ oxidation to an oxoammonium species. They have been used as mediators in a wide variety of alcohol oxidation reactions, including under electrochemical[46,131] and aerobic[132,133] reaction conditions. The use of $NO_x$ co-catalysts in the latter reactions provided the starting point for a fundamental study by Gerken and Stahl to investigate the ORR with an aminoxyl/$NO_x$ mediator/catalyst system (Figure 19A).[134] Cyclic voltammetry and controlled-potential electrolysis experiments highlighted the cooperative redox behavior of this system. A series of different nitroxyl mediators (TEMPO, ACT, 3-CARP, and ABNO; Figure 19B) were examined. TEMPO/TEMPO$^+$ electrochemistry was facile, but TEMPO did not react efficiently with $O_2$ (Figure 19C, blue trace). NO, generated by addition of acid to a solution of $NaNO_2$, reacted rapidly with $O_2$,

but the $NO_2$ product exhibited poor electrochemical behavior (Figure 19C, black trace). The combination of both mediators led to a significant and sustained increase in the observed currents (Figure 19C, red trace). Other aminoxyl mediators (ABNO, ACT, and 3-CARP) yielded similar results (Figure 19D), and the operating potential correlates with the potential (vs. $Fc^{+/0}$) of the aminoxyl/oxoammonium redox couple.

The thermodynamic potential for $O_2$ reduction under these reaction conditions was determined by measuring the $H^+/H_2$ open-circuit potential under the non-aqueous conditions and applying the relevant corrections.[135,136] The highest potential mediator, ACT, was shown to feature an ORR overpotential of roughly 300 mV, similar to overpotentials associated with the onset of ORR with conventional Pt catalysts. This system was not well suited for practical application (e.g., due to the use of an organic solvent and loss of $NO_x$ species to the gas phase), but it provides some of the most thorough insights to date into the mechanisms of electrochemical $O_2$ reduction with $NO_x$ and mixed aminoxyl/$NO_x$ mediator systems.

Park and coworkers reported a MedFC using aqueous acidic conditions with TEMPO as a mediator in the absence of a redox catalyst (Figure 20A).[137] The authors report the redox potential of TEMPO to be 0.76 V and used a conventional Pt/C $H_2$ anode ($H_2$|Pt/C||TEMPO|$O_2$). A fuel cell test with a cathode flow rate of 2 mL/min produced a maximum power density of 90 mW/$cm^2$ (Figure 20B). A constant potential experiment was conducted at 0.4 V, and the current was observed to go to zero in approximately 190 minutes (Figure 20C). A rough analysis of the total charge passed suggests that no regeneration of TEMPO occurs with $O_2$, consistent with previous observations (e.g., Figure 20B). The reduced TEMPO mediator will be present as $TEMPOH_2^+$ under these conditions and will not undergo facile reactions with $O_2$.[138]

### 2.6. Quinone/Hydroquinone mediators

Quinones have a rich redox chemistry. They undergo both electron-transfer or proton-coupled electron transfer, they are used in dehydrogenation and other oxidation reactions with organic molecules, and they serve as cocatalysts in aerobic oxidation reactions.[139,140] The last of these roles has direct relevance to the ORR because hydroquinone ($H_2Q$) reacts with activated oxygen species in the reduction of $O_2$ with a molecular Co(salophen) catalyst.[141] Stahl and Anson showed that the use of $H_2Q$ as an “electron-proton transfer mediator” led to a change in ORR product selectivity from $H_2O_2$ (two-electron reduction) to $H_2O$ (four electron reduction) during electrocatalytic $O_2$ reduction.[142] Cyclic voltammetry and bulk electrolysis experiments further showed that $H_2Q$ led to an enhanced rates and lower overpotentials for the Co(salophen)-catalyzed ORR in organic solvent (*N,N*-dimethylformamide, with acetic acid as the proton source; Figure 21). The conditions for the Co(salophen)/$H_2Q$ study reflected those used in the prior aerobic oxidation reactions, but the results have implications for more-conventional ORR effort by showing that a mediator could participate in a cooperative, inner-sphere mechanism and thereby influence the rate and/or selectivity of the reaction.

The first demonstration of hydroquinone-mediated ORR under PEMFC-like conditions was reported by Stahl and coworkers in 2018, using a water-soluble quinone mediator paired

with an off-electrode heterogeneous Co-N/C catalyst.[143] Water-soluble high-potential quinones containing sulfonate groups have been utilized in flow-battery applications[144] (Compounds A-C, Figure 22), but the previously reported materials rapidly decomposed and had inadequate stability for fuel cell operation. To address this limitation, a new tetra-substituted quinone bearing four alkylsulfide-linked sulfonate groups was designed and synthesized (Compound D, Figure 22). This mediator exhibited substantially improved stability with a half-life over >5000 h. Various M-N/C catalysts were tested for their ability to oxidize the corresponding hydroquinone to the quinone under fuel cell relevant conditions (1 M $H_2SO_4$ and 60 °C), and a Co-N/C catalyst using 1,10-phenanthroline as the nitrogen source during the pyrolytic catalyst preparation was identified as the most effective catalyst. A fully integrated fuel cell was constructed using a conventional Pt/C $H_2$ anode ($H_2$|Pt/C|| quinone|Co-N/C|$O_2$) and a Nafion membrane between the anode and cathode (Figure 23A). The cathodic solution contained 0.1 M quinone in 1 M $H_2SO_4$. This solution was circulated between the fuel cell cathode, where the oxidized mediator was reduced, and a packed-bed reactor, where the mediator was oxidized by $O_2$ using the Co-N/C catalyst. An *iR*-corrected peak power density of 251 mW/cm$^2$ (161 mW/cm$^2$ uncorrected) was obtained (Figure 23B). Under steady-state conditions, a stable current output was observed for over 8 h at a constant potential of 0.5 V (Figure 23C). Control experiments showed that a decrease in current density occurred when $O_2$ flow was shut off to the packed bed reactor, and the current density returned to its previous value when $O_2$ flow was resumed. It was noted that development of stable higher potential mediators would enable the fuel cell performance to match or exceed that of conventional fuel cells.

### 2.7. 2,2’-Azino-bis(3-ethylbenzothiazoline-6-sulphonate) mediator

2,2’-Azino-bis(3-ethylbenzothiazoline-6-sulfonate), $ABTS^{2-}$, is a water-soluble, redox-active organic molecule that has been used as a mediator for $O_2$ reduction with various enzymes at the cathode of enzymatic fuel cells (Figure 24). Mediators have found widespread use in enzymatic fuel cells to facilitate electron transfer between the electrode and the active site of an enzyme, which can be buried within the enzyme. A more detailed discussion of the role of mediators in enzymatic fuel cells is provided in Section 3.2 in the context of anodic reactions, and a review of $O_2$ reduction in enzymatic biofuel cells, including both mediated and direct electrochemical approaches, was recently published.[145] In general, mediated fuel cells employing enzymatic catalysts achieve power densities that are much lower (often, by two or three orders of magnitude) than those described in the previous sections.

The first use of $ABTS^{2-}$ in this context was reported by Palmore and Kim in 1999, using fungal laccase from *Pyricularia oryzae* as the enzyme catalyst.[146] Many laccases reduce $O_2$ at very high potentials, though prior reports using direct electrochemical methods displayed very low current densities. The outer-sphere electron-transfer reactivity of laccase accommodates a wide array of mediators. The authors considered mediators with an array of redox potentials, with the hope of identifying one close to the formal potential of the enzyme ($E°’$ = 0.539 V vs. SCE at pH 4.0, at which the formal potential for the reduction of $O_2$ to $H_2O$ is 0.723 V vs. SCE). $ABTS^{2-}$ was selected due to its high potential ($E°’$ = 0.440 V vs. SCE at pH 4.0), good solubility and reasonable stability.

The authors investigated the aerobic oxidation of $ABTS^{2-}$ to $ABTS^{\bullet-}$ catalyzed by laccase. Lower pH values favored higher laccase activity, and the stoichiometry of $ABTS^{2-}$ oxidized to $O_2$ reduced was found to be 4:1, consistent with full reduction of $O_2$ to water. A fuel cell employing a pH 4, 0.2 M acetate buffer was constructed with a Pt-gauze anode under 1 atm $H_2$ and a glassy carbon or Pt-foil cathode containing both laccase and $ABTS^{2-}$ under 1 atm $O_2$ ($H_2$|Pt||$ABTS^{2-}$ |laccase|$O_2$). The anode and cathode compartments were separated by a Nafion membrane. Polarization curves were obtained, and this system showed both a higher open-circuit potential and lower polarization relative to a Pt/$O_2$ or carbon/$O_2$ cathode system (Figure 25A). For example, at a current density of 25 μA/$cm^2$ the biocathode exhibits a potential of 0.50 V vs. SCE, while the Pt/$O_2$ and carbon/$O_2$ system have potentials of 0.04 V and −0.29 V, respectively. Measured power densities were substantially higher for the biocathode, with the mediator system achieving a power density of approximately 40 μW/$cm^2$, compared to ~15 μW/$cm^2$ for a Pt cathode and ~3 μW/$cm^2$ for a carbon cathode (Figure 25B). The performance of mediated laccase cathodes decreases at pH > 5. A biofuel cell pairing $ABTS^{2-}$ and fungal laccase at the cathode was reported to achieve a max power density of 99.8 μW/$cm^2$ at a pH 4.0, with a decrease to 2.0 μW/$cm^2$ at a pH 7.[147]

A pair of studies investigating the use of $ABTS^{2-}$ as a mediator at pH 7 were published by Ikeda and coworkers in 2001. The initial study explored electrocatalytic reduction of $O_2$ with bilirubin oxidase from *M. verrucaria* as the catalyst and $ABTS^{2-}$ as the mediator.[148] Cyclic voltammetry studies indicated catalytic $O_2$ reduction occurred under these conditions, with a half-wave potential of 490 mV vs. Ag/AgCl, which is close to the thermodynamic potential for $O_2$ reduction to $H_2O$ (615 mV vs. Ag/AgCl at pH 7.0; Figure 26). The mediator was found to decompose *via* disproportionation of $ABTS^{\bullet-}$ to $ABTS^{2-}$ and $ABTS^{0}$, which is unstable under these conditions. In a subsequent study, a biofuel cell with an $ABTS^{2-}$/bilirubin oxidase cathode system was paired with *Desulfovibrio vulgaris* bacteria and methyl viologen for $H_2$ oxidation at the anode.[149] A pH of 7 was maintained in each compartment, which were separated by an anion-exchange membrane. Results from this study showed that the cathode compartment exhibited good activity and stability, but the overall power output was limited by the anodic chemistry.

In 2007, Dunn and coworkers reported a fuel cell using bilirubin oxidase immobilized in a sol-gel with $ABTS^{2-}$ as a mediator for $O_2$ reduction.[150] The sol-gel substantially decreased diffusion of $ABTS^{2-}$ to the electrode. Using an anode consisting of a sol-gel immobilized glucose oxidase enzyme as the catalyst, ferrocene methanol as a soluble mediator, and glucose as the fuel (glucose|glucose oxidase|$FcCH_2OH$||$ABTS^{2-}$|bilirubin oxidase|$O_2$), an open circuit potential of 480 mV and a peak power density of approximately 0.12 mW/$cm^2$ were obtained. When air was used instead of $O_2$, the power density dropped to 0.086 mW/$cm^2$. Similar work was published by Xu and coworkers, using $ABTS^{2-}$ as a mediator with laccase at the cathode and glucose oxidase with either a ferrocene derivative or phenazine methylsulfate as anodic mediators.[151] A maximum power density of 5.8 μW/$cm^2$ was obtained in this case.

An enzymatic biofuel cell with a maximum power density of ~2 mW/$cm^2$ was reported by Zhu and coworkers.[152] At the cathode, laccase was bound to a graphene-gold nanoparticle (AuNP-graphene) hybrid electrode, and $ABTS^{2-}$ was used as a mediator. Glucose oxidase

was anchored to the same electrode material at the anode, and direct electron-transfer was possible (Figure 27A–B). Using 0.5 mM $ABTS^{2-}$ as a cathode mediator and 50 mM glucose as fuel for the anode, an open-circuit potential of 1.16 V and a maximum power density of 1.96 $mW/cm^2$ were achieved (Figure 27B). This system also displayed good stability; after 70 days of operation the OCP retained 80% of its original value (Figure 27C) and the maximum power of the cell decreased to 1.30 $mW/cm^2$, corresponding to 66% of the original value.

Chen, Hou, and coworkers reported a single-enzyme biofuel cell that utilizes immobilized laccase enzymes at both the anode and the cathode.[153] Bisphenol A (BPA), was oxidized at the anode and $O_2$ was reduced at the cathode. While the unmediated system was capable of producing power, enhanced performance was obtained when $ABTS^{2-}$ was introduced as a mediator for the cathode, with an approximately 3-fold increase in voltage after addition of ABTS (Figure 28).

Cosnier and coworkers entrapped $P_2ABTS^{2-}$ (bis-pyrene-$ABTS^{2-}$) in a glyconanoparticle and paired this mediator with solubilized bilirubin oxidase to mediate $O_2$ reduction in a "solubilized enzymatic fuel cell."[154] This entrapment strategy facilitates the use of higher concentrations of hydrophobic mediators, and the increased mediator size allows for the use of size-exclusion membranes to limit mediator and enzyme crossover. The cathode containing the entrapped $P_2ABTS^{2-}$ (PS-bCD-$P_2ABTS$) glyconanoparticle and bilibrubin oxidase was paired with an anode containing a 9,10-phenanthrenequinone (PS-bCD-PQ) glyconanoparticle and fungal flavin adenine dinucleotide-dependent glucose dehydrogenase (Figure 29). The glyconanoparticles were prepared by self-assembly of amphiphilic b-cyclodextrin modified polystyrene polymer, which was synthesized through click chemistry of functionalized cyclodextrin and polystyrene blocks,[155] and the resulting PS-bCD-$P_2ABTS$ glyconanoparticles were approximately 43 nm in size. A 3-chamber fuel cell was designed, with the central chamber connected to a peristaltic pump and separated from the anode and cathode compartments by dialysis membranes with a cutoff value of 25 kDa. Fresh solution containing pH 7.0 McIlvaine buffer, ambient $O_2$ concentration, and 5 mM glucose was flowed into the central compartment at a rate of 80 μL/min. The assembled fuel cell achieved a maximum power of 116 ± 21 μW. Charge-discharge experiments were conducted over 10 days. After seven days of testing, the peak power dropped to 85 ± 3 μW, for a power loss of approximately 26%. The spent fuel solution was tested and no evidence was found for the presence of enzymes or mediator. In contrast, a system without encapsulation of the mediators failed to charge after only 20 h, due to leaching of the mediators out of the cathode and anode compartments.

## 3. The Anode: Hydrogen, Alcohol, and Biomass Oxidation

A variety of fuels have been examined in PEMFCs. Hydrogen is the most widely used and is the current fuel for commercial fuel cell systems; however, challenges associated with the transportation and storage of $H_2$ continue to motivate efforts to identify alternative fuels. Methanol (MeOH) is the most common alternate fuel for low-temperature (<120 °C) fuel cells, in part, because methanol can undergo electrochemical oxidation to $CO_2$ without the need to break carbon-carbon bonds. Mediated approaches to electrochemical oxidation of $H_2$

and MeOH have been demonstrated in fuel cell applications, but the opportunities for MedFCs may be more significant for applications with challenging liquids, solids or other complex fuels that do not undergo facile direct electrochemical oxidation. In such cases, the redox chemistry with the fuel can occur off-electrode with a dissolved mediator. This approach allows for consideration of a wider variety of catalysts, since they do not need to be conductive or have other properties required of direct electrocatalysts. Results of mediated electrochemistry at the anode of fuel cells, including examples with chemical and enzymatic catalysts, are summarized below.

### 3.1. Fuel oxidations using chemical catalysts

**3.1.1. Introduction—**Early studies of MedFCs included studies of mediated anodes with $H_2$ as the fuel, but major advances in the performance of gas-diffusion electrodes and the ability to use low Pt catalyst loadings diminished interest and effort in such applications. Nonetheless, the historical efforts provide important context for mediator selection for oxidation reactions with more complex fuels, such as alcohols and biomass. An overview of the various mediated systems using chemical catalysts for anodic reactions is given in Table 7, each of which will be discussed in the following sections.

Two different MedFC configurations have been employed for the oxidation of biomass or related “challenging” fuels with mediators (Figure 30). The first features a one-stage process in which the fuel oxidation and electrochemical reduction of the mediator are coupled within a single continuous process (Figure 30A). The second features a two-stage process in which the fuel is oxidized by the mediator in an independent process, and electrochemical regeneration of the reduced mediator occurs in a separate process (Figure 30B). This latter strategy allows the chemical and electrochemical redox process to be conducted under different conditions (e.g., temperatures, time), while retaining the ability to translate chemical redox processes into electrical power.

**3.1.2. $TiO^{2+}/Ti^{3+}$ mediator—**The first use of mediators to facilitate $H_2$ oxidation was reported in 1959 by Carson and Feldman working at General Electric (see Section 2.1 for discussion on their cathode system).[40] They used an on-line reformer without gas purification, meaning that this mediator system must tolerate $CO_2$ and $H_2S$ impurities. Pd black was used as the catalyst for $TiO^{2+}$ reduction by $H_2$ in 6 N HCl (Figure 31). The activity of the catalyst increased over time, due to solubilization/precipitation of the Pd catalyst, arising from interconversion between insoluble Pd black ($Pd^0$) and $Pd^{2+}$ ions. The reaction of $Pd^{2+}$ ions with $H_2$ generated $Pd^0$, and the freshly deposited Pd black was found to be more active. The $Ti^{3+}/TiO^{2+}$ redox couple has an $E°$ of 0.1 V vs. NHE and, therefore, is well-positioned thermodynamically to mediate $H_2$ oxidation.

A kinetic study of this system was performed by Folkesson.[80] $TiCl_4$ was dissolved in 10% HCl with 2% $Pt/Al_2O_3$. The reduction with $H_2$ exhibited a first-order dependence on $[TiO^{2+}]$. A full fuel cell constructed using a vanadium/$NO_x/O_2$ cathode ($H_2|Pt/Al_2O_3|TiO^{2+}||VO^{2+}|NO_x|O_2$) achieved a peak power density of 15–20 $mW/cm^2$. The fuel cell was discharged through a 1-ohm resistor, and exhibited sustained performance for over 7 h (Figure 32).

**3.1.3. $Fe^{2+}/Fe^{3+}$ mediators—**The $Fe^{2+}/Fe^{3+}$ redox couple has been used as an anodic mediator for a variety of fuel oxidations. Complementary applications of the $Fe^{2+}/Fe^{3+}$ couple to mediate $O_2$ reduction were presented in Section 2.3.

Coordination of EDTA to $Fe^{3+}$ decreases the reduction potential from ~0.7 V vs. NHE to 0.117 V vs. NHE. Folkesson took advantage of this decrease in potential to use $Fe(EDTA)^{2-}$ as a mediator for $H_2$ oxidation, catalyzed by $Pd/Al_2O_3$, at pH 5 (Figure 33).[80] A fuel cell, incorporating $VO_2^+/VO^{2+}$ and $NO_x$ in a mediated cathode for $O_2$ reduction, exhibited rather low power densities of 3 $mW/cm^2$ ($H_2|Pd/Al_2O_3|Fe(EDTA)^{2-}||VO^{2+}|NO_x|O_2$). Some of the drawbacks of this system include poor solubility of $Fe(EDTA)^{2-}$ (max. solubility 0.075 M) and high resistance due to the raised anode solution pH. While the regeneration was shown to be effective, these issues have prevented further research into using $Fe(EDTA)^{2-}$as a mediator for $H_2$ oxidation.

Whitesides and coworkers reported the use of the $Fe^{2+}/Fe^{3+}$ redox couple in a variety of fuel cell applications (cf. Section 2.3 for cathode examples). In the first report, the $Fe^{2+}/Fe^{3+}$ redox couple was used to mediate methane oxidation with a Pt black catalyst (c.f. Figure 7).[82] An analogous MedFC approach was then demonstrated with methanol, ethylene glycol (and oxidized derivatives), and glycerol oxidation to $CO_2$ as the anodic process.[83] Other fuels, such as ethanol, acetic acid, or glucose, were oxidized, but $CO_2$ was not detected. Using a gas buret, the rate of $CO_2$ formation was measured. Potassium oxalate was oxidized to $CO_2$ the fastest, followed by ethylene glycol and glyoxal (Figure 34). Using a cell similar to that used with methane (cf. Figure 7), a fuel cell utilizing ethylene glycol as the fuel produced a maximum power density of 9.9 $mW/cm^3$ at a potential of 197 mV with a graphite felt electrode.

The $Fe^{2+}/Fe^{3+}$ mediator system was also extended to the use of sub-bituminous coal, Kraft lignin, and peat as fuels, without any added catalyst.[84] These efforts demonstrated the ability of mediators to enable the use of fuels that would be highly challenging in conventional fuel cell configurations. While biomass-derived sources were capable to be used as fuels, primary efforts focused on the use of sub-bituminous coal. When oxidizing the fuel in 5 M $H_2SO_4$ saturated with $Fe^{3+}$ at 100 °C, approximately 40% of the available electrons in the coal were liberated. Polarization curves for this system were collected, and a maximum power of 0.6 W per liter of slurry solution was obtained when using a solution containing 4 g of coal in 15 mL of 5 M $H_2SO_4$ saturated with $Fe_2(SO_4)_3$. Simulations of the data suggested that the cell resistance limited the performance, and it was suggested that volumetric power densities of over 7 W/L should be achievable with improved cell engineering. The fuel cell was run continuously for 1000 h (with necessary additions of coal every ~100 h) with no significant degradation in cell performance.

Deng and coworkers used the $Fe^{2+}/Fe^{3+}$ mediator couple to oxidize wheat straw in a fuel cell using $VO^{2+}/VO_2^+$ as the cathodic mediator.[85] Using suspensions of wheat straw in aqueous solutions of $FeCl_3$ and HCl, $Fe^{3+}$ was reduced to $Fe^{2+}$, eventually solubilizing the wheat straw. The fuel cell constructed using these redox couples in a two-stage process achieved power densities of over 100 $mW/cm^2$ when 10 g of wheat straw was used in 100 mL of electrolyte (Figure 35A). The performance stability of the cell was examined in a one-

stage process, and, with a discharge voltage of 0.3 V, a stable current density of 320 mA/cm$^2$ was achieved for 12 h (Figure 35B). Based on the values given, each $Fe^{2+}$ ion was oxidized approximately 1.4 times over the course of this test. The degradation products of wheat grass were hypothesized to contain vanillin and other aromatics, which over time were further oxidized to $CO_2$. Analysis of the biomass after completing the fuel cell test suggested that hemicellulose was the primary reactive component, with cellulose and lignin remaining largely intact.

In 2017, Li and coworkers reported a MedFC using various carbohydrates as the fuel. A combination of $FeCl_3$ with low loadings of $H_3PW_{12}O_{40}$ or $H_3PMo_{12}O_{40}$ POM was the most effective mediator system for electricity generation.[110] Their initial studies focused on testing high loadings (0.3 M) of $H_3PMo_{12}O_{40}$ or $H_3PW_{12}O_{40}$ as the sole catalyst/mediator for oxidation of glucose, but later studies found that using 1 M $FeCl_3$ and 0.06 M $H_3PW_{12}O_{40}$ or 1 M $FeCl_3$ and 0.03 M $H_3PMo_{12}O_{40}$ yielded similar results as 0.3 M $H_3PMo_{12}O_{40}$ (Figure 36). A maximum power density of approximately 2.6 mW/cm$^2$ was achieved. These experiments were conducted in a two-stage process, in which the glucose fuel was heated with the catalyst/mediator system at 85–95 °C for 2 h before introduction into the fuel cell at room temperature. Additionally, both 0.3 M $H_3PMo_{12}O_{40}$ and 1 M $FeCl_3$ + 0.06 M $H_3PW_{12}O_{40}$ were competent catalyst systems for the oxidation of starch (max power densities of ~1.6 mW/cm$^2$), while 1 M $FeCl_3$ + 0.06 M $H_3PW_{12}O_{40}$ was more efficient for the oxidation of cellulose, which enabled a maximum power density of 0.72 mW/cm$^2$, compared to 0.46 mW/cm$^2$ with 0.3 M $H_3PMo_{12}O_{40}$. These results indicate that the addition of $FeCl_3$ could provide a means to reduce the POM loading in biomass oxidation (see Section 3.1.4 for POM-only based methods).

$FeCl_3$ was used as a mediator for the oxidation of glucose and other biomass sources by Deng and coworkers in 2018.[86] The kinetics of this oxidation process were studied, and a nearly first-order dependence of the rate on [glucose] and [$FeCl_3$] was observed under the acidic conditions used. The byproducts of glucose oxidation were identified as $CO_2$, formic acid, acetic acid, and 4-hydroxybutyric acid. The best fuel cell performance, with a power density of approximately 125 mW/cm$^2$, was achieved with a two-stage approach in which 0.33 M glucose and 2.0 M $FeCl_3$ were heated at reflux for 4 h prior to electrochemical reoxidation of the $Fe^{2+}$. The charged solution was capable of maintaining a current density of 250 mA/cm$^2$ (stated 105 mW/cm$^2$ power density) over the course of 1 h. In a closely related process, $Fe^{3+}$-mediated oxidation of biomass (e.g., lignin and sugars) has been conducted in electrolysis cells to produce $H_2$ *via* proton reduction at the cathode, rather than produce power *via* reduction of $O_2$ at the cathode (Figure 37).[156–158]

**3.1.4. Polyoxometalate anodic mediators—**Polyoxometalates (POMs) have been described in several sections above, most extensively as catalysts/mediators in mediated $O_2$ reduction (see Section 2.2). They have also been used as catalysts and/or mediators for the oxidation of hydrogen, alcohols and biomass in fuel cells, as briefly noted in the previous section. These soluble mediators interact effectively with suspensions of heterogeneous and/or polymeric biomass materials, and display higher activity for C–C bond cleavage and are less easily poisoned by biomass impurities relative to heterogeneous catalysts supported on electrodes.

In connection with studies of redox flow batteries, Oei and Kummer were investigating a series of mediators (e.g., $Sn^{2+}/Sn^{4+}$, E° = 0.15 V vs. NHE; $Cu^{2+}/Cu$, E° = 0.153 V vs. NHE; $Fe^{2+}/Fe^{3+}$, E° = 0.77 V vs. NHE) and testing the ability of the oxidized mediator to be reduced by $H_2$ following electrochemical oxidation.[76] Silicotungstic acid ($H_4SiW_{12}O_{40}$) exhibited especially favorable properties, with a reduction potential close to 0 V vs. NHE and an ability to be reduced by $H_2$.[63] While the uncatalyzed reduction at pH 0.5–1 is too slow to observe at room temperature, a variety of catalysts, including $PtO_2$, $PtCl_4$, or Pt/$SiO_2$, in addition to tungsten carbide and Pd(4,4′,4″,4‴-tetrasulphophthalocyanine), enhanced the rate. At 75 °C, the silicotungstic acid was reduced to a lesser extent than at 25 °C due to a temperature-dependent shift in its $E°$, and $H_2$ evolved when a solution reduced at 25 °C was heated to 75 °C. Polarization curves using a $VO^{2+}/VO_2^+$ mediated cathode displayed a cell voltage of 568 mV at 80 mA/cm$^2$ current density. In an extended test of the fully constituted system using a Pt/$SiO_2$ catalyst for reduction of $H_4SiW_{12}O_{40}$, good anode performance was maintained over 20 h, and the performance of the system was limited by the cathode performance. A follow-up study revealed improved cell performance using a $VO^{2+}/VO_2^+$ mediated cathode with $HNO_3$ as a catalyst, reflecting enhanced cathode system stability (Figure 38).[79]

In 2014, Deng and coworkers demonstrated photochemical and thermal oxidation of starch solutions and other biomass sources by POMs at the anode of a MedFC,[159] using a conventional Pt/C $O_2$ cathode. The biomass solution with POM was thermally or photochemically pre-treated and then flowed through the anode compartment in a two-stage process (c.f. Figure 30B). Using this approach with $H_3PMo_{12}O_{40}$ as the POM, power densities of 0.28 mW/cm$^2$ (photochemical pretreatment) and 0.44 mW/cm$^2$ (thermal pretreatment) were measured. In a continuous experiment, in which the POM/starch solution was continuously exposed to light irradiation and heated to 95 °C, a steady current density of 2.5 mA/cm$^2$ was observed for over 20 h. Polarization curves using poplar and switch grass as fuels and photochemical pretreatment displayed peak power densities of 0.65 and 0.62 mW/cm$^2$, respectively.

A subsequent report by Deng and coworkers described a MedFC with POM mediators for both the anode and cathode (cf. Figure 12 in Section 2.2):[107] $H_3PW_{11}MoO_{40}$ (0.3 M) as the anodic mediator and $H_{12}P_3Mo_{18}V_7O_{85}$ (0.3 M) as the cathodic mediator. A two-stage process was used for the anode, in which the $H_3PW_{11}MoO_{40}$ solution was heated with the biomass at 100 °C for 4 h prior to electrochemical treatment and, following this pretreatment procedure, the two POM solutions were passed through their respective electrode compartments and polarization curves were recorded. A variety of biomass sources were tested using this two-stage protocol (Figure 39A). Fresh grass displayed the highest power densities (51 mW/cm$^2$), followed by switchgrass (45 mW/cm$^2$), starch solution (34 mW/cm$^2$), and cellulose (22 mW/cm$^2$). One-stage performance of this system (c.f. Figure 30A) using starch as the fuel source was also demonstrated, displaying a power density of 30 mW/cm$^2$ at a constant discharge current of 160 mA/cm$^2$ for greater than 10 h (Figure 39B). A large portion of the biomass was converted into $CO_2$: 88% of the initial glucose, 82% of the cellulose, and 65% of the lignin was converted to $CO_2$, as measured by total organic content remaining after 12 thermal treatment cycles. Photochemical treatment led to nearly complete conversion to $CO_2$ after 200 hours of photolysis; however, the authors did not

report electrochemical performance over these cycles. Overall, these studies highlight the ability of POMs to cleave C–C bonds in biomass while also being capable of regeneration at the anode.

A similar MedFC was reported by Zhu and coworkers using various lignins as the biomass source and $H_3PMo_{12}O_{40}$ as the POM at the anode with a conventional Pt/C $O_2$ cathode.[113] Polarization curves were collected at room temperature following the reaction of a POM/lignin combinations under a variety of conditions (i.e., in a two-stage approach; cf. Figure 30B). Peak power densities approached 0.35 mW/cm$^2$ for reaction mixtures derived from lignin loadings of 25 g/L and a POM concentration of 0.1 M. Replacement of the Pt/C $O_2$ cathode with a POM-mediated cathode system generated power densities of up to 5 mW/cm$^2$ at 90 °C. The POM source for the cathode was identical to that used at the anode ($H_3PMo_{12}O_{40}$), and power generation was achieved from the different redox states of the POM in the two electrode compartments.

In 2016, Deng and coworkers reported a MedFC using polyols as the fuel in a two-stage anodic process.[108] The anodic mediator/fuel solution, containing 2 M polyol and 0.2 M $H_3PMo_{12}O_{40}$, was subjected to irradiation for 17.5 h with a 250 W metal halide lamp at 25 °C. This solution was then passed through the anode compartment of the MedFC, which employed a 0.3 M $H_{12}P_3Mo_{18}V_7O_{85}$ as a cathodic POM mediator. Using this approach, polarization curves were collected using various alcohol-based fuels. In contrast to conventional fuel cells, in which methanol is typically the best alcohol fuel, the authors showed that glucose performed much better than methanol. The maximum power density attained with glucose was ~ 31.5 mW/cm$^2$, while use of methanol led to a power density of ~8 mW/cm$^2$. The authors also evaluated ethylene glycol, glycerol, erythritol, xylitol, and sorbitol (Figure 40A), and the fuels with more hydroxyl groups led to enhanced power densities at identical fuel concentration (2 M, Figure 40B) or at the same effective hydroxyl concentration of 6 M (i.e. 6 M methanol, 3 M ethylene glycol or 2 M glycerol). UV-visible experiments suggested that increased association between polyhydroxylated fuels and the POM increased the POM reduction by fuels containing more hydroxyl groups. This pre-association was also supported by NMR spectroscopic data. As observed previously,[107] carbon dioxide is the major product arising from these POM-mediated photochemical oxidation reactions of polyols.

Chao and coworkers reported a biomass fuel cell with glucose and other sugars as the fuel, using $H_3PMo_{12}O_{40}$ as the anodic mediator and $H_{12}P_3Mo_{18}V_7O_{85}$ as the cathodic mediator.[112] A two-stage anodic process was used, and a maximum MedFC performance of 40 mW/cm$^2$ was obtained using an anodic solution prepared by photolysis of the POM and glucose solution at 80 °C for 8 hours. Thermal measurements showed that the temperature of the photolysis reaction increased substantially during irradiation, which in turn enhanced the rate of glucose oxidation. The overall efficiency, considering all energy inputs and outputs, of this fuel cell was calculated to be 36.7%. Other sugars, such as fructose and xylose, as well as polysaccharides, such as raffinose and maltose, were found to be nearly as effective of fuels as glucose.

Deng and coworkers reported a MedFC that used coal as a fuel and POM mediators in the anode.[109] Lignite, the lowest grade of coal, was used as the coal source, and it was combined with $H_3PMo_{12}O_{40}$ under a variety of conditions to examine reduction of the POM mediator in the first stage of a two-stage anodic process. The best fuel cell results were obtained by treatment of 10 g lignite in 0.1 L of a 0.3 M POM solution at 200 °C for 5 h. The resulting solution of reduced POM mediator was cooled, filtered to remove coal particulates, and then used at the anode of a MedFC operated at 80 °C with a $H_{12}P_3Mo_{18}V_7O_{85}$-mediated cathode. The maximum power density observed was 120 mW/cm$^2$. Continuous discharging of the fuel cell using a single batch of reduced anodic POM solution was conducted at 150 mA/cm$^2$, and the maximum power density decreased from 60 to ~30 mW/cm$^2$ over 10 h. The coal oxidation was repeated three times with the same batch of coal, consuming approximately 9% of the coal mass in each case. Diminished performance was observed on the third run. Characterization of the coal residue after the third reaction showed a decrease in the total organic carbon, indicating oxidation of the coal to $CO_2$ or water-soluble low molecular weight species, and $^{13}C$ NMR spectroscopic data suggested that aliphatic-like carbonaceous material was preferentially oxidized over aromatic content.

Deng and coworkers also reported a MedFC that utilized sewage sludge as the fuel.[111] This system employed $H_3PMo_{12}O_{40}$ as the anodic POM mediator and $H_{12}P_3Mo_{18}V_7O_{85}$ as the cathodic POM mediator. The authors examined the role of temperature and treatment time on the oxidation of the sewage sludge by $H_3PMo_{12}O_{40}$. Power densities of 13.56 mW/cm$^2$, 16.07 mW/cm$^2$, and 17.91 mW/cm$^2$ were obtained from anodic solutions prepared by treatment of the sewage sludge at 80 °C for 6 h, 12 h, and 24 h, respectively. Further improvements in power densities were achieved by treatment of the sludge for 24 h at 100 °C and 150 °C (49.8 mW/cm$^2$ and 61.4 mW/cm$^2$, respectively; Figure 41). The first oxidation treatment removed over 60 wt% of the sludge sample, which increased to 85 wt% after a second treatment. The authors additionally showed that the POM could undergo repeated cycling with addition of fresh fuel after each cycle. Four cycles were conducted with each showing similar performance.

In 2017, Zhao and coworkers demonstrated the oxidation of lignin in wheat straw to produce electricity using a two-stage process incorporating $H_3PMo_{12}O_{40}$ as an anodic mediator.[160,161] Enzyme-digestible carbohydrates were obtained as a by-product of the biomass oxidative pretreatment. The extent of deliginification, the level of xylan and glucan dissolution, the ability of the remaining glucans to be enzymatically hydrolyzed, and the degree of reduction of the POM were assessed under a variety of conditions. Solutions containing reduced POM were introduced into the anode compartment of a MedFC, in which the cathode solution contained a solution of $FeCl_3$. After testing a variety of conditions, the maximum power density obtained was approximately 11 mW/cm$^2$.

POMs have also been utilized as mediators for biomass oxidation in combination with electrochemical production of $H_2$ and $CO_2$ reduction at the cathode. In these systems, instead of reducing $O_2$ at the cathode to generate power, power is applied to the system and either protons are oxidized to produce $H_2$ (Figure 42)[156,162–163] or $CO_2$ is reduced to CO

and hydrocarbons.[164] The anodic performance of these systems is quite similar to the fuel cell systems.

**3.1.5. Other transition metal-based mediators—**Two additional examples of transition metal-based mediators have been only briefly studied. The first case was reported by Kummer and Oei, who were searching for a mediator solution for $H_2$ oxidation with higher volumetric charge capacity than silicotungstic acid (c.f. Section 3.1.4).[79] Their work was inspired by a precedent for 2 $e^-$ oxidation of a trinuclear molybdenum ion, $[(Mo^{3+})_2Mo^{4+}]$, to $[Mo^{4+}]_3$ with an $E°$ very close to 0 V vs. NHE. Using Pt catalysts, a solution containing $Mo^{6+}$ was cleanly reduced to $Mo^{4+}$ by $H_2$, but only half of the species were further reduced to the $Mo^{3+}$ state, compared to the expected value of two-thirds. This outcome fell short of expectations, but it still led to more reduced metal sites than the one-twelfth observed in silicotungstic acid. When used in a fuel cell along with a $VO_2^+/VO^{2+}$-mediated, $NO_x$-catalyzed $O_2$ cathode ($H_2|Pt|Mo^{3+}||VO^{2+}|NO_x|O_2$), a current density of 85 $mA/cm^2$ at approximately 550 mV (*iR*-free voltage of 725 mV) was obtained. No long-term stability experiments were reported using this mediated anode.

In 2018, Bullock and coworkers reported a fundamental study of electrochemical $H_2$ oxidation under non-aqueous conditions using a mediator/co-catalyst system comprising $Cp*Cr(CO)_3$ and an $Fe(P_2N)$ complex (Figure 43).[165] In this report, $H_2$ underwent homolytic cleavage by two equivalent of $Cp*Cr(CO)_3$ to form two $Cp*Cr(CO)_3H$ species. This complex can transfer an H-atom to $[Fe(P^{Et}N^{Ph}P^{Et})(CO)_3]^+$, and the resulting species undergoes deprotonation and electrochemical oxidation to regenerate the five-coordinate Fe species. A catalytic wave was observed by cyclic voltammetry at the $Fe^{+/0}$ redox wave, and it increased with higher 2-methylpyridine concentration. Each complex was required for competent $H_2$ oxidation, and controlled potential electrolysis with 2,6-di-tert-butylpyridine as a base gave a lower limit of 5 turnovers for Co and 21 turnovers for Fe.

**3.1.6. Quinone/Hydroquinone mediators—**In the mid-1980s, Weetall and coworkers at Corning Glass Works investigated the use of various biomass sources as fuels for a MedFC, using sulfonated anthraquinone (AQ) derivatives as anodic mediators. They examined simple alcohols,[166] carbohydrates,[167] and sulfonated lignin or Kraft Black liquor[168] (a byproduct of wood-pulping) as fuels. To facilitate the oxidation of the alcohol or carbohydrate fuels, visible light irradiation was necessary to excite the anthraquinone mediator. Basic (pH > 12) conditions were used. With ethylene glycol as the fuel (10 volume %), currents of approximately 1 mA were observed, corresponding to a current density of about 0.1 $mA/cm^2$. No potentials, power densities, or sustained performance data for simple alcohol fuels were given. More thorough analysis was performed when carbohydrates, such as glucose, sucrose, or unpurified molasses were used. The highest power output was obtained with glucose as a fuel (0.57 $mW/cm^2$), followed by invertase-treated sucrose (0.43 $mW/cm^2$) and fructose (0.41 $mW/cm^2$). In each of these experiments, 6 mM anthraquinone sulfonate was used as mediator. The authors calculated that 6.4 pounds of glucose would be required to generate one kWh of energy using their cell setup. Under similar conditions using lignin-based fuels, peak power densities of approximately 0.34 $mW/cm^2$ were obtained. Further experiments indicated that the initial polymeric lignin material was

converted into low-molecular weight fragments during fuel cell operation, though the identities of these fragments was not further investigated. It is likely that the performances of the cells could have been substantially increased through further engineering of the cell design. For example, the authors observed a 50% increase in currents merely by mixing the system.

Stahl and coworkers reported a MedFC utilizing a water-soluble anthraquinone mediator, anthraquinone-2,6-disulfonic acid (AQDS) in 1 M $H_2SO_4$ paired with an off-electrode Pt/C catalyst for mediated electrochemical $H_2$ oxidation.[105] The fuel cell was initially constructed using a conventional Pt/C $O_2$ cathode; however, substantial mass-transport losses were observed in the polarization curves due to cathode flooding. To address these concerns, a POM-mediated cathode utilizing 0.3 M $Na_4H_3PMo_8V_4O_{40}$ was used (Figure 44). Polarization curves were obtained, and a peak *iR*-free power density of 528 mW/cm$^2$ was reported (228 mW/cm$^2$ without *iR*-correction). The system also displayed sustained performance at a current density of 50 mA/cm$^2$ for over 8 h. These MedFC performance metrics are substantially lower than those of conventional PEMFCs, but considerable better than metrics achieved with previous applications of MedFCs using $H_2$ as the fuel (cf. sections 3.1.3, 3.1.4, and 3.1.5) Moreover, formic acid and methanol were shown to reduce the AQDS mediator using the Pt/C catalyst, suggesting this approach could potentially be adapted to achieve improved fuel cell performance with fuels more complex than $H_2$.

**3.1.7. $V^{3+}/VO^{2+}$ mediator—**A patent published in 1997 by Larsson and Folkesson reported a MedFC using vanadium salts and a Pt catalyst to oxidize glucose to $CO_2$ as the anodic reaction (Figure 45) and $VO^{2+}/VO_2^+$ as the cathodic redox couple (glucose|Pt|$VO^{3+}$||$VO^{2+}$|catalyst|$O_2$).[169] In this cell, $VO^{2+}$ was reduced to $V^{3+}$ (with some further reduction to $V^{2+}$). Using vanadium species in both the cathode and anode eliminated concerns with mediator crossover, resembling advantages evident in all-vanadium redox flow batteries.[74] A cell capable of producing 10 kW with a power density of 10.5 mW/cm$^2$ (cell voltage of 0.7 V with current density of 15 mA/cm$^2$) was developed, using an anode solution of 180 liters containing 0.3 M $VOSO_4$, 5 M $H_3PO_4$, 0.003 M sugar, and 229 g Pt. Overall, 4 stacks were connected in parallel, with each stack consisting of 130 cells in series, in order to deliver the desired power output. A further kinetic study of the oxidation of sugars by $VO^{2+}$ was reported by the same authors in 2005.[170] They found that low concentrations of sugar were necessary for complete oxidation to $CO_2$. A variety of sugars (sucrose, fructose, glucose, arabinose, xylose) all behaved similarly. Continued optimization of this cell led to power conversion efficiencies of 41–45%, which were suggested to exceed efficiencies accessible by thermal combustion of the sugar.[81]

**3.1.8. Viologen-based mediators—**Viologens (1,1’-dialkyl-4,4’-bipyridyls) are cationic, low-potential, redox-active organic species that have been used as mediators for the oxidation of glucose and other carbohydrate derivatives under basic conditions. In 2009, a pair of publications, one from Wheeler and coworkers[171] and one from Scott and Liaw,[172] reported fuel cells incorporating viologens as mediators for electrochemical glucose oxidation.

Wheeler and coworkers focused on the oxidation of glucose by methyl viologen ($MV^{2+}$, Figure 46A) under mildly basic conditions (pH 9–12).[171] Anaerobic experiments indicated ~8 equiv of $MV^{2+}$ were reduced in the oxidation of glucose when high $MV^{2+}$:glucose ratios were used, compared to the 24 equiv theoretically necessary for full oxidation. However, exposure to $O_2$ under these conditions led to enhanced consumption of glucose, and, at a 12:1 $MV^{2+}$/glucose ratio, significant amounts of carbonate and formate were observed. Preliminary experiments with a simpler substrate (dihydroxyacetone) indicated that a fuel cell could operate using $MV^{2+}$ as a mediator and a cathode containing a cobalt oxide-based catalyst originally developed for zinc-air batteries. Liaw and coworkers demonstrated improved performance in a related fuel cell,[172] showing that with 3 M KOH, 2 M glucose, and 28 mM $MV^{2+}$, a power density of 2.5 mW/cm$^2$ could be obtained with an air-breathing cathode (Figure 46B–C). Liaw proposed that glucose oxidation proceeded only to d-gluconolactone. However, no characterization data for this proposed species was reported. In a later study, Liaw and coworkers provided spectroscopic evidence that the major product of glucose oxidation was gluconic acid when indigo carmine was used as a mediator.[173] One explanation for the discrepancy between the fate of glucose between the Liaw and Wheeler reports is the difference in solution basicity used in these two studies, which may influence the reaction pathways during glucose oxidation.

A later paper, published in 2013 by Liu and coworkers, reported activities similar to those of Liaw and coworkers for their fuel cell using $MV^{2+}$ as a mediator for glucose oxidation.[174] Further work was performed by Liu, Zhang, and coworkers, who reported a power density of 0.52 mW/cm$^2$ at room temperature with 1 M glucose, 3 M KOH, and 15 mM $MV^{2+}$.[175] They detected the formation of both acetate and formate products in their cell.

Wang, Liu, and coworkers reported the use of cellulose as a fuel with a $MV^{2+}$ mediator using a solution containing 5 M NaOH, 1 wt% (w/v) cellulose, and 15 mM $MV^{2+}$.[176] This system achieved a peak power density of 45 μW/cm$^2$. The degradation products of cellulose oxidation were identified by HPLC as oxalic acid, glucaric acid, glyceric acid, glycolic acid, formic acid, and acetic acid.

To increase the performance of a glucose-powered fuel cell using viologen mediators, Watt and coworkers investigated the mechanisms of glucose oxidation and mediator degradation.[177] Under mildly basic conditions, they identified the reaction of an enediol formed from glucose under basic conditions with $MV^{2+}$ as the important step for selectivity. High selectivity required high $MV^{2+}$ loadings to prevent the formation of inactive intermediates. Additionally, it was noticed that dialkyl viologens decomposed under basic conditions (pH > 13) to monoalkyl viologens, so the activity of monoalkyl viologens for glucose oxidation was examined.[178] While glucose oxidation proceeded approximately 50% slower using monoalkyl viologens, the monoalkyl viologens displayed substantially higher stability than the dialkyl variants. In this initial report, higher OCP values also were reported for the monomethyl viologen (0.9 V) than for the dimethyl viologen (0.72 V).[179] Further kinetic studies were undertaken, and increased temperatures were found to substantially increase the rate of alcohol oxidations by methyl viologen and mono-methyl viologen.[180] To assist in the recovery of the viologen mediators, Watt and coworkers also examined the ability of soluble, polymeric viologens to act as mediators in glucose oxidation. Less basic conditions (pH =

11) were required to prevent decomposition of the viologen polymers.[181] While reoxidation with $O_2$ allowed for effective glucose oxidation, attempts to perform the reoxidation electrochemically led to precipitation of the mediators from solution.

## 3.2. Fuel oxidations using enzymatic catalysts

**3.2.1. Introduction—**Enzymatic fuel cells are a broad class of devices, in which enzymes are used as catalysts for oxidant reduction or fuel oxidation.[55–57] Enzymatic fuel cells are different from microbial fuel cells, which use entire organisms to catalyze the desired reactions.[59] While the enzymes are occasionally used as soluble species in solution, they are typically tethered or otherwise immobilized onto the electrode. Some enzymes can undergo direct electron transfer at the electrode, but the buried active sites of many enzymes often leads to slow direct electron transfer. This problem is often addressed through the use of mediators, which can be soluble or immobilized on the electrode. Immobilization of both the enzyme and mediator is most commonly employed, as it has the benefit of removing the need for a membrane, thereby facilitating the miniaturization of enzymatic fuel cells, and minimizes the chance of releasing toxic mediators in implantable or wearable devices. Historical examples of common immobilized mediators include osmium- or ruthenium-containing redox polymers,[182] and in recent years redox polymers containing organic mediators, such as quinones, viologens, or phenothiazines have been developed.[183] The discussion here emphasizes dissolved mediators, analogous to the chemical systems described above. Most enzymatic fuel cells operate at or near ambient conditions (room temperature or slightly above) at moderate or neutral pH values and generate low amounts of power. Power densities are typically ≤1 mW/cm$^2$, commensurate with that appropriate for implantable devices or sensors. A summary of enzymatic fuel cells using at least one soluble mediator is given in Table 8.

**3.2.2. Phenazine-based mediators—**Hill and coworkers reported an enzymatic fuel cell in which methanol dehydrogenase was used to oxidize methanol to formate with phenazine methosulfate (PMS) or phenazine ethylsulfate (PES) as a mediator (Figure 47A)[184] in combination with a conventional Pt/C $O_2$ cathode. PES exhibits greater stability and was shown to give better performance. The fuel cell was operated at pH 9.5 and temperatures from 25–30 °C. The current reached a saturation limit at higher concentrations of mediator and enzyme, and sustained operation was examined with two loadings of the enzyme (Figure 47B). The open circuit potential was ~0.3 V, and a maximum current of ~3 mA (corresponding to a current density of 0.4 mA/cm$^2$ based on the reported Pt electrode dimensions) was obtained across a 10 W resister with 4.6 mg enzyme, 3.5 mM PES, and 62 mM MeOH in 4 mL anode solution. Over the course of 80 min of fuel cell operation, the current dropped to ~1.5 mA (~0.2 mA/cm$^2$). The authors suggested that this decrease could be due to PES blocking of proton flow through the membrane. A pH difference was observed between the anode and cathode compartments at the end of cell operation, supporting this conclusion.

Later, Yue and Lowther revisited this system and attempted to improve on the results by including the enzyme formate dehydrogenase to oxidize the formate product obtained from methanol dehydrogenase.[185] The authors used conditions similar to those of Hill and

coworkers, but they incorporated a carbon anode instead of a Pt mesh anode. The authors selected PMS as the mediator since they observed approximately 10% higher activities for MeOH and formaldehyde oxidation with PMS than with PES in control experiments. Over the course of a 60 min experiment using immobilized enzymes and soluble PMS, the current decreased from 2.14 mA (0.054 mA/cm$^2$) to 1.57 mA (0.039 mA/cm$^2$). It is unclear why the current densities of this system were substantially lower than those of Hill and coworkers. Further testing indicated that the formate dehydrogenase enzyme used in these experiments led to negligible current (only 0.03 mA) when formic acid was directly used as a fuel. This result contrasted the enzyme activity tests, which showed similar activity for formic acid oxidation catalyzed by formate dehydrogenase using PMS and for methanol oxidation catalyzed by methanol dehydrogenase with PMS.

**3.2.3. Tetramethyl-4-phenylenediamine mediator—**In an effort to incorporate mediators more stable than PES or PMS (see section 3.2.2), Hill and coworkers examined a variety of organic species as oxidants for methanol oxidation catalyzed by the quinoprotein alcohol dehydrogenase.[186] Through these efforts, *N,N,N′,N′*-tetramethyl-4-phenylenediamine (TMPD, Figure 48A) was identified as the best mediator. Cyclic voltammetry studies at pH 10.5 showed substantial catalytic activity at the TMPD reduction potential in the presence of methanol and enzyme. In the absence of substrate or enzyme, a reversible 1 e$^-$ wave was observed at 0.01 V vs. SCE (+ 0.25 V vs. NHE). The stability of the TMPD mediator was then compared to PES in a fuel cell. Over a 6 h electrolysis at pH 10.5, the current decayed nearly to zero when PES was used as the mediator (Figure 48B, trace B). When TMPD was used at the mediator under the same conditions, the current remained stable over the entire 6 h electrolysis (Figure 48B, trace A), and decreased by less than 10% over 24 h. Polarization curves were collected, and a peak power of 12 μW was obtained, corresponding to a power density of 2 μW/cm$^2$. The low power density likely reflects, at least in part, the high mediator potential. While no open-circuit potential was reported, the potential at the lowest current indicated was only ~160 mV. The authors noted that this cell was not limited by the cathode chemistry, since no fuel cell improvement was observed when pure $O_2$ was purged into the cathode compartment rather than air. Formate dehydrogenase was included to oxidize the formate since formate inhibits the alcohol dehydrogenase, but poor enzyme performance at the relevant pH led to no improvement in the fuel cell performance.

Ranta and coworkers also studied the stability of TMPD in fuel cells utilizing MeOH/methanol dehydrogenase at pH 10.[187] A $KMnO_4$ solution was used as the oxidant at the cathode. Polarization curves revealed a peak power density of 0.25 mW/cm$^2$ at a current density of 0.38 mA/cm$^2$ and cell voltage of 0.67 V. Most of the polarization losses arose from the anode. The product of methanol oxidation with this enzyme is formate, which led to a decrease in pH that led to a decrease in the system performance during extended operation. TMPD decay (*via* dimerization or oligomerization) was observed, with an estimated half-life of approximately 5 days during fuel cell operation.

In 2009, Leech and coworkers reported an enzymatic fuel cell using a glucose oxidase enzyme as a catalyst for glucose oxidation with TMPD as a mediator.[188] The cathode consisted of a laccase enzyme co-immobilized with an osmium redox polymer acting as a

redox mediator. This study primarily focused on the cathode reaction, but the authors required a highly active anode catalyst and mediator combination. A maximum power density of 52 μW/cm$^2$ was observed, with the performance of the system being limited by the cathodic reaction.

**3.2.4. Dichlorophenolindophenol mediator—**In 1984, Laane and coworkers reported a biofuel cell using glucose as a fuel and D–glucose oxidase as the catalyst with a dichlorophenolindophenol (DCIP, Figure 49A) mediator.[189] Glucose was oxidized to gluconic acid, which the authors identified as a valuable industrial chemical. In their initial studies, $O_2$ reduction to $H_2O$ on a Pt electrode was the cathodic reaction, and sustained currents of 0.3 mA were obtained for over 200 min of cell operation. In a later experiment, a gold cathode was used to reduce $O_2$ to $H_2O_2$, which the authors used to oxidize barbituric acid to 5-chlorbarbituric acid with chloroperoxidase as a catalyst (Figure 49B). Limited information was given about the power generation capabilities of this system. Over 3 days of operation, 10 mg gluconic acid and 8 mg 5-chlorobarbituric acid were generated, corresponding to $1.8 \times 10^4$ turnovers for D-glucose oxidase.

**3.2.5. Viologen-based mediators—**In efforts to increase the power densities of an enzymatic fuel cell using MeOH as a fuel, Palmore and coworkers were interested in decreasing the overpotential between the anodic mediator and MeOH.[190] Previously reported mediators typically have overpotentials of at least 700 mV (cf. sections 3.2.2. and 3.2.3.), presumably because lower overpotential mediators were not sufficiently active with the chosen enzymes. However, the high potentials greatly reduce the potential power output of the fuel cell. To enable the use of lower-potential mediators, three $NAD^+$-dependent enzymes were used to catalyze the oxidation of methanol to $CO_2$: alcohol dehydrogenase (ADH), aldehyde dehydrogenase (AldDH), and formate dehydrogenase (FDH). Three equivalents of $NAD^+$ were required to complete the 6 $e^-$ oxidation of MeOH. The $NAD^+$/NADH redox couple has slow electrode kinetics, however, that often require overpotentials of >1 V to achieve suitable electron-transfer rates.[191] To facilitate the oxidation of NADH, the enzyme diaphorase was used with another soluble mediator, benzyl viologen ($BV^{2+}$), and a fuel cell was constructed using these mediators and enzymes in the anodic compartment and a Pt-black $O_2$ cathode (Figure 50). The cell exhibited an OCP of approximately 0.8 V, and polarization measurements exhibited a peak power density of 0.68 mW/cm$^2$. The rate-determining step in the fuel cell was identified as the oxidation of NADH to $NAD^+$, catalyzed by diaphorase with $BV^{2+}$ as the oxidant.

Enzymes have been extensively studied for electrocatalytic $H_2$ oxidation,[192] but most of these studies utilize heterogenized hydrogenase enzymes. Recently, Minteer and coworkers reported a fuel cell using a solubilized hydrogenase enzyme and methyl viologen ($MV^{2+}$) as a mediator.[193] $N_2$ reduction, catalyzed by nitrogenase and mediated by $MV^{2+}$, was performed at the cathode (Figure 51). With the same mediator used in both anode and cathode, this cell would not supply power at equilibrium, but the shift in equilibrium concentrations caused by substrate oxidation/reduction yielded a potential difference. This cell demonstrated an OCP of 228 mV and achieved a maximum power density of 1.50 μW/cm$^2$. Dinitrogen was reduced to ammonia in this fuel cell, with an overall yield of 286

nmol $NH_3$/mg MoFe protein and a cathodic Faradaic efficiency of 26.4%. This enzymatic fuel cell is noteworthy for its ability to produce $NH_3$ from $N_2$ and $H_2$ while also generating electricity. The authors also demonstrated that an anode consisting of glucose directly oxidized by $MV^{2+}$ under carbonate buffer (pH=11) conditions was also feasible (see section 3.1.7). The OCP under these conditions was 238 mV and the maximum power density was 0.76 μW/cm$^2$.

**3.2.6. Ferrocene-based mediators—**Ferrocene derivatives, such as ferrocene methanol or ferrocene carboxylic acid, have found widespread use as mediators for enzymatic reactions, though many of these examples employed in sensing applications rather than power generation.[194] Dong and coworkers employed a porous carbon electrode with an immobilized glucose oxidase enzyme was paired with ferrocene monocarboxylic acid as a mediator in the anodic compartment of an enzymatic fuel cell.[147] The cathode compartment contained a laccase enzyme and $ABTS^{2-}$ as the mediator. A peak power density of 99.8 μW/cm$^2$ at pH 4 decreased to 2.0 μW/cm$^2$ at pH 7 due to the lower activity of the laccase enzyme in the cathode compartment at higher pH (see section 2.7 for further discussion).

Dunn and coworkers reported an enzymatic fuel cell with glucose oxidase immobilized in a carbon nanotube-containing sol-gel matrix, using ferrocene methanol as a mediator and glucose as the fuel.[150] The cathode compartment contained immobilized bilirubin oxidase and $ABTS^{2-}$ as a soluble mediator for $O_2$ reduction (see Section 2.7). An open circuit potential of 480 mV was obtained with this cell. This value is substantially larger than the difference in redox potentials between $ABTS^{2-}$ (0.480 V vs. Ag/AgCl) and (Fc)$CH_2OH$ (0.21 V vs. Ag/AgCl). The authors suggested that glucose oxidase had sufficient electron transport to the electrode to influence the open circuit potential (the potential of the enzyme was reported to be −0.340 V vs. Ag/AgCl). The system displayed minimal activation polarization, suggesting that this electron transfer continues to be reasonably facile. Similar work was published by Xu and coworkers, using $ABTS^{2-}$ as a mediator with laccase at the cathode and glucose oxidase with ferrocene carboxylic acid as the anodic mediators.[151]

**3.2.7. Quinone/Hydroquinone mediators—**Wang, Kim, and coworkers reported a biofuel cell using glucose oxidase attached to carbon nanotubes with 1,4-benzoquinone as a soluble mediator.[195] Polarization tests using a conventional Pt/C $O_2$ cathode indicated minimal cell polarization up to current densities approaching 0.1 mA/cm$^2$, until mass-transport limitations led to a significant decrease in performance (Figure 52). A maximum power density of 77 μW/cm$^2$ was observed. The enzyme activity was suggested to be capable to supporting power densities approaching 270 μW/cm$^2$.

Zhu and Zhang reported the use of a water-soluble anthraquinone derivative, 2,7-anthraquinone-disulfonic acid (AQDS), as a mediator for oxidation of glucose 6-phosphate using glucose 6-phosphate dehydrogenase (G6PDH) and diaphorase as enzymatic catalysts.[196] NADH was used to mediate electron transfer between glucose 6-phosphate dehydrogenase and diaphorase. The authors compared the use of soluble mediators and enzymes with immobilized mediators and enzymes (Figure 53A), including (a) immobilized enzymes and an immobilized naphthoquinone mediator, menadione (VK3), (b) soluble

enzymes with immobilized VK3, and (c and d) soluble enzymes with either soluble benzyl viologen or soluble AQDS. The results with AQDS as a soluble mediator and non-immobilized enzymes gave the best performance, as determined from polarization curves, with a maximum power density of 1.1 $mW/cm^2$ at room temperature. This value could be increased to 2.4 $mW/cm^2$ at 37 °C. Long-term performance tests showed that the cell with AQDS and immobilized mediators continued to display optimal activity, though overall the performance decreased by 65%, while a cell with immobilized mediator and enzymes only decreased by 35% (Figure 53B).

Cosnier and coworkers encapsulated 9,10-phenanthrenequinone in a glyconanoparticle (PS-bCD-PQ) and used fungal FAD-dependent glucose dehydrogenase for the oxidation of glucose in a “solubilized enzymatic fuel cell”.[154] This encapsulation increases the concentration of the hydrophobic quinone mediator from ~ 5 μM to 68.4 μM (for a 2:1 quinone/glyconanoparticle ratio). Discussion of the performance of the assembled fuel cell is provided in Section 2.7.

**3.2.8. Nitroxyl/Oxoammonium mediators—**Minteer, Sigman, and coworkers use a nitroxyl-based mediator in combination with an enzyme for the complete oxidation of glycerol to $CO_2$. The proposed pathway features non-enzymatic nitroxyl-mediated oxidation of glycerol to mesoxalic acid, followed by decarboxylation of mesoxalic acid by oxalate oxidase.[197] Further nitroxyl-mediated (non-enzymatic) oxidation of glyoxylic acid forms oxalic acid, which undergoes enzymatic oxidation to $CO_2$. Most nitroxyl mediators were found to be inactive as oxidation catalysts under the acidic conditions required for oxalate oxidase (i.e., pH 4–5), but 4-amino-TEMPO exhibited suitable activity. Bulk electrolysis studies with glycerol, 4-amino-TEMPO and oxalate oxidase at pH 5.2 generated current densities up to 1.2 $mA/cm^2$. Intermediates such as glyceric acid, tartronic acid, mesoxalic acid, and glyoxylic acid were detected by HPLC. Using $^{13}C$-labeled glycerol, $^{13}CO_2$ was also detected by NMR. This mediated electrochemical system is different from the other enzymatic processes discussed in this article in that the organic nitroxyl mediator does not shuttle electrons between the enzyme and the electrode, but rather directly mediates electrochemical oxidation of the fuel (glycerol). The enzyme processes intermediates derived from glycerol oxidation that are not amenable to nitroxyl-mediated oxidation, and thereby enables complete oxidation of glycerol to $CO_2$.

Oxalate oxidase requires $O_2$ to support decarboxylative production of $CO_2$ from mesoxalic acid and oxalic acid. Consequently, the four electrons transferred in these steps are not captured electrochemically. To address this issue, 4-amino-TEMPO was paired with other enzymes capable of promoting non-oxidative decarboxylation. Such performance was achieved with oxalate decarboxylase, a redox-neutral enzyme that enabled collection of all possible electrons in the electrochemical oxidation of glycerol (Figure 54).[198] Another study employed the NAD-dependent formate hydrogenase with 4-amino-TEMPO to oxidize glycerol to $CO_2$.[199] Unlike oxalate decarboxylase and oxalate oxidase, which require acidic pH (e.g., pH 4–5), formate hydrogenase is effective at higher pH (e.g., pH 8) where the 4-aminoTEMPO exhibits higher activity. The catalytic activity of the combined system, with $NAD^+$, formate hydrogenase, and 4-amino-TEMPO, for the oxidation of mesoxalate was evident by cyclic voltammetry. Removal of any of the components led to significant or

complete loss of catalytic activity. Complete oxidation of glycerol to $CO_2$ from bulk electrolysis was confirmed by NMR.

One problem in using nitroxyl species as mediators for fuel oxidation at the anode of a fuel cell is the high redox potential of these species, which limits the cell voltage that can be achieved in a fuel cell. In an effort to identify nitroxyls with a more suitable redox potential while retaining high rates of electrocatalytic alcohol oxidation, Sigman, Minteer, and coworkers developed a structure-activity relationship for nitroxyl catalysts.[200] The catalytic activity of the nitroxyl radical was found to be empirically correlated with the potential difference between proton-coupled oxidation of the (protonated) hydroxylamine and oxidation of the nitroxyl. By analyzing this relationship, the authors were able to assign different nitroxyl species to one of four groups, associated with their catalytic activity (y-axis) and their nitroxyl/oxoammonium redox potential (x-axis) (Figure 55A). The four groups correspond to (a) good anodic catalysts (low redox potential and high catalytic activity), (b) good synthetic catalysts (high potentials and high catalytic activity), (c) anti-oxidants (low catalytic activity and low potential), and (d) EPR labels (high potential and low catalytic activity). From this analysis, two species were highlighted as optimal targets for fuel cell applications (numbered **14** and **19** in the original study) (Figure 55B).

## 4. Conclusions and Outlook

This content above highlights historical and recent advances in the applications of soluble redox mediators to electrochemical power generation. The development and testing of mediated fuel cells (MedFCs) have greatly expanded in recent years, with advances leading to new approaches to the catalytic reduction of $O_2$ at the cathode and to the oxidation of $H_2$, alcohols, biomass, and other fuels at the anode. Replacement of Pt with non-PGM cathodes in fuel cell cathodes remains a high priority. Whereas historical efforts commonly featured $Br_2$- or $NO_x$-based mediators, these materials seem unlikely to provide long-term solutions due to challenges related to the volatility, toxicity and/or corrosivity of these species. Polyoxometalates continue to be the focus of attention because their excellent stability and good reactivity with $O_2$, and their ability to access reasonable overpotentials makes them promising mediators and/or catalysts for the ORR and mediated cathode systems. POM mediators have some disadvantages related to their high molecular weight, which contributes to a decreased specific energy density. The recent demonstration of organic cathode mediators in combination with off-electrode ORR catalysts provides a novel approach to implement Pt-free ORR catalysts (e.g., Fe- or Co-N/C materials) and may allow for improved utilization of these catalytic materials. The design of highly stable, high-potential mediators represents a key challenge that will need to be addressed to expand on recent demonstrations. In addition, exploration of other conditions, such as the use alkaline conditions and anion exchange membranes, may open new avenues for catalyst and mediator compositions. Mediated electrochemistry introduces significant opportunities for fuel cell power generation with complex fuels, such as polyols and other biomass-derived materials, hydrocarbons, and even low-grade coal and sewage. Low-potential POMs have emerged as some of the most effective anodic mediators, reflecting their low cost, good stability, effective redox behavior, and compatibility with chemicals present in complex fuels that inhibit or poison many other types of catalysts (e.g., sulfur or other heteroatom-containing

compounds). Thus far, many implementations of mediated fuels with complex chemicals employ a two-stage process in which the first stage features oxidation of the fuel by the mediator in a (non-electrochemical) batch process, and the mediator is regenerated electrochemically in a second stage. Assessment of the merits of this approach relative to a one-stage continuous electrolysis process represents an important issue for future efforts in the field. Organic mediators have been commonly used to support fuel oxidation, especially in enzymatic fuel cells. Organic mediators are appealing because of the ability to tune their redox kinetics and electrochemical potentials, as revealed by studies of viologens and organic nitroxyls. For enzymatic fuel cell systems, efforts will likely continue to focus on immobilized enzymes and mediators, but recent reports highlight potential performance enhancements possible when the mediator and/or enzyme are dissolved in solution. The latter strategy may find utility for systems in which refreshing the solutions to restore the enzyme and mediator activity is feasible.

Thus far, mediated fuel cells, especially those using alcohols, biomass, or other complex fuels achieve lower power output than conventional fuel cells. Nonetheless, the ability to eliminate the requirement for Pt and other PGM catalysts and derive power from non-conventional fuel sources provides strong motivation to continue exploration of this technology, including the development of new mediators that achieve improved stability, lower overpotentials for the processes of interest, better kinetics; and the development of new catalysts that serve as effective partners with mediators to allow electrochemically driven off-electrode redox reactions or that exhibit cooperative redox behavior with the mediator, allowing for faster rates or lower overpotentials.

## Acknowledgements

Our research on in this field has been exploring a number of different topics and has been supported different funding sources: the Center for Molecular Electrocatalysis, an Energy Frontier Research Center funded by the U.S. Department of Energy, Office of Science, Office of Basic Energy Sciences (molecular mediators for catalytic oxygen reduction); the Great Lakes Bioenergy Research Center, DOE Office of Science DE-SC0018409 (research on biomass-based fuels; U.S. Department of Energy, Office of Science, Office of Basic Energy Sciences, Catalysis Program, DE-FG02-05ER15690 (copper-catalyzed oxidation reactions); and the NIH NIGMS, R01 GM100143 and R35 GM134929 (use of molecular mediators for organic chemical synthesis).

## Appendix I.: Summary of Mediated Fuel Cells Using Chemical Catalysts. (See Table 8 for a Summary of Mediated Fuel Cells Using Enzymatic Catalysts.)

| Anode | | | Cathode | | | |
|---|---|---|---|---|---|---|
| ***fuel*** | ***catalyst*** | ***mediator*** | ***mediator*** | ***catalyst*** | ***oxidant*** | ***ref.*** |
| $H_2$ | Pd black | $TiO^{2+}/Ti^{3+}$ | $Br^-/Br_2$ | $NO_x$ | $O_2$ | 40 |
| | Pt | – | | | | 73 |
| | | | $VO^{2+}/VO_2^+$ | HCl | | 75 |
| | | $Mo^{3+}/Mo^{4+}$ | | $NO_x$ | | 79 |
| | | $H_4SiW_{12}O_{40}$ | | | | 79 |

| Anode | | | Cathode | | | |
|---|---|---|---|---|---|---|
| ***fuel*** | ***catalyst*** | ***mediator*** | ***mediator*** | ***catalyst*** | ***oxidant*** | ***ref.*** |
| | | $Ti^{3+}/TiO^{2+}$ | | | | 80 |
| | $Pd/Al_2O_3$ | $Fe(EDTA)^{2-}$/ $Fe(EDTA)^{-}$ | | | | 80 |
| | Pt | $H_4SiW_{12}O_{40}$ | | POM | | 76–78 |
| | Pt/C | AQ | V-containing POM | | | 105 |
| | Pt/C | – | | | | 63, 95–102, 104 |
| | | | $Fe^{2+}/Fe^{3+}$ | Fe(pc) | | 61 |
| | | | $K_3Fe(CN)_6$ | Mn complex | | 118 |
| | | | Fc species | Fe complex | | 119–123 |
| | | | $HNO_3$ | | | 128–129 |
| | | | nitroxyl | – | | 137 |
| | | | quinone | Co–N/C | | 143 |
| alcohols | Pt | – | $HNO_3$ | | | 124–127 |
| coal | – | $Sn^{4+}/Sn^{2+}$ | $Br^{-}/Br_2$ | $NO_x$ | | 70 |
| $CH_4$, alcohols, coal | Pt | $Fe^{2+}/Fe^{3+}$ | $VO^{2+}/VO_2^{+}$ | $NO_x$ | | 82–84 |
| biomass | – | | | | | 85, 86 |
| sugars | Pt | $V^{3+}/VO^{2+}$ | | Pt | | 81, 169 |
| sugars | POM | $Fe^{2+}/Fe^{3+}$ | V-containing POM | | | 110 |
| biomass | POM | | | | | 107, 111, 112 |
| alcohols | | | | | | 108 |
| lignin | | | | | | 113 |
| coal | | | | | | 109 |
| biomass | | | – | Pt/C | | 113, 159 |
| alcohols, sugars or lignin | – | AQ | – | – | | 166–168 |
| sugars | – | viologen | – | Co | | 171–175, 177 |
| – | – | $V^{2+}/V^{3+}$ | $VO^{2+}/VO_2^{+}$ | $NO_x$ | | 79 |
| Zn | – | – | $Fe^{2+}/Fe^{3+}$ | charcoal | | 114 |

## Biographies

Colin W. Anson obtained his B.A. in Chemistry in 2011 from Colby College, located in Waterville, Maine. Later that year, he joined the research group of Professor Shannon Stahl at the University of Wisconsin-Madison, where he obtained his Ph.D. in Chemistry in 2017. His doctoral work focused on the use of organic quinones as mediators for electrocatalytic $O_2$ reduction using molecular cobalt catalysts. He continued this research during his postdoctoral work, targeting fuel cell-relevant applications of this concept. Currently, he is an Associate Scientist in the Stahl group, where he works on electrochemical energy conversion and biomass valorization projects.

Shannon S. Stahl obtained his B.S. in Chemistry in 1992 from the University of Illinois at Urbana–Champaign and earned his Ph.D from Caltech in 1997, where he worked with Professor John Bercaw. He was an NSF postdoctoral fellow with Professor Stephen Lippard at Massachusetts Institute of Technology from 1997 to 1999. He is currently the Steenbock Professor of Chemical Sciences at the University of Wisconsin–Madison, where he began his independent career in 1999. His research group specializes in catalysis and electrochemistry, with an emphasis on catalytic aerobic oxidation reactions and electrocatalytic reactions related to chemical synthesis and energy conversion.

## References


(1). Gyuk I; Johnson M; Vetrano J; Lynn K; Parks W; Handa R; Kannberg L; Hearne S; Waldrip K; Braccio R Grid Energy Storage; U.S. Department of Energy, Office of Electricity Delivery & Energy Reliability: Washington, DC, 2013.

(2). Annual Energy Outlook 2019 with Projections to 2050; U.S. Department of Energy, Office of Energy Analysis, U.S. Energy Information Administration: Washington, DC, 2019.

(3). Jamison L Monthly Energy Review May 2019, Section 10. Renewable Energy; pgs 171–191; U.S. Department of Energy, Office of Energy Analysis, U.S. Energy Information Administration: Washington, DC, 2019.

(4). Goodenough JB; Park K-S The Li-Ion Rechargable Battery: A Perspective. J. Am. Chem. Soc 2013, 135, 1167–1176. [PubMed: 23294028]

(5). Yabuuchi N; Kubota K; Dahbi M; Komaba S Research Development on Sodium-Ion Batteries. Chem. Rev 2014, 114, 11636–11682. [PubMed: 25390643]

(6). Winter M; Barnett B; Xu K Before Li Ion Batteries. Chem. Rev 2018, 118, 11433–11456. [PubMed: 30500179]

(7). Zhao C; Liu L; Qi X; Lu Y; Wu F; Zhao J; Yu Y; Hu Y-S; Chen L Solid-State Sodium Batteries. Adv. Energy Mater 2018, 8, 1703012.

(8). Soloveichik GL Flow Batteries: Current Status and Trends. Chem. Rev 2015, 115, 11533–11558. [PubMed: 26389560]

(9). Winsberg J; Hagemann T; Janoschka T; Hager MD; Schubert US Redox-Flow Batteries: From Metal to Organic Redox-Active Materials. Angew. Chem. Int. Ed 2017, 56, 686–711.

(10). Yang Z; Zhang J; Kintner-Meyer MCW; Lu X; Choi D; Lemmon JP; Liu J Electrochemical Energy Storage for Green Grid. Chem. Rev 2011, 111, 3577–3613. [PubMed: 21375330]

(11). Winter M; Brodd RJ What Are Batteries, Fuel Cells, and Supercapacitors? Chem. Rev 2004, 104, 4245–4270. [PubMed: 15669155]

(12). Nocera DG Solar Fuels and Solar Chemicals Industry. Acc. Chem. Res 2017, 50, 616–619. [PubMed: 28945407]

(13). Detz RJ; Reek JNH; van der Zwaan BCC The Future of Solar Fuels: When Could They Become Competitive? Energy Environ. Sci 2018, 11, 1653–1669.

(14). Fuel Cells; U.S. Department of Energy, Energy Efficiency & Renewable Energy, Fuel Cell Technologies Office, 11 2015 https://www.energy.gov/sites/prod/files/2015/11/f27/fcto_fuel_cells_fact_sheet.pdf, accessed 08/26/2019.

(15). Mehta V; Cooper JS Review and Analysis of PEM Fuel Cell Design and Manufacturing. J. Power Sources 2003, 114, 32–53.

(16). The Future of Hydrogen, International Energy Agency: Paris, 2019.

(17). Gottesfeld S; Dekel DR; Page M; Bae C; Yan Y; Zelenay P; Kim YS Anion Exchange Membrane Fuel Cells: Current Status and Remaining Challenges. J. Power Sources 2018, 375, 170–184.

(18). Jiao K; Li X Water Transport in Polymer Electrolyte Membrane Fuel Cells. Prog. Energy Combust. Sci 2011, 37, 221–291.

(19). Kreuer K-D; Paddison SJ; Spohr E; Schuster M Transport in Proton Conductors for Fuel-Cell Applications: Simulations, Elementary Reactions, and Phenomenology. Chem. Rev 2004, 104, 4637–4678. [PubMed: 15669165]

(20). De las Heras A; Vivas FJ; Segura F; Andújar JM From the Cell to the Stack. A Chronological Walk through the Techniques to Manufacture the PEFCs Core. Renewable Sustainable Energy Rev 2018, 96, 29–45.

(21). Hermann A; Chaudhuri T; Spagnol P Bipolar Plates for PEM Fuel Cells: A Review. Int. J. Hydrogen Energy 2005, 30, 1297–1302.

(22). Garsany Y; Atkinson RW III; Gould BD; Swider-Lyons KE High Power, Low-Pt Membrane Electrode Assemblies for Proton Exchange Membrane Fuel Cells. J. Power Sources 2018, 408, 38–45.

(23). Gasteiger HA; Kocha SS; Sompalli B; Wagner FT Activity Benchmarks and Requirements for Pt, Pt-alloy, and Non-Pt Oxygen Reduction Catalysts for PEMFCs. Appl. Catal. B 2005, 56, 9–35.

(24). Martinez U; Babu SK; Holby EF; Zelenay P Durability Challenges and Perspective in the Development of PGM-Free Electrocatalysts for the Oxygen Reduction Reaction. Curr. Opin. Electrochem 2018, 9, 224–232.

(25). Thompson ST; Wilson AR; Zelenay P; Myers DJ; More KL; Neyerlin KC; Papageorgopoulos D ElectroCat: DOE's Approach to PGM-Free Catalyst and Electrode R&D. Solid State Ionics 2018, 319, 68–76.

(26). Gewirth AA; Varnell JA; DiAscro AM Nonprecious Metal Catalysts for Oxygen Reduction in Heterogeneous Aqueous Systems. Chem. Rev 2018, 118, 2313–2339. [PubMed: 29384375]

(27). Ballard Plans World's First PEMFC Product with Low-Cost Nisshinbo Non-Precious Metal Catalyst. Fuel Cell Bull 2017, 9, 1.

(28). Banham D; Choi J-Y; Kishimoto T; Ye S Integrating PGM-Free Catalysts into Catalyst Layers and Proton Exchange Membrane Fuel Cell Devices. Adv. Mater 2019, 31, 1804846.

(29). Liu H; Song C; Zhang L; Zhang J; Wang H; Wilkinson DP A Review of Anode Catalysis in the Direct Methanol Fuel Cell. J. Power Sources 2006, 155, 95–110.

(30). Li X; Faghri A Review and Advances of Direct Methanol Fuel Cells (DMFCs) Part I: Design, Fabrication, and Testing with High Concentration Methanol Solutions. J. Power Sources 2013, 226, 223–240.

(31). Soloveichik GL Liquid Fuel Cells. Beilstein J. Nanotechnol 2014, 5, 1399–1418. [PubMed: 25247123]

(32). Kurzweil P History: Secondary Batteries In Encyclopedia of Electrochemical Power Systems; Garche J, Ed.; Elsevier: Amsterdam, 2009, pp 565–578.

(33). Bartolozzi M Development of Redox Flow Batteries. A Historical Bibliography. J. Power Sources 1989, 27, 219–234.

(34). Noack J; Roznyatovskaya N; Herr T; Fischer P The Chemistry of Redox-Flow Batteries. Angew. Chem. Int. Ed 2015, 54, 9776–9809.

(35). Luo J; Hu B; Hu M; Zhao Y; Liu TL Status and Prospects of Organic Redox Flow Batteries toward Sustainable Energy Storage. ACS Energy Lett 2019, 4, 2220–2240.

(36). Huskinson B; Marshak MP; Suh C; Er S; Gerhardt MR; Galvin CJ; Chen X; Aspuru-Guzik A; Gordon RG; Aziz MJ A Metal-Free Organic-Inorganic Aqueous Flow Battery. Nature 2014, 505, 195–198. [PubMed: 24402280]

(37). Lin K; Chen Q; Gerhardt MR; Tong L; Kim SB; Eisenach L; Valle AW; Hardee D; Gordon RG; Aziz MJ et al. Alkaline Quinone Flow Battery. Science 2015, 349, 1529–1532. [PubMed: 26404834]

(38). Janoschka T; Martin N; Hager MD; Schubert US An Aqueous Redox-Flow Battery with High Capacity and Power: The TEMPTMA/MV System. Angew. Chem. Int. Ed 2016, 55, 14427–14430.

(39). Gong K; Fang Q; Gu S; Li SFY; Yan Y Nonaqueous Redox-Flow Batteries: Organic Solvents, Supporting Electrolytes, and Redox Pairs. Energy Environ. Sci 2015, 8, 3515–3530.

(40). Carson WN Jr.; Feldman ML A Redox Type. Proc. Ann. Power Sources Conf 1959, 13, 111–113.

(41). Matsen JM Chemically Regenerative, Fuel Cell Systems. Adv. Chem. Ser 1967, 64, 277–291.

(42). Tolmachev YV; Vorotyntsev MA Fuel Cells with Chemically Regenerative Redox Cathodes (Review). Russ. J. Electrochem 2014, 50, 403–411.

(43). Steckhan E Indirect Electroorganic Syntheses–A Modern Chapter of Organic Electrochemistry. Angew. Chem. Int. Ed 1986, 25, 683–701.

(44). Ogibin YN; Elinson MN; Nikishin GI Mediator Oxidation Systems in Organic Electrosynthesis. Russ. Chem. Rev 2009, 78, 89–140.

(45). Francke R; Little RD Redox Catalysis in Organic Electrosynthesis: Basic Principles and Recent Developments. Chem. Soc. Rev 2014, 43, 2492–2521. [PubMed: 24500279]

(46). Nutting JE; Rafiee M; Stahl SS Tetramethylpiperidine *N*-Oxyl (TEMPO), Phthalimide *N*-Oxyl (PINO), and Related *N*-Oxyl Species: Electrochemical Properties and Their Use in Electrocatalytic Reactions. Chem. Rev 2018, 118, 4834–4885. [PubMed: 29707945]

(47). Hagfeldt A; Boschloo G; Sun L; Kloo L; Pettersson H Dye-Sensitized Solar Cells. Chem. Rev 2010, 110, 6595–6663. [PubMed: 20831177]

(48). Bella F; Gerbaldi C; Barolo C; Grätzel M Aqueous Dye-Sensitized Solar Cells. Chem. Soc. Rev 2015, 44, 3431–3473. [PubMed: 25864577]

(49). McCloskey BD; Addison D A Viewpoint on Heterogeneous Electrocatalysis and Redox Mediation in Nonaqueous Li-$O_2$ Batteries. ACS Catal 2017, 7, 772–778.

(50). Yan R; Wang Q Redox-Targeting-Based Flow Batteries for Large-Scale Energy Storage. Adv. Mater 2018, 30, 1802406.

(51). Wallace AG; Symes MD Decoupling Strategies in Electrochemical Water Splitting and Beyond. Joule 2018, 2, 1390–1395.

(52). Hu L; Zhai T; Li H; Wang Y Redox-Mediator-Enhanced Electrochemical Capacitors: Recent Advances and Future Perspectives. ChemSusChem 2019, 12, 1118–1132. [PubMed: 30427120]

(53). Cao L; Skyllas-Kazacos M; Wang D-W Solar Redox Flow Batteries: Mechanism, Design, and Measurement. Adv. Sustainable Syst 2018, 1800031.

(54). Pattabiraman R; Venkatesan VK; Udupa HVK Applications of Redox Systems in Fuel Cells. J. Sci. Ind. Res 1981, 40, 432–447.

(55). Cracknell JA; Vincent KA; Armstrong FA Enzymes as Working or Inspirational Electrocatalysts for Fuel Cells and Electrolysis. Chem. Rev 2008, 108, 2439–2461. [PubMed: 18620369]

(56). Kavanagh P; Leech D Mediated Electron Transfer in Glucose Oxidising Enzyme Electrodes for Applications to Biofuel Cells: Recent Progress and Perspectives. Phys. Chem. Chem. Phys 2013, 15, 4859–4869. [PubMed: 23443881]

(57). Rasmussen M; Abdellaoui S; Minteer SD Enzymatic Biofuel Cells: 30 Years of Critical Advancements. Biosens. Bioelectron 2016, 76, 91–102. [PubMed: 26163747]

(58). Logan BE; Hamelers B; Rozendal R; Schröder U; Keller J; Freguia S; Aelterman P; Verstraete W; Rabaey K Microbial Fuel Cells: Methodology and Technology. Environ. Sci. Tech 2006, 40, 5181–5192.

(59). Santoro C; Arbizzani C; Erable B; Ieropoulos I Microbial Fuel Cells: From Fundamentals to Applications. A review. J. Power Sources 2017, 356, 225–244. [PubMed: 28717261]

(60). Mohan SV; Velvizhi G; Krishna KV; Babu ML Microbial Catalyzed Electrochemical Systems: A Bio-Factory with Multi-Facet Applications. Bioresour. Technol 2014, 165, 355–364. [PubMed: 24791713]

(61). Han S-B; Kwak D-H; Park HS; Choi I-A; Park J-Y; Ma K-B; Won J-E; Kim D-H; Kim S-J; Kim M-C et al. Chemically Regenerative Redox Fuel Cells Using Iron Redox Couples as a Liquid Catalyst with Cocatalysts. ACS Catal 2016, 6, 5302–5306.

(62). Sen K; Creeth A; Metz S A Combined Experimental/Theoretical Approach to Accelerated Fuel Cell Development by Quantitative Prediction of Redox Potentials. J. Power Sources 2018, 399, 443–447.

(63). Gunn NLO; Ward DB; Menelaou C; Herbert MA; Davies TJ Investigation of a Chemically Regenerative Redox Cathode Polymer Electrolyte Fuel Cell using a Phosphomolybdovanadate Polyoxoanion Catholyte. J. Power Sources 2017, 348, 107–117.

(64). Oei D-G. Chemically Regenerative Redox Fuel Cells. J. Appl. Electrochem 1982, 12, 41–51.

(65). Kongkanand A; Mathias MF The Priority and Challenge of High-Power Performance of Low-Platinum Proton-Exchange Membrane Fuel Cells. J. Phys. Chem. Lett 2016, 7, 1127–1137. [PubMed: 26961326]

(66). Banham D; Ye S Current Status and Future Development of Catalyst Materials and Catalyst Layers for Proton Exchange Membrane Fuel Cells: An Industrial Perspective. ACS Energy Lett 2017, 2, 629–638.

(67). Wilson A; Marcinkoski J; Papageorgopoulos D Fuel Cell System Cost – 2016. DOE Hydrogen and Fuel Cells Program Record # 16020 Approved 11 21, 2016.

(68). Nie Y; Li L; Wei Z Recent Advancements in Pt and Pt-Free Catalysts for Oxygen Reduction Reaction Chem. Soc. Rev 2015, 44, 2168–2201. [PubMed: 25652755]

(69). Shao M; Chang Q; Dodelet J-P; Chenitz R Recent Advances in Electrocatalysts for Oxygen Reduction Reaction. Chem. Rev 2016, 116, 3594–3657. [PubMed: 26886420]

(70). Posner AM Redox Fuel Cell. Fuel 1955, 34, 330–338.

(71). Merton-Bingham BE; Posner AM Nitrogen Peroxide as a Catalyst for the Autoxidation of Hydrobromic Acid. J. Am. Chem. Soc 1955, 77, 2634–2638.

(72). Reneke WE Air Regeneration of Bromine-Bromide Fuel Cell Catholyte Ph.D. Dissertation, University of Florida, Gainesville, FL, 1961.

(73). Juda W Fuel Cell U.S. Patent 3,152,013, 10 6, 1964.

(74). Skyllas-Kazacos M; Rychick M; Robins R All-Vanadium Redox Battery U.S. Patent 4,786,567, 11 22, 1988.

(75). Schaefer HF; Kordesch KV Fuel Cell Half-Cell Containing Vanadium Redox Couple U.S. Patent 3,279,949, 10 18, 1966.

(76). Kummer JT; Oei D-G. A Chemically Regenerative Redox Fuel Cell. J. Appl. Electrochem 1982, 12, 87–100.

(77). Kummer JT; Oei D-G Chemically Regenerable Redox Fuel Cell and Method of Operating the Same U.S. Patent 4,396,687, 8 2, 1983.

(78). Kummer JT; Oei D-G Chemically Regenerable Redox Fuel Cell and Method of Operating the Same U.S. Patent 4,407,902, 10 4, 1983.

(79). Kummer JT; Oei D-G. A Chemically Regenerative Redox Fuel Cell. II. J. Appl. Electrochem 1985, 15, 619–629.

(80). Folkesson B Chemically Regenerative Redox Fuel Cells II. Regeneration Reaction Studies. J. Appl. Electrochem 1990, 20, 907–911.

(81). Larsson R; Folkesson B; Spaziante PM; Veerasai W; Exell RHB A High-Power Carbohydrate Fuel Cell. Renewable Energy 2006, 31, 549–552.

(82). Bergens SH; Gorman CB; Palmore GTR; Whitesides GM A Redox Fuel Cell That Operates with Methane as Fuel at 120 °C. Science 1994, 265, 1418–1420. [PubMed: 17833814]

(83). Gorman CB; Bergens SH; Whitesides GM Platinum-Catalyzed Oxidations of Organic Compounds by Ferric Sulfate: Use of a Redox Fuel Cell to Mediate Complete Oxidation of Ethylene Glycol by Dioxygen at 80 °C. J. Catal 1996, 158, 92–96.

(84). Weibel DB; Boulatov R; Lee A; Ferrigno R; Whitesides GM Modeling the Anodic Half-Cell of a Low-Temperature Coal Fuel Cell. Angew. Chem. Int. Ed 2005, 44, 5682–5686.

(85). Gong J; Liu W; Du X; Liu C; Zhang Z; Sun F; Yang L; Xu D; Guo H; Deng Y Direct Conversion of Wheat Straw into Electricity with a Biomass Flow Fuel Cell Mediated by Two Redox Ion Pairs. ChemSusChem 2017, 10, 506–513. [PubMed: 27976550]

(86). Zu X; Sun L; Gong J; Liu X; Liu Y; Du X; Liu W; Chen L; Yi G; Zhang W et al. Ferric Ion Pair Mediated Biomass Redox Flow Fuel Cell and Related Chemical Reaction Kinetics Study. Chem. Eng. J 2018, 348, 476–484.

(87). Odyakov VF; Zhizhina EG; Maksimovskaya RI; Matveev KI New Methods for the Synthesis of Molybdenum-Vanadium-Phosphoric Heteropoly Acids. Kinet. Catal 1995, 36, 733–738.

(88). Zhizhina EG; Odyakov VF; Matveev KI Thermochemical Study of Reduction and Oxidation Reactions of Molybdovanadophosphoric Heteropolyacids in Aqueous Solutions. Eur. J. Inorg. Chem 1999, 1009–1014.

(89). Odyakov VF; Zhizhina EG; Matveev KI Redox Potentials of Molydovanadophosphoric Heteropoly Acids in Aqueous Solutions. J. Mol. Catal. A: Chem 2000, 158, 453–465.

(90). Zhizhina EG; Odyakov VF; Simonova MV; Matveev KI Kinetics of Oxidation of Reduced Phosphorus-Molybdenum-Vanadium Heteropoly Acid Species with Dioxygen in Aqueous Solutions. Kinet. Catal 2005, 46, 354–363.

(91). Odyakov VF; Zhizhina EG; Maksimovskaya RI Synthesis of Molybdovanadophosphoric Heteropoly Acid Solutions Having Modified Composition. Appl. Catal. A 2008, 342, 126–130.

(92). Zhizhina EG; Odyakov VF Regeneration of the Oxidation Catalysts Based on the Aqueous Solutions of Non-Keggin Mo-V-P Heteropoly Acids by Molecular Oxygen. Int. J. Chem. Kinet 2014, 46, 567–576.

(93). Odyakov VF; Zhizhina EG; Rodikova YA; Gogin LL Mo-V-Phosphoric Heteropoly Acids and Their Salts: Aqueous Solution Preparation – Challenges and Perspectives. Eur. J. Inorg. Chem 2015, 3618–3631.

(94). Weinstock IA; Schreiber RE; Neumann R Dioxygen in Polyoxometalate Mediated Reactions. Chem. Rev 2018, 118, 2680–2717 [PubMed: 29192770]

(95). Creeth A Pt-Free PEM Cathode Technology with Fundamental Durability Benefits: FlowCath[â]. Fuel Cell Bull 2011, 2011, 12–15.

(96). Singh R; Shah AA; Potter A; Clarkson B; Creeth A; Downs C; Walsh FC Performance and Analysis of a Novel Polymer Electrolyte Membrane Fuel Cell using a Solution Based Redox Mediator. J. Power Sources 2012, 201, 159–163.

(97). Creeth AM; Potter AR Redox Fuel Cells with a Catholyte Solution Containing a Polyoxometallate U.S. Patent 9,005,828, 4 14, 2015.

(98). Knuckey K; Kangati B; Downs C; Potter A Regenerative Fuel Cell with Catholyte Comprising a Polyoxometalate and a Vanadium (IV)-Compound U.S. Patent 9,362,584, 6 7, 2016.

(99). Rochester DL; Herbert MA; Creeth AM Polyozometallates for Use at Elevated Temperatures and Pressures U.S. Patent App. 2016/0156059, 6 2, 2016.

(100). Knuckey KJ; Creeth AM; Baynes N. d. B.; Rochester D; Clarkson B Fuel Cells for use at Elevated Temperatures and Pressures U.S. Patent 10,326,156, 6 18, 2019.

(101). Matsui T; Morikawa E; Nakada S; Okanishi T; Muroyama H; Hirao Y; Takahashi T; Eguchi K Polymer Electrolyte Fuel Cells Employing Heteropolyacids as Redox Mediators for Oxygen Reduction Reactions: Pt-Free Cathode Systems. ACS Appl. Mater. Interfaces 2016, 8, 18119–18125. [PubMed: 27348019]

(102). Ward DB; Gunn NLO; Uwigena N; Davies TJ Performance Comparison of Protonic and Sodium Phosphomolybdovanadate Polyoxoanion Catholytes within a Chemically Regenerative Redox Cathode Polymer Electrolyte Fuel Cell. J. Power Sources 2018, 375, 68–76.

(103). Longman R; Clarkson B Fuel Cells U.S. Patent 9,385,391, 7 5, 2016.

(104). Ward DB; Davies TJ Effect of Temperature and Catholyte Concentration on the Performance of a Chemically Regenerative Fuel Cell. Johnson Matthey Technol. Rev 2018, 62, 189–203.

(105). Preger Y; Johnson MR; Biswas S; Anson CW; Root T; Stahl SS Anthraquinone-Mediated Fuel Cell Anode Accessing High Power Density with an Off-Electrode Heterogeneous Catalyst. Manuscript under review, ACS Energy Lett

(106). Zhao X; Liu W; Deng Y; Zhu JY Low-Temperature Microbial and Direct Conversion of Lignocellulosic Biomass to Electricity: Advances and Challenges. Renewable Sustainable Energy Rev 2017, 71, 268–282.

(107). Liu W; Mu W; Deng Y High-Performance Liquid-Catalyst Fuel Cell for Direct Biomass-into-Electricity Conversion. Angew. Chem. Int. Ed 2014, 53, 13558–13562.

(108). Wu W; Liu W; Mu W; Deng Y Polyoxometalate Liquid-Catalyzed Polyol Fuel Cell and the Related Photoelectrochemical Reaction Mechanism Study. J. Power Sources 2016, 318, 86–92.

(109). Zhang Z; Liu C; Liu W; Cui Y; Du X; Xu D; Guo H; Deng Y Innovative Design of Coal Utilization – A Green Pathway for Direct Conversion of Coal to Electricity through Flow Fuel Cell Technology. Appl. Energy 2017, 200, 226–236.

(110). Xu F; Li H; Liu Y; Jing Q Advanced Redox Flow Fuel Cell using Ferric Chloride as Main Catalyst for Complete Conversion from Carbohydrates to Electricity. Sci. Rep 2017, 7, 5142. [PubMed: 28698567]

(111). Zhang Z; Liu C; Liu W; Du X; Cui Y; Gong J; Guo H; Deng Y Direct Conversion of Sewage Sludge to Electricity using Polyoxometalate Catalyzed Flow Fuel Cell. Energy 2017, 141, 1019–1026.

(112). Liu W; Gong Y; Wu W; Yang W; Liu C; Deng Y; Chao Z.-s. Efficient Biomass Fuel Cell Powered by Sugar with Photo- and Thermal-Catalysis by Solar Irradiation. ChemSusChem 2018, 11, 2229–2238. [PubMed: 29920986]

(113). Zhao X; Zhu JY Efficient Conversion of Lignin to Electricity Using a Novel Direct Biomass Fuel Cell Mediated by Polyoxometalates at Low Temperatures. ChemSusChem 2016, 9, 197–207. [PubMed: 26692572]

(114). Lamb AB; Elder LW Jr. The Electromotive Activation of Oxygen. J. Am. Chem. Soc 1931, 53, 137–163.

(115). Posner AM The Kinetics of Autoxidation of Ferrous Ions in Concentrated HCl Solutions. Trans. Faraday Soc 1953, 49, 382–388.

(116). Posner AM The Kinetics of the Charcoal Catalyzed Autoxidation of $Fe^{2+}$ Ion in Dilute HCl Solutions. Trans. Faraday Soc 1953, 49, 389–395.

(117). Chen Y-WD; Santhanam KSV; Bard AJ Solution Redox Couples for Electrochemical Energy Storage I. Iron (III)-Iron(II) Complexes with O-Phenanthroline and Related Ligands. J. Electrochem. Soc 1981, 128, 1460–1467.

(118). Creeth AM Fuel Cells U.S. Patent Appl. 2008/0274385, 11 6, 2008.

(119). Knuckey K; Creeth A Fuel Cells U.S. Patent 8,492,048, 7 23, 2013.

(120). Knuckey K; Creeth A Fuel Cells U.S. Patent 9,136,554, 9 15, 2015.

(121). Knuckey K; Rochester D Redox Fuel Cell with Catholyte Redox Mediator U.S. Patent 8,951,695, 2 10, 2015.

(122). Knuckey K; Rochester D; Creeth AM Redox Fuel Cells U.S. Patent 8,647,781, 2 11, 2014.

(123). Knuckey K; Rochester D Fuel Cells U.S. Patent Appl. 2011/0027671, 2 3, 2011.

(124). Heath CE; Tarmy BL; Holt EL; Levine DG; Moerikofer AW; Shropshire JA; Worsham CH Soluble Carbonaceous Fuel-Air Fuel Cell. Report No. 1, Contract No. DA 36–039 SC-89156, 6 1962.

(125). Shropshire JA; Tarmy BL The Nitric Acid-Oxygen Redox Electrode in Acid Electrolyte. Adv. Chem 1969, 47, 153–165.

(126). Tarmy BL; Holt EL; Levine DG; Moerikofer AW; Shropshire JA; Worsham CH Soluble Carbonaceous Fuel-Air Fuel Cell. Report No. 2, Contract No. DA 36–039 SC-89156, 12 1962.

(127). Tarmy BL; Feng I-M; Holt EL; Levine DG; Lewis K; Moerikofer AW; Okrent EH; Shropshire JA; Wilson JA; Worsham CH Soluble Carbonaceous Fuel-Air Fuel Cell. Report No. 3, Contract No. DA 36–039 AMC-00134, 6 1963.

(128). Han S-B; Song Y-J; Lee Y-W; Ko A-R; Oh J-K; Park K-W High-Performance Hydrogen Fuel Cell using Nitrate Reduction Reaction on a Non-Precious Catalyst. Chem. Commun 2011, 47, 3496–3498.

(129). Han S-B; Kwak D-H; Park HS; Choi I-A; Park J-Y; Kim S-J; Kim M-C; Hong S; Park K-W High-Performance Chemically Regenerative Redox Fuel Cell Using a NO3–/NO Regeneration Reaction. Angew. Chem. Int. Ed 2017, 56, 2893–2897.

(130). Ma K-B; Han S-B; Kwon S-H; Kwak D-H; Park K-W. High-Performance Direct Ethanol Fuel Cell using Nitrate Reduction Reaction. Int. J. Hydrogen Energy 2018, 43, 17265–17270.

(131). Rafiee M; Miles KC; Stahl SS Electrocatalytic Alcohol Oxidation with TEMPO and Bicyclic Nitroxyl Derivatives: Driving Force Trumps Steric Effects. J. Am. Chem. Soc 2015, 137, 14751–14757. [PubMed: 26505317]

(132). Lauber MB; Stahl SS Efficient Aerobic Oxidation of Secondary Alcohols at Ambient Temperature with an ABNO/$NO_x$ Catalyst System. ACS Catal 2013, 3, 2612–2616.

(133). Shibuya M; Osada Y; Sasano Y; Tomizawa M; Iwabuchi Y Highly Efficient, Organocatalytic Aerobic Alcohol Oxidation. J. Am. Chem. Soc 2011, 133, 6497–6500. [PubMed: 21473575]

(134). Gerken JB; Stahl SS High-Potential Electrocatalytic $O_2$ Reduction with Nitroxyl/$NO_x$ Mediators: Implications for Fuel Cells and Aerobic Oxidation Catalysis. ACS Cent. Sci 2015, 1, 234–243. [PubMed: 27162977]

(135). Roberts JAS; Bullock RM Direct Determination of Equilibrium Potentials for Hydrogen Oxidation/Production by Open Circuit Potential Measurements in Acetonitrile. Inorg. Chem 2013, 52, 3823–3835. [PubMed: 23488870]

(136). Pegis ML; Roberts JAS; Wasylenko DJ; Mader EA; Appel AM; Mayer JM Standard Reduction Potentials for Oxygen and Carbon Dioxide Couples in Acetonitrile and *N,N*-Dimethylformamide. Inorg. Chem 2015, 54, 11883–11888. [PubMed: 26640971]

(137). Han S-B; Kwak D-H; Park HS; Park J-Y; Ma K-B; Won J-E; Kim D-H; Kim M-C; Park K-W A Chemically Regenerative Redox Fuel Cell using (2,2,6,6-tetramethylpiperidin-1-yl)oxyl Redox Reaction in Acid Medium. J. Power Sources 2018, 393, 32–36.

(138). Gerken JB; Pang YQ; Lauber MB; Stahl SS Structural Effects on the pH-Dependent Redox Properties of Organic Nitroxyls: Pourbaix Diagrams for TEMPO, ABNO, and Three TEMPO Analogs. J. Org. Chem 2018, 83, 7323–7330. [PubMed: 29182282]

(139). Piera J; Bäckvall J-E Catalytic Oxidation of Organic Substrates by Molecular Oxygen and Hydrogen Peroxide by Multistep Electron Transfer–A Biomimetic Approach. Angew. Chem. Int. Ed 2008, 47, 3506–3523.

(140). Wendlandt AE; Stahl SS Quinone-Catalyzed Selective Oxidation of Organic Molecules. Angew. Chem. Int. Ed 2015, 54, 14638–14658.

(141). Anson CW; Ghosh S; Hammes-Schiffer S; Stahl SS Co(salophen)-Catalyzed Aerobic Oxidation of *p*-Hydroquinone: Mechanism and Implications for Aerobic Oxidation Catalysis. J. Am. Chem. Soc 2016, 138, 4186–4193. [PubMed: 26924338]

(142). Anson CW; Stahl SS Cooperative Electrocatalytic $O_2$ Reduction Involving Co(salophen) with p-Hydroquinone as an Electron–Proton Transfer Mediator. J. Am. Chem. Soc 2017, 139, 18472–18475. [PubMed: 29198114]

(143). Preger Y; Gerken JB; Biswas S; Anson CW; Johnson MR; Root TW; Stahl SS Quinone-Mediated Electrochemical $O_2$ Reduction Accessing High Power Density with an Off-Electrode Co-N/C Catalyst. Joule 2018, 2, 2722–2731.

(144). Hoober-Burkhardt L; Krishnamoorthy S; Yang B; Murali A; Nirmalchandar A; Prakash GKS; Narayanan SR A New Michael-Reaction-Resistant Benzoquinone for Aqueous Organic Redox Flow Batteries. J. Electrochem. Soc 2017, 164, A600–A607.

(145). Mano N; de Poulpiquet A $O_2$ Reduction in Enzymatic Biofuel Cells. Chem. Rev 2018, 118, 2392–2468. [PubMed: 28930449]

(146). Palmore GTR; Kim H-H Electro-Enzymatic Reduction of Dioxygen to Water in the Cathode Compartment of a Biofuel Cell. J. Electroanal. Chem 1999, 464, 110–117.

(147). Liu Y; Wang M; Zhao F; Liu B; Dong S A Low-Cost Biofuel Cell with pH-Dependent Power Output Based on Porous Carbon as Matrix. Chem. Eur. J 2005, 11, 4970–4974. [PubMed: 15968703]

(148). Tsujimura S; Tatsumi H; Ogawa J; Shimizu S; Kano K; Ikeda T Bioelectrocatalytic Reduction of Dioxygen to Water at Neutral pH using Bilirubin Oxidase as an Enzyme and 2,2'-azinobis(3-ethylbenzothiazolin-6-sulfonate) as an Electron Transfer Mediator. J. Electroanal. Chem 2001, 496, 69–75.

(149). Tsujimura S; Fujita M; Tatsumi H; Kano K; Ikeda T Bioelectrocatalysis-Based Dihydrogen/Dioxygen Fuel Cell Operating at Physiological pH. Phys. Chem. Chem. Phys 2001, 3, 1331–1335.

(150). Lim J; Malati P; Bonet F; Dunn B Nanostructured Sol-Gel Electrodes for Biofuel Cells. J. Electrochem. Soc 2007, 154, A140–A145.

(151). Xu W; Danilov D; Gao L; Oudenhoven JFM; Pop V; Notten PHL Kinetic Study of Homogeneously Mediated Electrode Reactions in Glucose-Based BioFuel Cells. ECS Trans 2014, 48, 59–71.

(152). Chen Y; Gai P; Zhang J; Zhu J-J Design of an Enzymatic Biofuel Cell with Large Power Output. J. Mater. Chem. A 2015, 3, 11511–11516.

(153). Ji C; Hou J; Wang K; Ng YH; Chen V Single-Enzyme Biofuel Cells. Angew. Chem. Int. Ed 2017, 56, 9762–9766.

(154). Hammond JL; Gross AJ; Giroud F; Travelet C; Borsali R; Cosnier S Solubilized Enzymatic Fuel Cell (SEFC) for Quasi-Continuous Operation Exploiting Carbohydrate Block Copolymer Glyconanoparticle Mediators. ACS Energy Lett 2019, 4, 142–148.

(155). Gross AJ; Chen X; Giroud F; Travelet C; Borsali R; Cosnier S Redox-Active Glyconanoparticles as Electron Shuttles for Mediated Electron Transfer with Bilirubin Oxidase in Solution. J. Am. Chem. Soc 2017, 139, 16076–16079. [PubMed: 29088534]

(156). Du X; Liu W; Zhang Z; Mulyadi A; Brittain A; Gong J; Deng Y Low-Energy Catalytic Electrolysis for Simultaneous Hydrogen Evolution and Lignin Depolymerization. ChemSusChem 2017, 10, 847–854. [PubMed: 28102938]

(157). Yang L; Liu W; Zhang Z; Du X; Gong J; Dong L; Deng Y Hydrogen Evolution from Native Biomass with $Fe^{3+}/Fe^{2+}$ Redox Couple Catalyzed Electrolysis. Electrochim. Acta 2017, 246, 1163–1173.

(158). Ju H; Giddey S; Badwal SPS Role of Iron Species as Mediator in a PEM Based Carbon-Water Co-Electrolysis for Cost-Effective Hydrogen Production. Int. J. Hydrogen Energy 2018, 43, 9144–9152.

(159). Liu W; Mu W; Liu M; Zhang X; Cai H; Deng Y Solar-Induced Direct Biomass-to-Electricity Hybrid Fuel Cell using Polyoxometalates as Photocatalyst and Charge Carrier. Nat. Commun 2014, 5, 3208. [PubMed: 24504242]

(160). Zhao X; Ding Y; Du B; Zhu JY; Liu D Polyoxometalate-Mediated Lignin Oxidation for Efficient Enzymatic Production of Sugars and Generation of Electricity from Lignoellulosic Biomass. Energy Technol 2017, 5, 1179–1185.

(161). Ding Y; Du B; Zhao X; Zhu JY; Liu D Phosphomolybdic Acid and Ferric Iron as Efficient Electron Mediators for Coupling Biomass Pretreatment to Produce Bioethanol and Electricity Generation from Wheat Straw. Bioresour. Technol 2017, 228, 279–289. [PubMed: 28081526]

(162). Liu W; Cui Y; Du X; Zhang Z; Chao Z; Deng Y High Efficiency Hydrogen Evolution from Native Biomass Electrolysis. Energy Environ. Sci 2016, 9, 467–472.

(163). Sarma BB; Neumann R Polyoxometalate-Mediated Electron Transfer-Oxygen Transfer Oxidation of Cellulose and Hemicellulose to Synthesis Gas. Nat. Commun 2014, 5, 4621. [PubMed: 25082188]

(164). Yang L; Liu W; Zhang Z; Du X; Dong L; Deng Y Low Energy Electro-Reduction of Carbon Dioxide Coupling with Anodic Glycerol Oxidation Catalyzed by Chemical Regenerative Phosphomolybdic Acids. J. Power Sources 2019, 420, 99–107.

(165). Chambers GM; Wiedner ES; Bullock RM $H_2$ Oxidation Electrocatalysis Enabled by Metal-to-Metal Hydrogen Atom Transfer: A Homolytic Approach to a Heterolytic Reaction. Angew. Chem. Int. Ed 2018, 57, 13523–13527.

(166). Hertl W; Weetall HH A Photo-Chemical Electrical Fuel Cell Part I. Alcohol Fuels. Bioelectrochem. Bioenerg 1985, 14, 357–366.

(167). Hertl W; Weetall HH A Photo-Chemical Electrical Fuel Cell Part II. Carbohydrate Fuels. Bioelectrochem. Bioenerg 1985, 14, 367–373.

(168). Weetall HH; Forsyth BD; Hertl W A Direct Fuel Cell for the Production of Electricity from Lignin. Biotechnol. Bioeng 1985, 27, 927–979.

(169). Larsson R; Folkesson B Method for Producing Electric Energy in a Biofuel-Powered Fuel Cell U.S. Patent 5,660,940, 8 26, 1997.

(170). Larsson R; Folkesson B A Catalytic Oxidation of Sugar by Vanadium(IV). J. Mol. Catal. A: Chem 2005, 229, 183–190.

(171). Wheeler DR; Nichols J; Hansen D; Andrus M; Choi S; Watt GD Viologen Catalysts for a Direct Carbohydrate Fuel Cell. J. Electrochem. Soc 2009, 156, B1201–B1207.

(172). Scott D; Liaw BY Harnessing Electric Power from Monosaccharides – a Carbohydrate-Air Alkaline Fuel Cell Mediated by Redox Dyes. Energy Environ. Sci 2009, 2, 965–969.

(173). Scott DM; Tsang TH; Chetty L; Aloi S; Liaw BY Mechanistic Understanding of Monosaccharide-Air Flow Battery Electrochemistry. J. Power Sources 2011, 196, 10556–10562.

(174). Liu X; Hao M; Feng M; Zhang L; Zhao Y; Du X; Wang G A One-Compartment Direct Glucose Alkaline Fuel Cell with Methyl Viologen as Electron Mediator. Appl. Energy 2013, 106, 176–183.

(175). Yang Y-L; Liu X-H; Hao M-Q; Zhang P-P Performance of a Low-Cost Direct Glucose Fuel Cell with an Anion-Exchange Membrane. Int. J. Hydrogen Energy 2015, 40, 10979–10984.

(176). Hao M; Liu X; Feng M; Zhang P; Wang G Generating Power from Cellulose in an Alkaline Fuel Cell Enhanced by Methyl Viologen as an Electron-Transfer Catalyst. J. Power Sources 2014, 251, 222–228.

(177). Watt GD; Hansen D; Dodson D; Andrus M; Wheeler D Electrical Energy from Carbohydrate Oxidation during Viologen-Catalyzed $O_2$-Oxidation: Mechanistic Insights. Renewable Energy 2011, 36, 1523–1528.

(178). Read A; Hansen D; Aloi S; Pitt WG; Wheeler DR; Watt GD Monoalkyl Viologens are Effective Carbohydrate $O_2$-Oxidation Catalysts for Electrical Energy Generation by Fuel Cells. Renewable Energy 2012, 46, 218–223.

(179). Hansen DC; Pan Y; Stockton J; Pitt WG; Wheeler DR Cyclic Voltammetry Investigation of Organic Species Considered for Use as Catalysts in Direct-Carbohydrate Fuel Cells. J. Electrochem. Soc 2012, 159, H834–H841.

(180). Watt GD A New Future for Carbohydrate Fuel Cells. Renewable Energy 2014, 72, 99–104.

(181). Rigby CR; Han H; Bhowmik PK; Bahari M; Chang A; Harb JN; Lewis RS; Watt GD Soluble Viologen Polymers as Carbohydrate Oxidation Catalysts for Alkaline Carbohydrate Fuel Cells. J. Electroanal. Chem 2018, 823, 416–421.

(182). Barton SC; Gallaway J; Atanassov P Enzymatic Biofuel Cells for Implantable and Microscale Devices. Chem. Rev 2004, 104, 4867–4886. [PubMed: 15669171]

(183). Ruff A Redox Polymers in Bioelectrochemistry: Common Playgrounds and Novel Concepts. Curr. Opin. Electrochem 2017, 5, 66–73.

(184). Plotkin EV; Higgins IJ; Hill HAO Methanol Dehydrogenase Bioelectrochemical Cell and Alcohol Detector. Biotechnol. Lett 1981, 3, 187–192.

(185). Yue PL; Lowther K Enzymatic Oxidation of C1 Compounds in a Biochemical Fuel Cell. Chem. Eng. J 1986, 33, B69–B77.

(186). Davis G; Hill HAO; Aston WJ; Higgins IJ; Turner APF Bioelectrochemical Fuel Cell and Sensor Based on a Quinoprotein, Alcohol Dehydrogenase. Enzyme Microb. Technol 1983, 5, 383–388.

(187). Zhang X-C; Ranta A; Halme A Direct Methanol Biocatalytic Fuel Cell–Considerations of Restraints on Electron Transfer. Biosens. Bioelectron 2006, 21, 2052–2057. [PubMed: 16554148]

(188). Kavanagh P; Boland S; Jenkins P; Leech D Performance of a Glucose/$O_2$ Enzymatic Biofuel Cell Containing a Mediated *Melanocarpus albomyces* Laccase Cathode in a Physiological Buffer. Fuel Cells 2009, 9, 79–84.

(189). Laane C; Pronk W; Franssen M; Veeger C Use of a Bioelectrochemical Cell for the Synthesis of (Bio)chemicals. Enzyme Microb. Technol 1984, 6, 165–168.

(190). Palmore GTR; Bertschy H; Bergens SH; Whitesides GM A Methanol/Dioxygen Biofuel Cell that Uses $NAD^+$-Dependent Dehydrogases as Catalysts: Application of an Electro-Enzymatic Method to Regenerate Nicotinamide Adenine Dinucleotide at Low Overpotentials. J. Electroanal. Chem 1998, 443, 155–161.

(191). Moiroux J; Elving PJ Effects of Absorption, Electrode Material, and Operational Variables on the Oxidation of Dihydronicotinamide Adenine Dincucleotide at Carbon Electrodes. Anal. Chem 1978, 50, 1056–1062.

(192). Lojou E Hydrogenases as Catalysts for Fuel Cells: Strategies for Efficient Immobilization at Electrode Interfaces. Electrochim. Acta 2011, 56, 10385–10397.

(193). Milton RD; Cai R; Abdellaoui S; Leech D; De Lacey AL; Pita M; Minteer SD Bioelectrochemical Haber-Bosch Process: An Ammonia-Producing $H_2/N_2$ Fuel Cell. Angew. Chem. Int. Ed 2017, 56, 2680–2683.

(194). Cass AEG; Davis G; Francis GD; Hill HAO; Aston WJ; Higgins IJ; Plotkin EV; Scott LDL; Turner APF Ferrocene-Mediated Enzyme Electrode for Amperometric Determination of Glucose. Anal. Chem 1984, 56, 667–671. [PubMed: 6721151]

(195). Zhao X; Jia H; Kim J; Wang P Kinetic Limitations of a Bioelectrochemical Electrode Using Carbon Nanotube-Attached Glucose Oxidase for Biofuel Cells. Biotech. Bioengin 2009, 104, 1068–1074.

(196). Zhu Z; Zhang Y-HP Use of Nonimmobilized Enzymes and Mediators Achieved High Power Densities in Closed Biobatteries. Energy Sci. Eng 2015, 3, 490–497.

(197). Hickey DP; McCammant MS; Giroud F; Sigman MS; Minteer SD Hybrid Enzymatic and Organic Electrocatalytic Cascade for the Complete Oxidation of Glycerol. J. Am. Chem. Soc 2014, 136, 15917–15920. [PubMed: 25350383]

(198). Abdellaoui S; Hickey DP; Stephens AR; Minteer SD Recombinant Oxalate Decarboxylase: Enhancement of a Hybrid Catalytic Cascade for the Complete Electro-Oxidation of Glycerol. Chem. Commun 2015, 51, 14330–14333.

(199). Abdellaoui S; Chavez MS; Matanovic I; Stephens AR; Atanassov P; Minteer SD Hybrid Molecular/Enzymatic Catalytic Cascade for Complete Electro-Oxidation of Glycerol using a Promiscuous NAD-Dependent Formate Dehydrogenase from *Candida boidinii*. Chem. Commun 2017, 53, 5368–5371.

(200). Hickey DP; Schiedler DA; Matanovic I; Doan PV; Atanassov P; Minteer SD; Sigman MS Predicting Electrocatalytic Properties: Modeling Structure-Activity Relationships of Nitroxyl Radicals. J. Am. Chem. Soc 2015, 137, 16179–16186. [PubMed: 26635089]

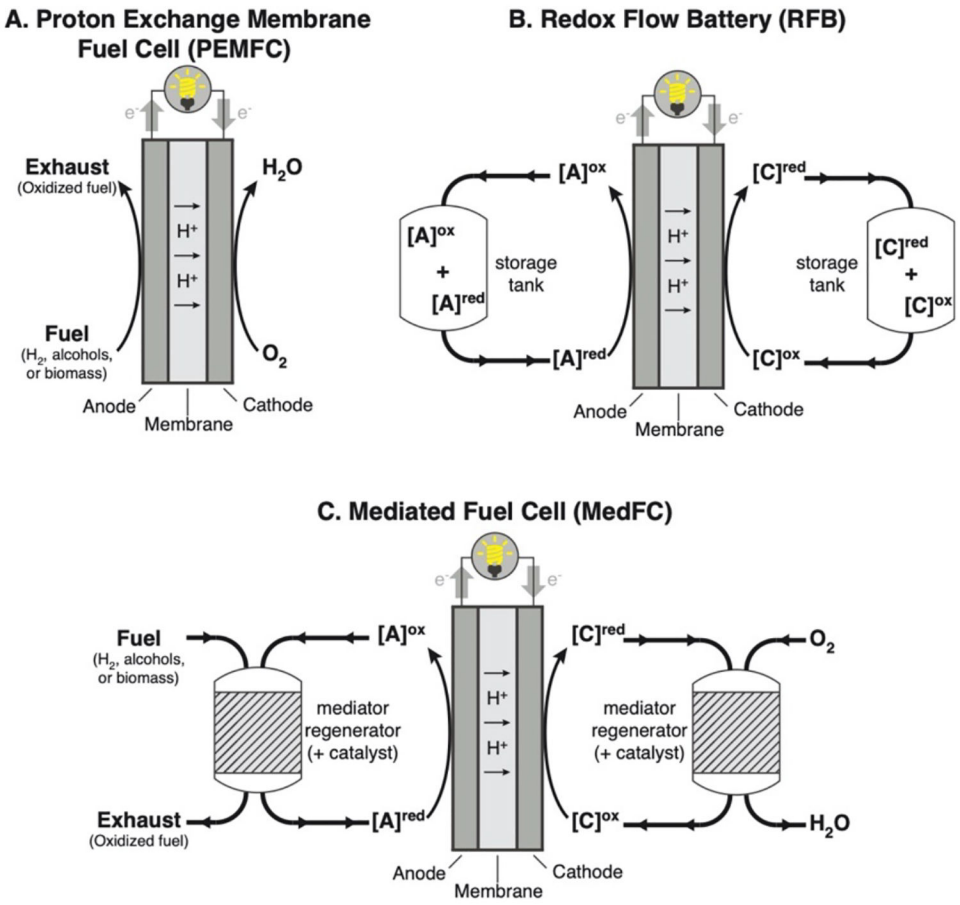


**Figure 1.**

General schematic of an A) PEM fuel cell, B) flow battery in discharge mode with [A] representing the anodic (e.g. low potential) redox couple and [C] representing the cathodic (e.g. high potential) redox couple, and C) mediated fuel cell with mediators for both anode and cathode.

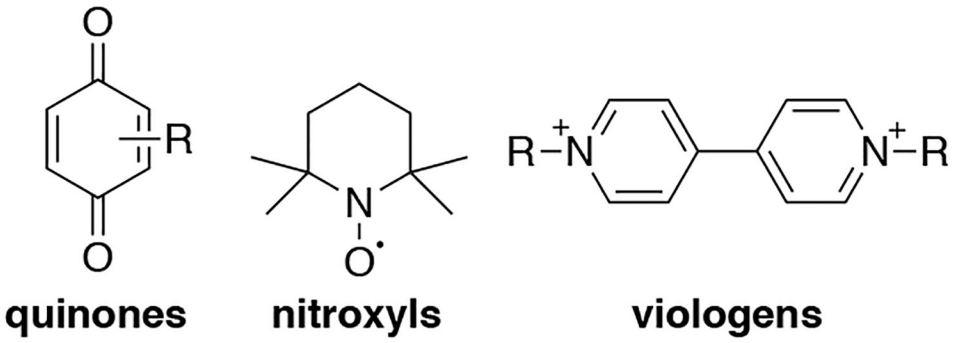


**Figure 2.**
Structures of representative organic mediators examined for redox flow battery applications.

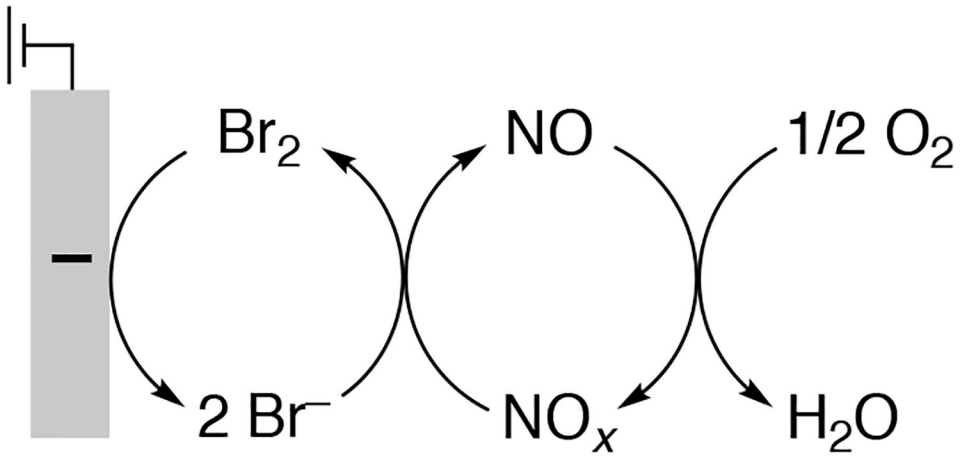


**Figure 3.**

Redox sequence for bromine-mediated cathode with a $NO_x$-based catalyst ($||Br_2|NO_x|O_2$). For relevant studies, see references 40, 70–73.

**A) Mechanism proposed by Posner and Merton-Binham**

$$HNO_2 + HBr \rightleftharpoons \text{"X"}$$

$$\text{"X"} + NOBr \xrightarrow{\textit{rate-limiting step}} 2\,NO + Br_2 + (x\,H_2O)$$

$$2\,NO + O_2 \longrightarrow 2\,NO_2$$

$$NO_2 + HBr \longrightarrow NOBr + {}^{\bullet}OH$$

$${}^{\bullet}OH + HBr \longrightarrow H_2O + Br^{\bullet}$$

$$NO_2 + HBr \longrightarrow HNO_2 + Br^{\bullet}$$

**B) Mechanism proposed by Reneke**

$$2\,NO_{(g)} + O_{2(g)} \longrightarrow 2\,NO_{2(g)}$$

$$2\,NO_{2(g)} \rightleftharpoons N_2O_{4(g)}$$

$$NO_{2(g)} \longrightarrow NO_{2(aq)}$$

$$NO_{2(aq)} + 2\,HBr \longrightarrow Br_2 + NO_{(aq)} + H_2O$$

$$NO_{(aq)} \longrightarrow NO_{(g)}$$

**Figure 4.**
Proposed mechanisms for HBr oxidation to $Br_2$ by $NO_x$ catalysts.

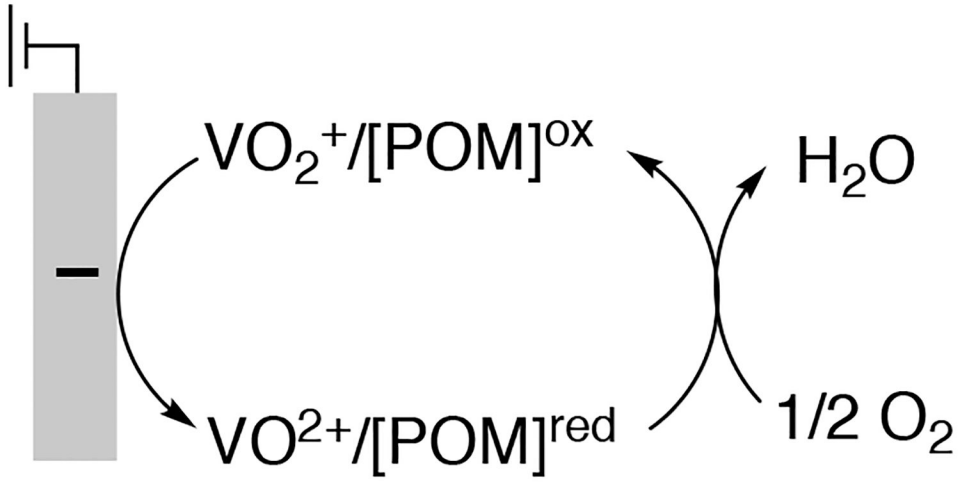


**Figure 5.**

Redox sequence proposed for V-mediated cathode with POM catalyst for $O_2$ reduction (|| $VO^{2+}$|POM|$O_2$). For relevant systems using this mediated cathode, see references 76–78.

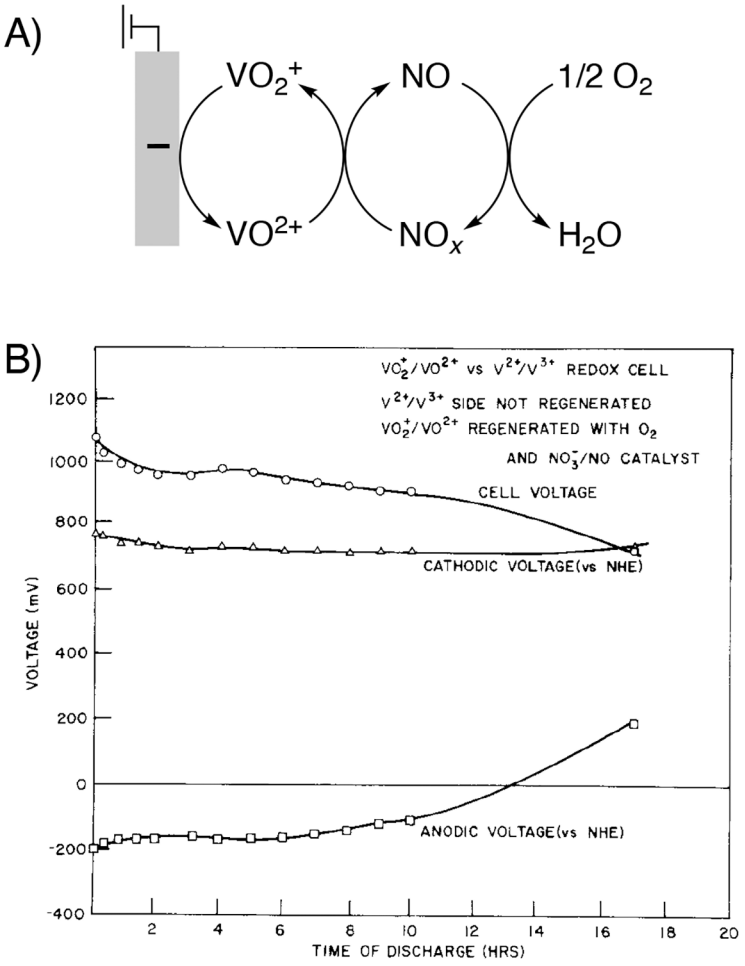


**Figure 6.**

(A) Redox sequence for vanadium-mediated cathode with $NO_x$ catalyst for $O_2$ reduction (|| $VO^{2+}$|$NO_x$|$O_2$). For systems featuring this mediated cathode, see references 79–86. (B) Sustained performance curve of a mediated cathode utilizing a $VO^{2+}/VO_2^+$ redox mediator, reoxidized with $NO_x$-based catalysts. The anode solution contained a $V^{2+}/V^{3+}$ redox mediator which was not regenerated during the experiment ($V^{3+}$||$VO^{2+}$|$NO_x$|$O_2$). Cell was discharged through a 5-ohm external load with a flow rate of 230 mL/min. Adapted from ref. 79. Copyright 1985, Chapman and Hall Ltd.

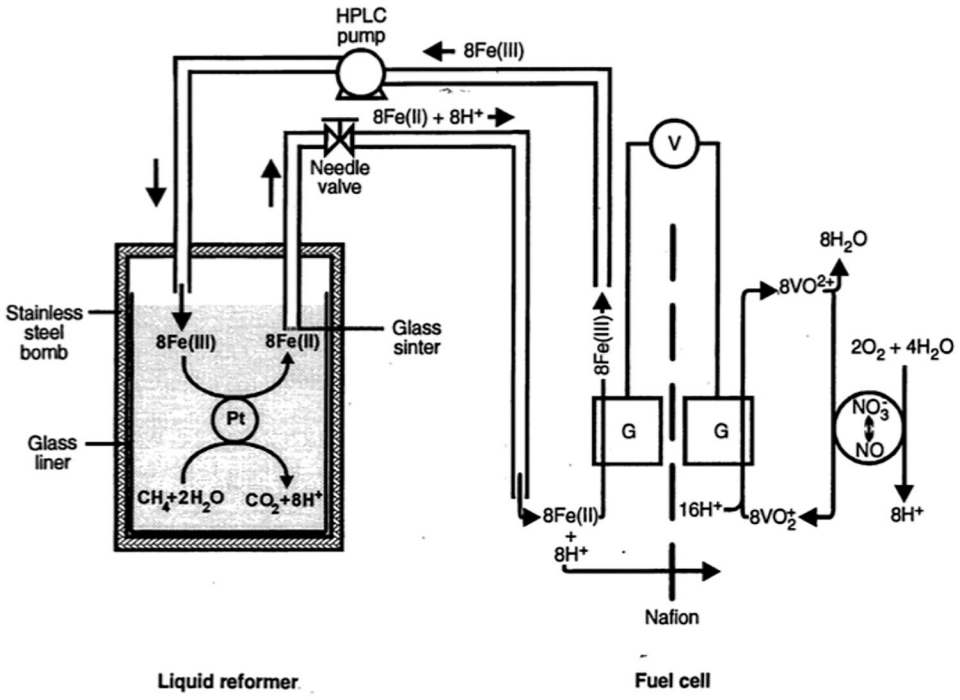


**Figure 7.**

Schematic of doubly mediated fuel cell ($CH_4|Pt|Fe^{2+}||VO^{2+}|NO_x|O_2$) using methane as fuel developed by Whitesides and coworkers. Adapted from ref. 82. Copyright 1994, American Association for the Advancement of Science.

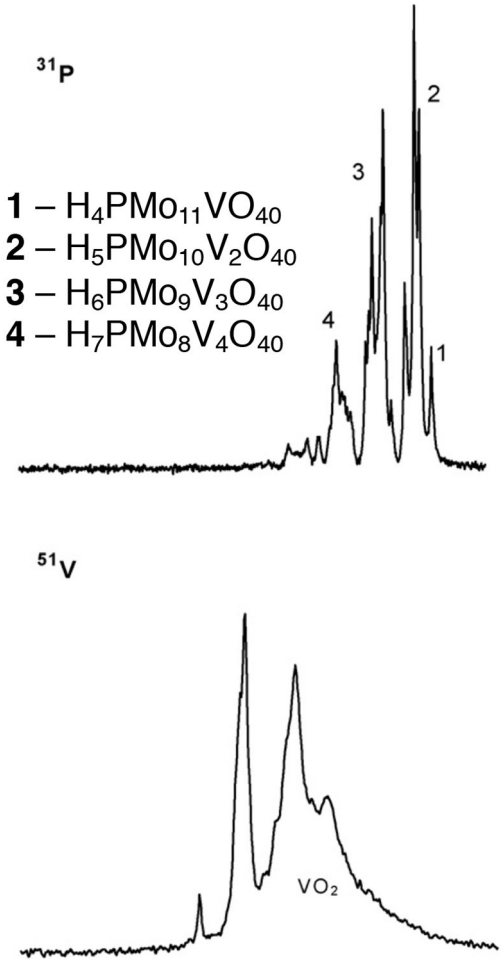


**Figure 8.**

$^{31}P$ and $^{51}V$ NMR spectra of 0.25 M solution of $H_{12}P_3Mo_{18}V_7O_{85}$. Numerals 1, 2, 3, and 4 correspond to collection of lines of HPA-*x* Keggin POMs $H_{3+x}PMo_{12-x}V_xO40$, where $x = 1–4$, see reference 87. Adapted from ref. 91. Copyright 2008, Elsevier B.V.

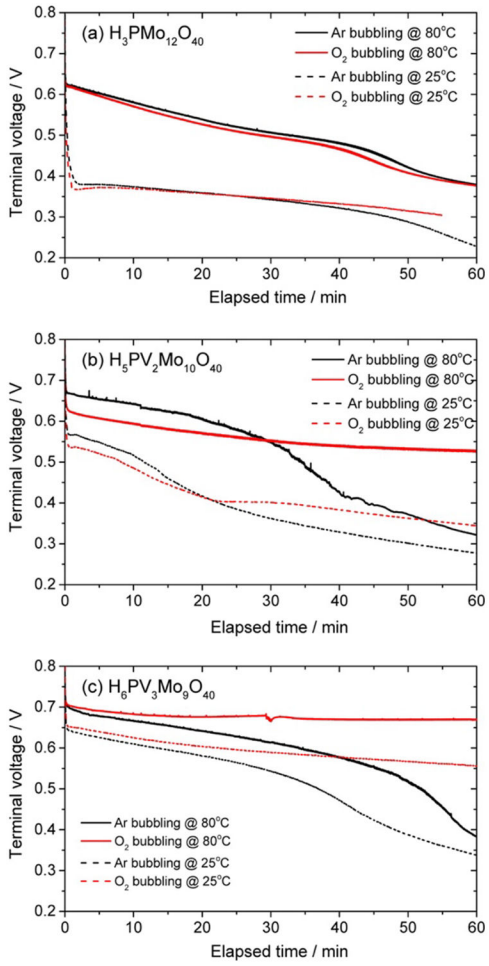


**Figure 9.**

Voltage time-courses of POM-mediated cathodes ($H_2$|Pt||POM|$O_2$) at a current density of 5.36 mA/cm$^2$ at either 25 °C or 80 °C under $O_2$ or Ar for 0.01 M solutions of (a) $H_3PMo_{12}O_{40}$, (b) $H_5PV_2Mo_{10}O_{40}$, and (c) $H_6PV_3Mo_9O_{40}$. Adapted from ref. 101. Copyright 2016, American Chemical Society.

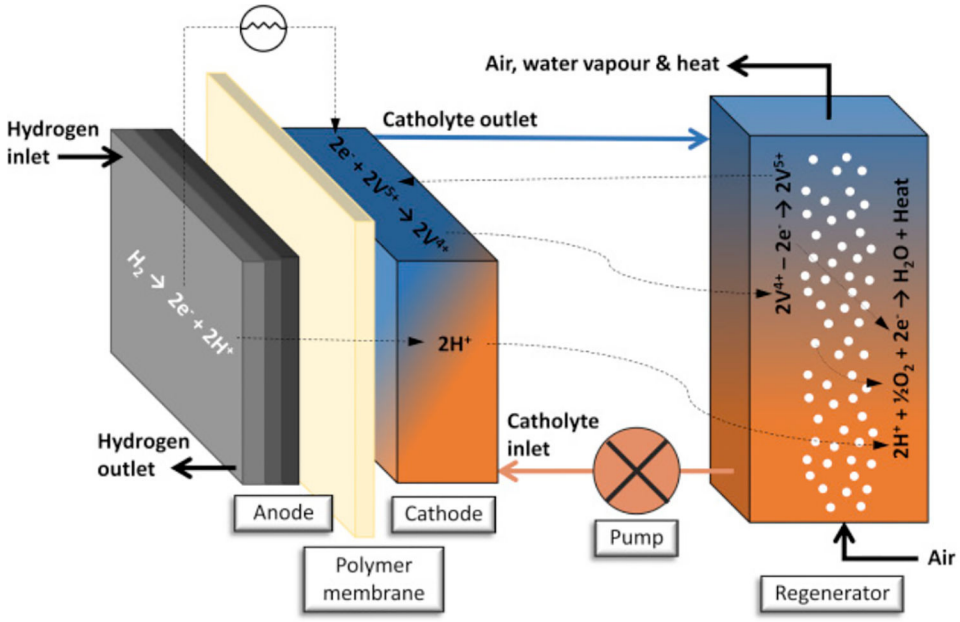


**Figure 10.**

Schematic of POM-mediated cathode fuel cell ($H_2$|Pt||POM|$O_2$) reported by Davies and coworkers. Adapted from ref. 63. Copyright 2017, Elsevier B.V.

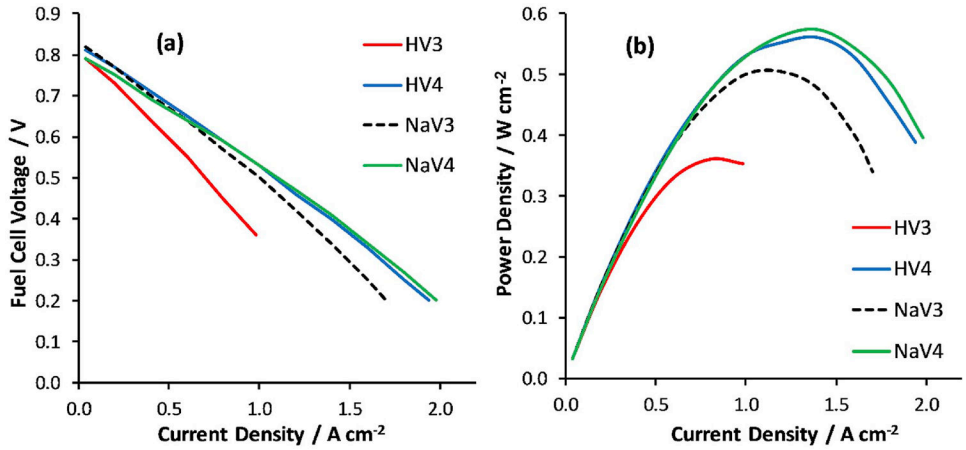


**Figure 11.**

Projected (a) *i*-V and (b) power density curves generated from simulated steady state performance for HV3, HV4, NaV3, and NaV4 POM solutions ($H_2$|Pt||POM|$O_2$). Adapted from ref. 102. Copyright 2017, Elsevier B.V.

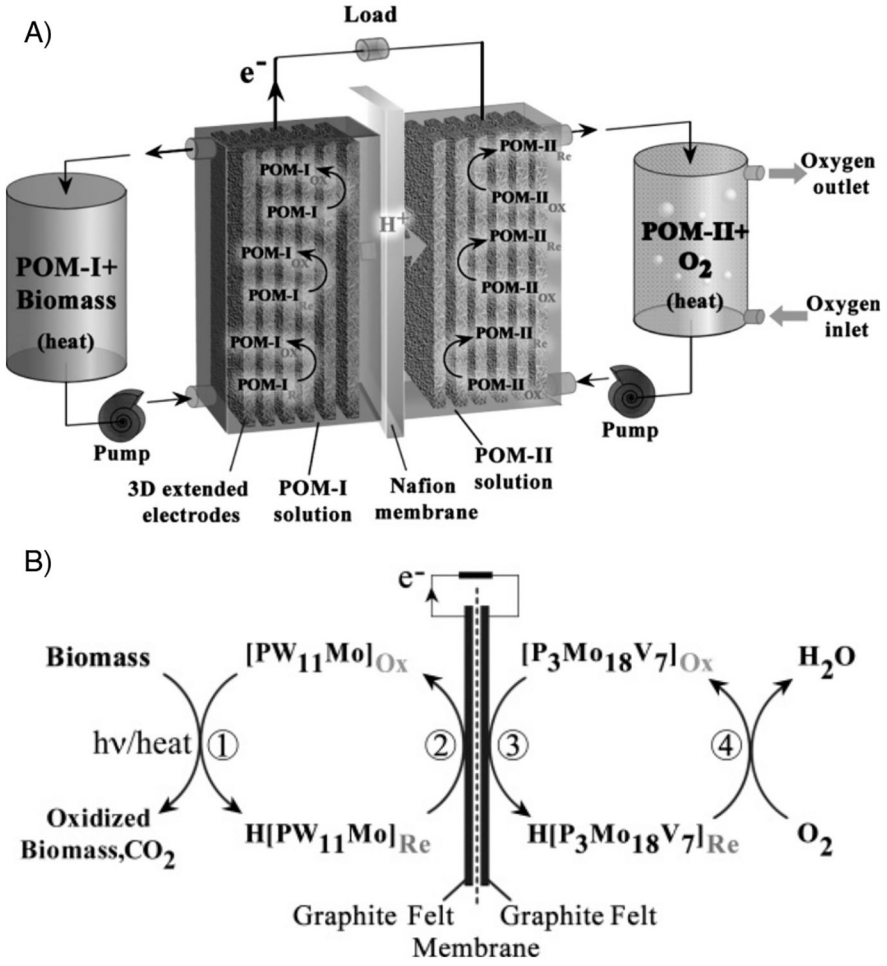


**Figure 12.**

A) Schematic for the doubly mediated fuel cell using POM-I as mediator for biomass oxidation and POM-II as mediator for $O_2$ reduction (biomass|POM-I||POM-II|$O_2$). B) Further details showing electrode reactions and regeneration reactions of POM-I and POM-II. Adapted from ref. 107. Copyright 2014 Wiley-VCH Verlag GmbH & Co.

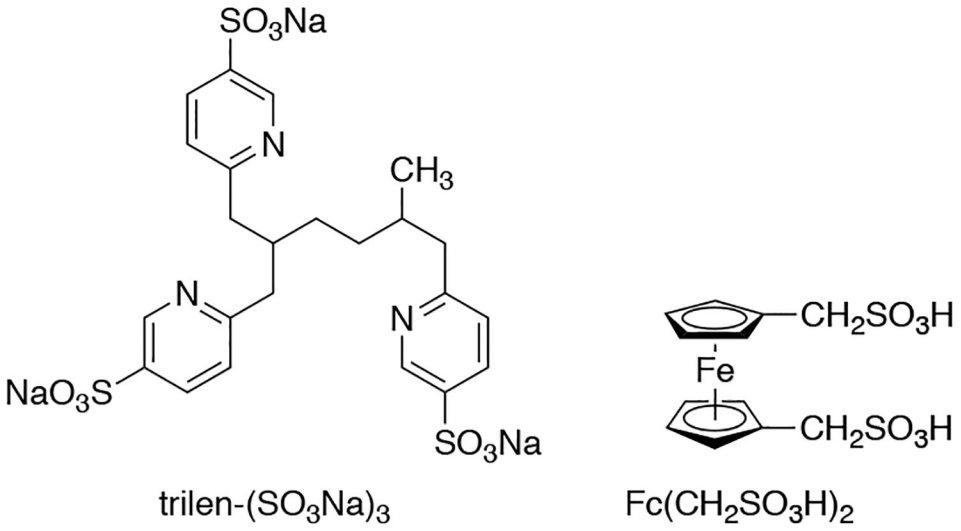


**Figure 13.**
Ligand used with $Fe^{2+}$ (trilen-$SO_3Na)_3$ and to oxidize $Fc(CH_2SO_3H)_2$ mediator.

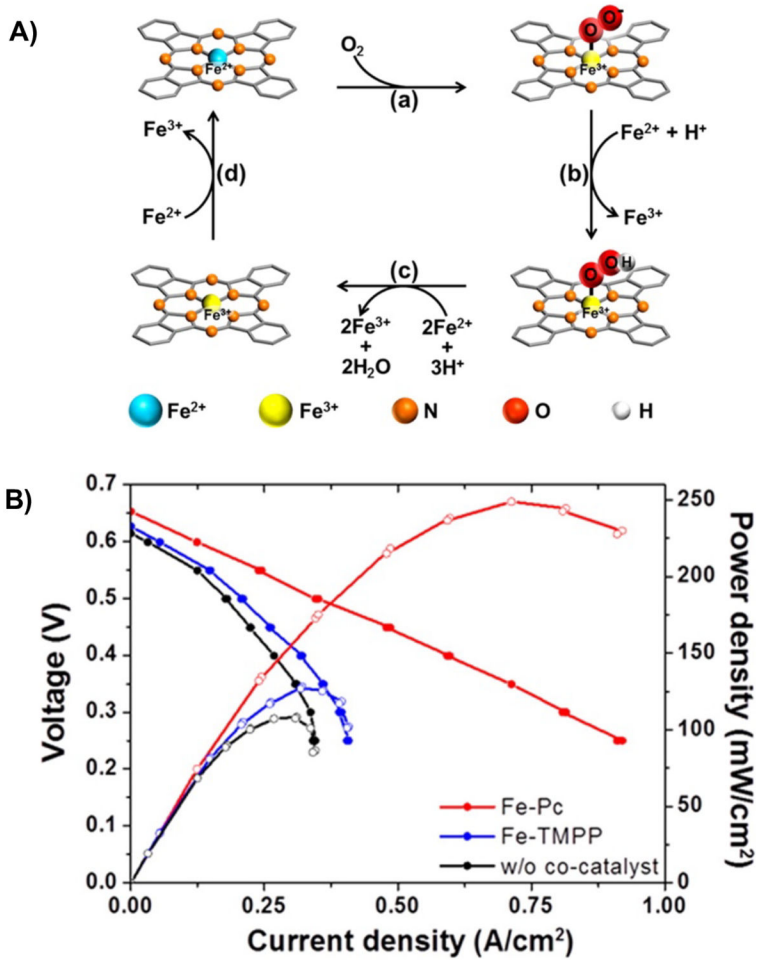


**Figure 14.**

(A) Proposed mechanism for $Fe^{2+}$ oxidation by $O_2$ catalyzed by Fe(pc). (B) Polarization curves measured using 0.5 M $FeSO_4$ + 1.0 M $H_2SO_4$ solutions after oxidation at 80 °C with $O_2$ for 5 h in the presence of no catalyst (black traces), [$Fe^{III}$((4-OMephenyl)porphyrin)]Cl (Fe-TMPP) as catalyst (blue traces), or Fe(Pc) as catalyst (red traces). $H_2$ was used as the fuel at a Pt/C electrode ($H_2$|Pt/C||$Fe^{2+}$|Fe(pc)|$O_2$). Adapted from ref. 61. Copyright 2016 American Chemical Society.

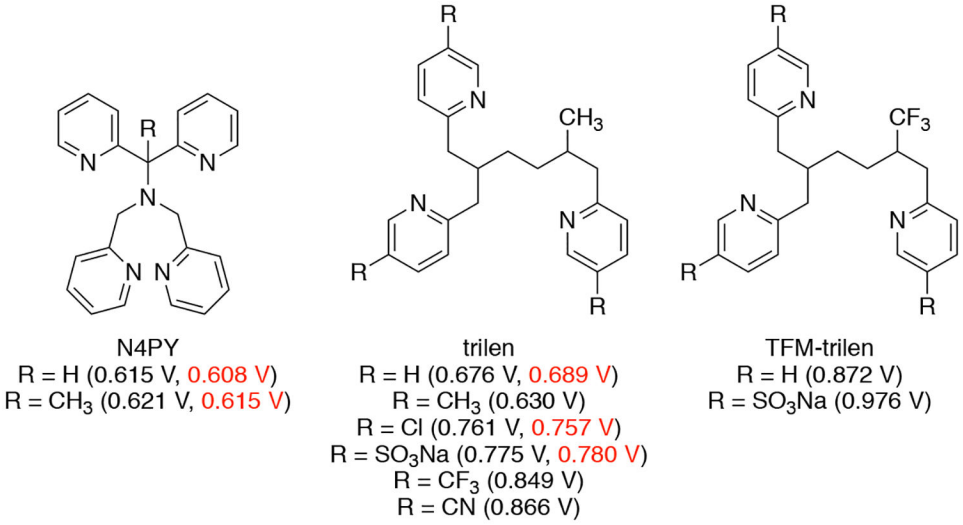


**Figure 15.**

Ligands studied computationally by Metz and coworkers to determine the redox potentials of the Fe complexes.[62] Experimentally determined redox potentials are shown in red, while the calculated redox potentials are shown in black.

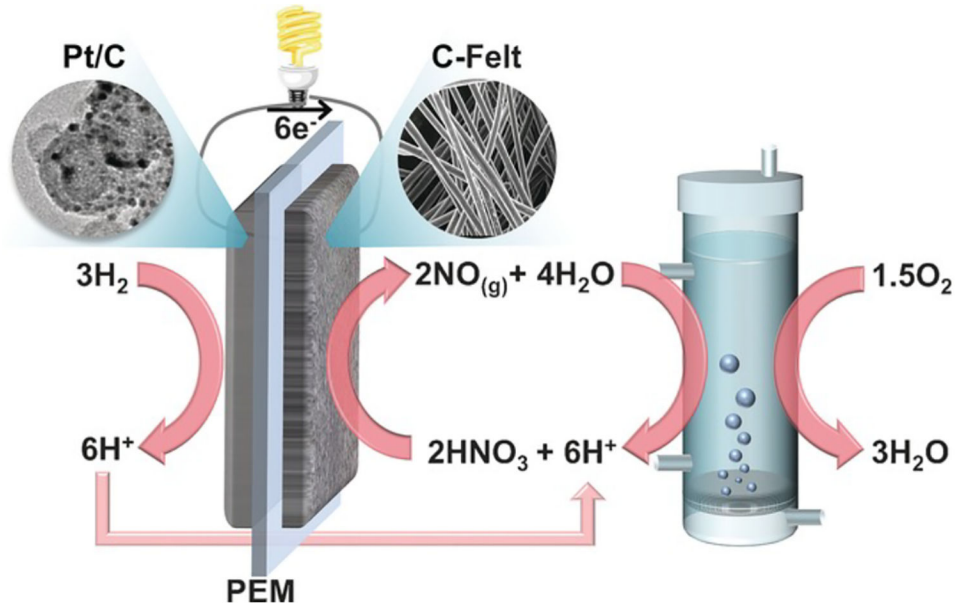


**Figure 16.**

Schematic of a mediated fuel cell using the $NO_3^-$/NO redox mediator to mediate $O_2$ reduction. Adapted from ref. 129. Copyright 2017 Wiley-VCH Verlag GmbH & Co. KGaA.

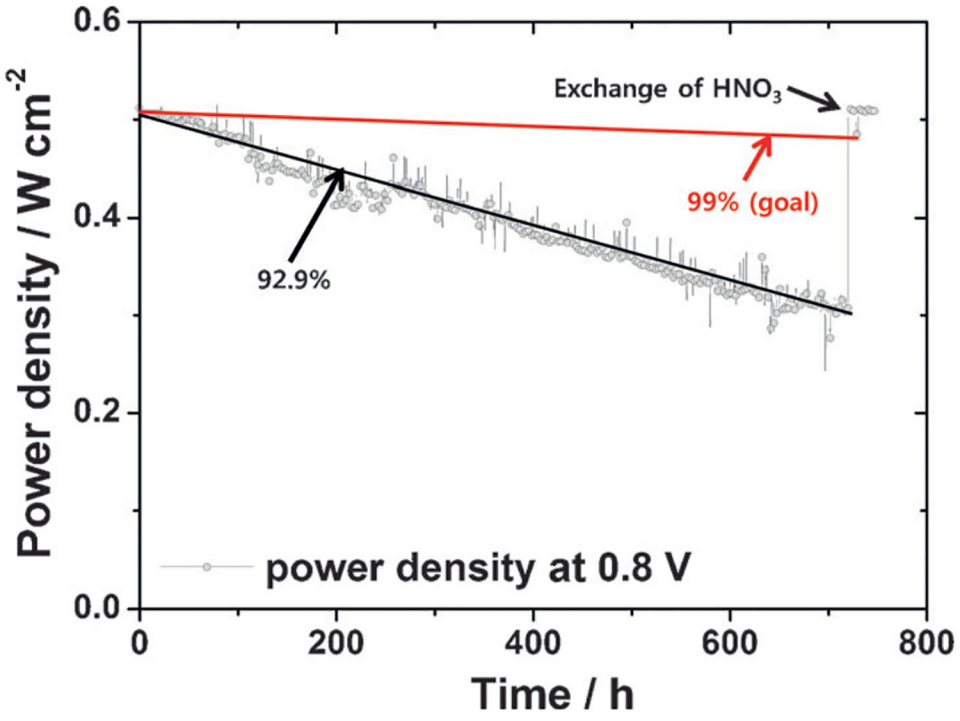


**Figure 17.**

Long term stability test of $HNO_3$-mediated cathode with nitrogen-doped carbon-felt electrode. Cell run at 80 °C with $H_2$ anode. Adapted from ref. 129. Copyright 2017 Wiley-VCH Verlag GmbH & Co. KGaA.

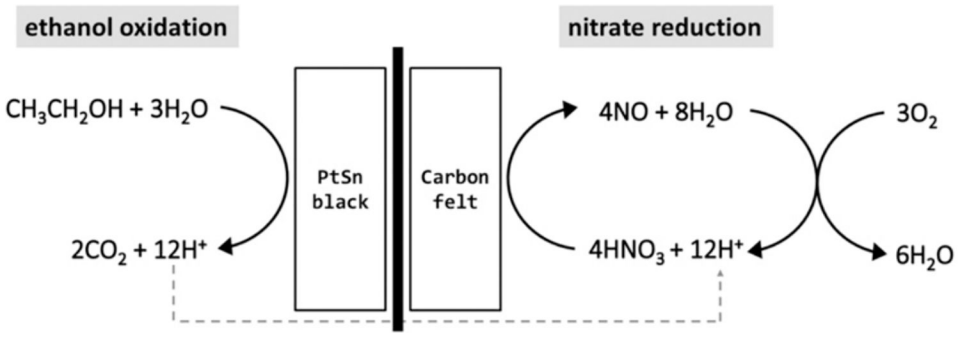


**Figure 18.**

Schematic of a direct ethanol fuel cell using an $HNO_3$ mediated cathode. Adapted from ref. 130. Copyright 2018 Hydrogen Energy Publications LLC.

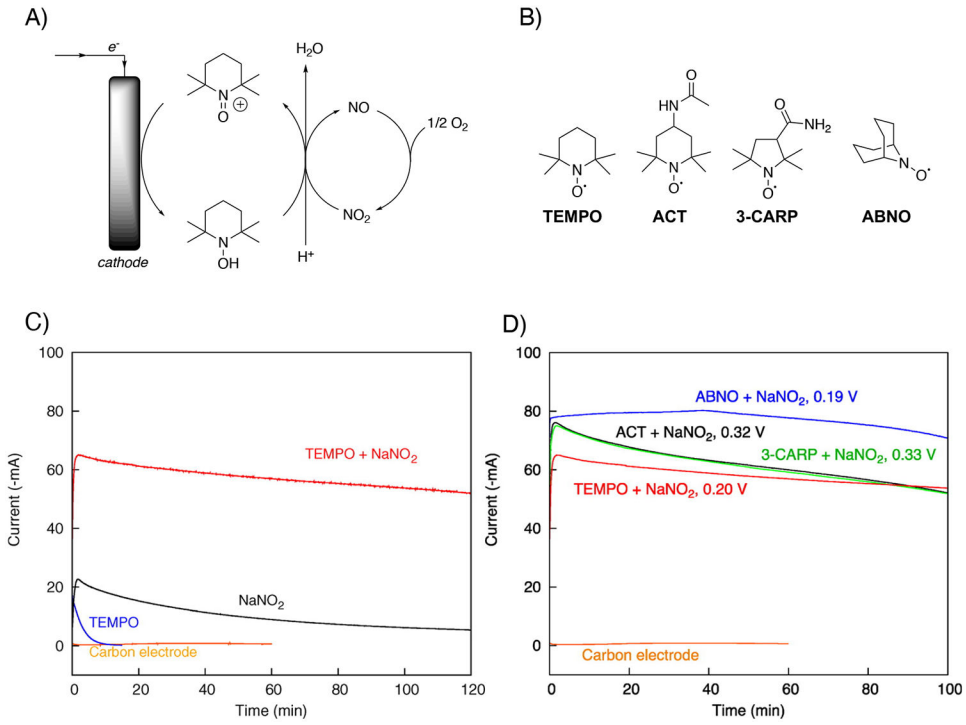


**Figure 19.**

A) Simplified scheme for TEMPO-mediated $O_2$ reduction using a $NO_x$-based catalyst B) Different nitroxyls examined in the study. C) Controlled-potential electrolysis traces in the presence and absence of mediator and/or catalyst (TEMPO and $NO_x$, respectively). D) Controlled-potential electrolysis traces in the presence of $NO_x$ and various nitroxyl mediators (red = TEMPO; black = ACT; blue = ABNO; green = 3-CARP). Adapted from ref. 134. Copyright 2015 American Chemical Society.

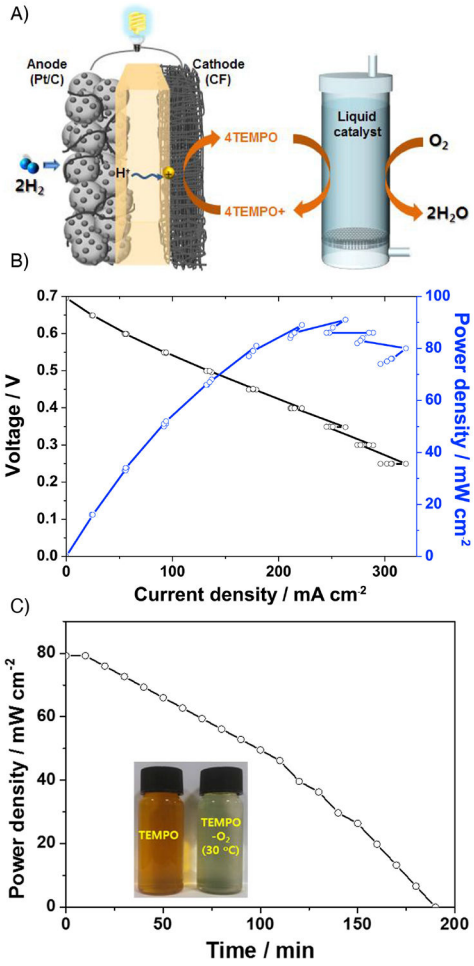


**Figure 20.**

A) Schematic of mediated cathode fuel cell using TEMPO mediator. B) Polarization curve of the mediated fuel cell using TEMPO as a cathodic mediator and a conventional $H_2$ anode. Conditions: 0.3 M TEMPO and 1 M $H_2SO_4$ in the cathode, fuel cell temperature 30 °C. C) Time-on-stream test using a TEMPO-mediated cathode. Inset shows original color of TEMPO solution (left) and solution color after time-on-stream experiment (right). Adapted from ref. 137. Copyright 2018, Elsevier B.V.

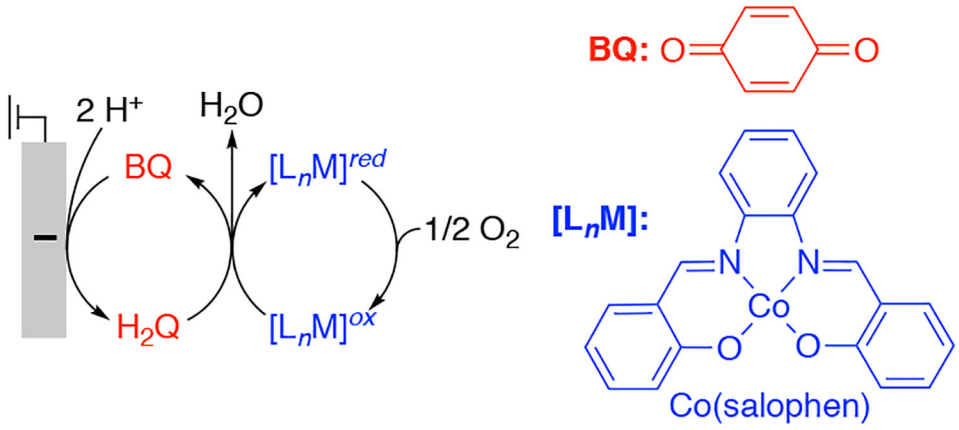


**Figure 21.**
Simplified scheme for quinone-mediated $O_2$ reduction utilizing Co(salophen) as a soluble catalyst. Adapted from ref. 142. Copyright 2017, American Chemical Society.

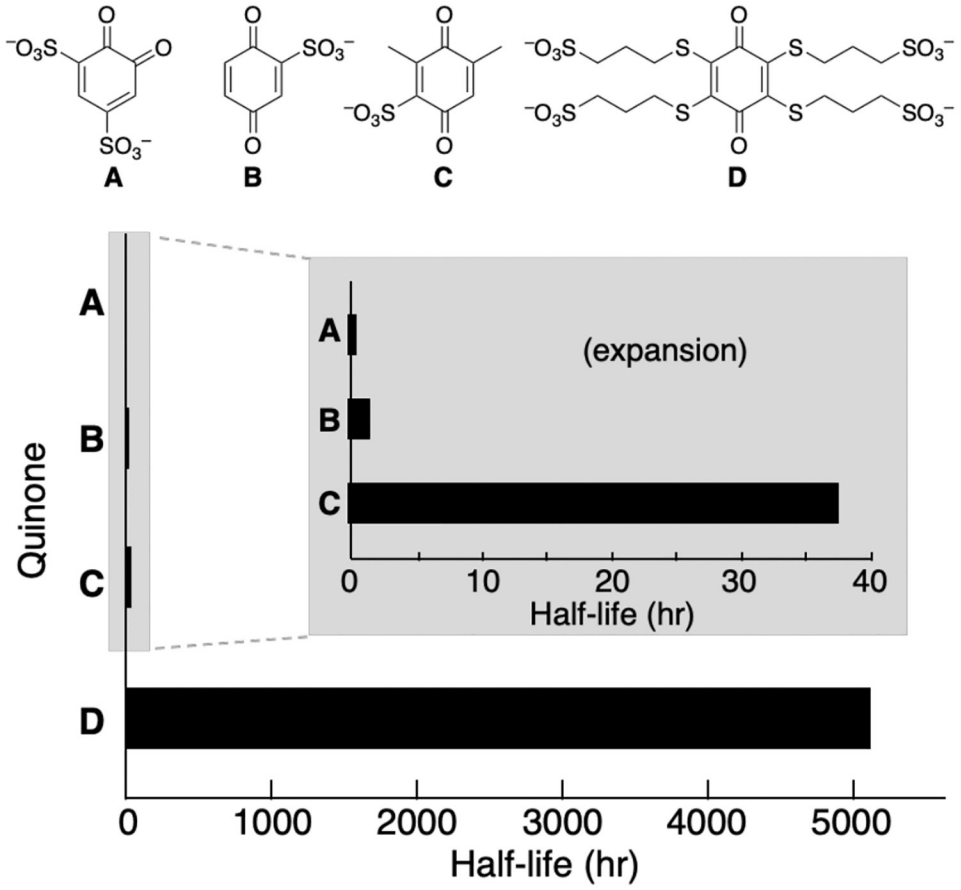


**Figure 22.**

Stability of quinone structures previously tested for flow battery applications, A-C, and new tetrasubstituted quinone D. The stability was assessed by 1H NMR, and the half-lives were calculated by assessing the first-order rate constant for quinone decomposition. Conditions: 0.1 M quinone concentration in 0.5 M $D_2SO_4$ + 0.05 M $CH_3SO_3H$ in $D_2O$ at 60 °C. Adapted from ref. 143. Copyright 2018, Elsevier B.V.

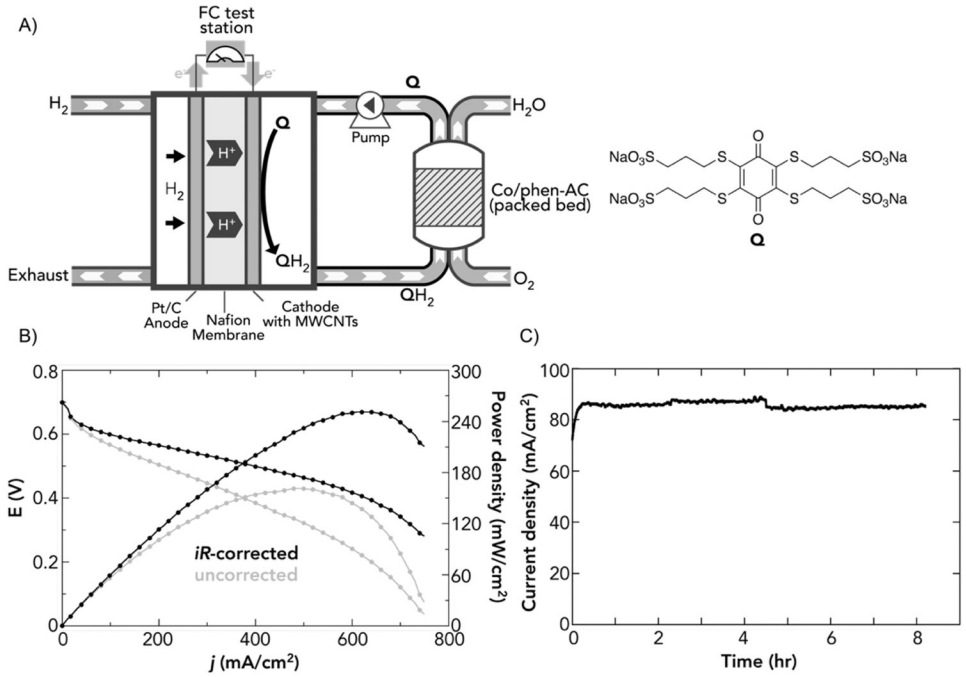


**Figure 23.**

A) Schematic of mediated cathode utilizing quinone mediator and Co-Phen/AC catalyst, $H_2$|Pt/C||quinone|Co-phen/AC|$O_2$. B) Polarization curves and C) time-on-stream performance for quinone-mediated fuel cell cathode with a Co-N/C catalyst. Conditions: 0.1 M quinone mediator, 1 M $H_2SO_4$, 60 °C, $H_2$ fuel with Pt/C anode, MWCNT-coated carbon paper cathode, Nafion 117 membrane, 5 g Co-N/C catalyst in packed bed reactor. Time-on-stream experiment conducted at a constant potential of 0.5 V. Adapted from ref. 143. Copyright 2018, Elsevier B.V.

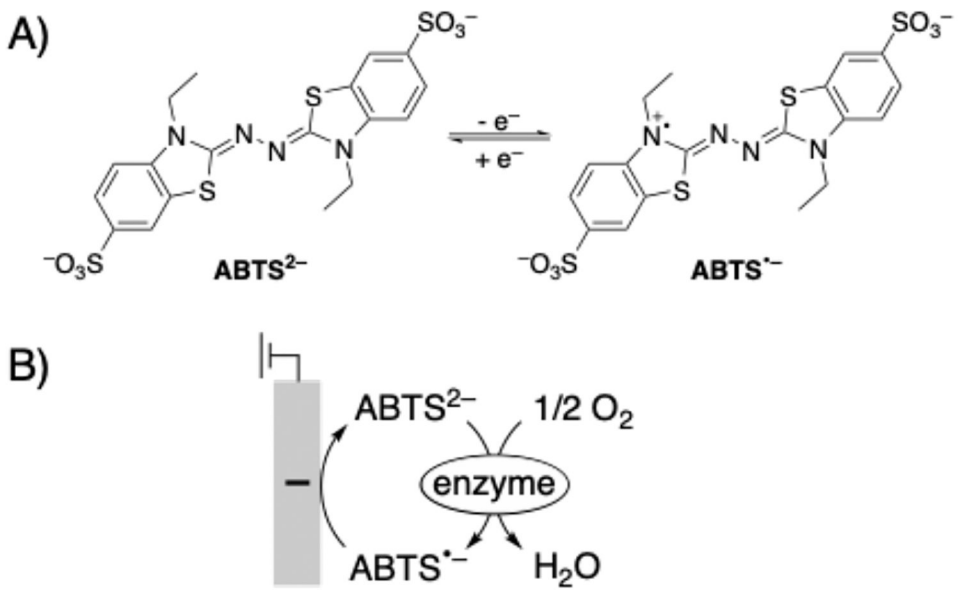


**Figure 24.**

(A) Structure of ABTS$^{2-}$ and (B) redox sequence for ABTS$^{2-}$-mediated cathode with enzymes as catalyst. For systems using this mediated cathode, see references 146–154.

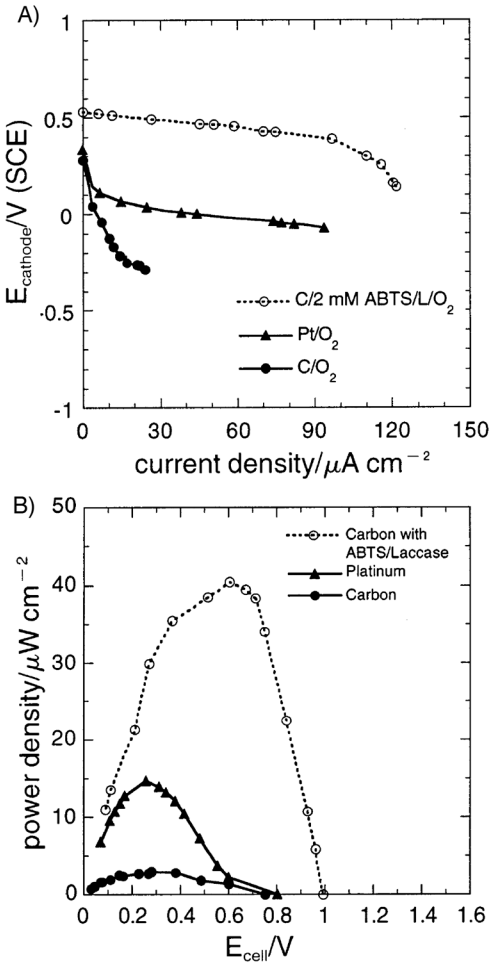


**Figure 25.**

A) Polarization curves of a fuel cell constructed with a laccase/$ABTS^{2-}$ biocathode (dotted line with open circles), Pt cathode (solid line with filled triangles), or carbon cathode (solid line with filled circles). B) Power density for the mediated fuel cell (dotted line with open circles) compared with a Pt cathode (solid line with filled triangles) and a carbon cathode (solid line with filled circles). Adapted from ref. 146. Copyright 1999 Elsevier Science S.A.

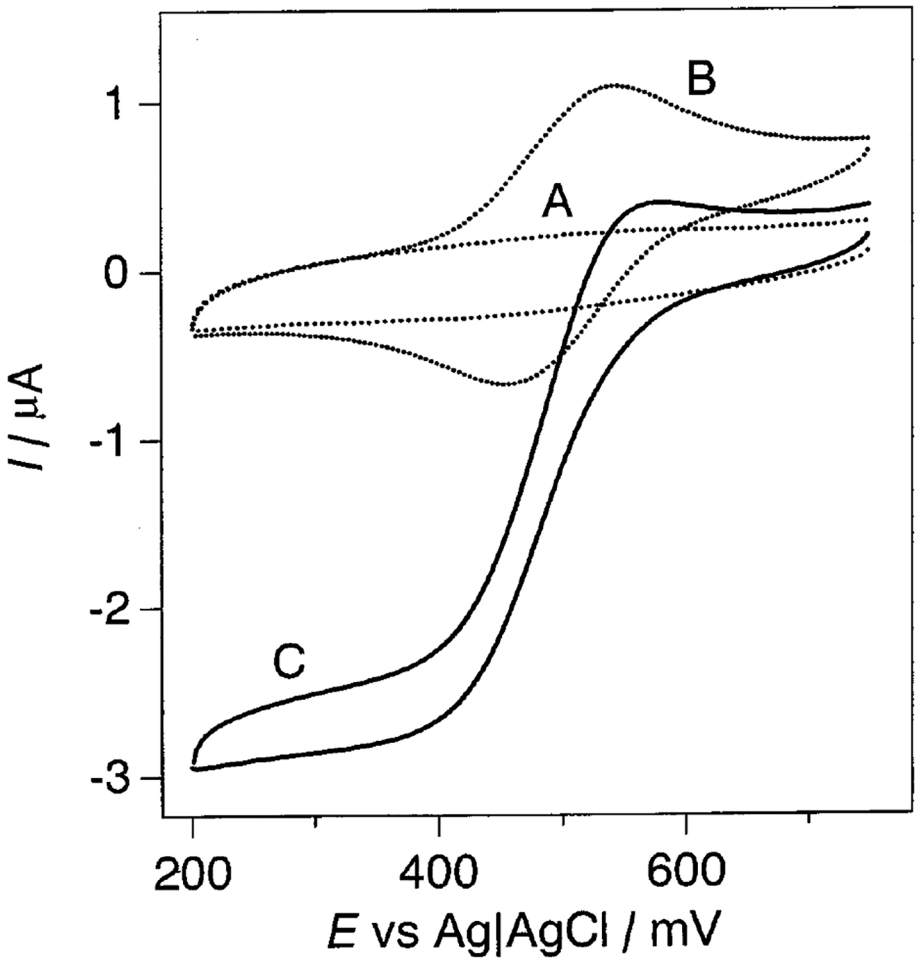


**Figure 26.**

Cyclic voltammagrams of: A) pH 7.0 phosphate buffer, B) pH 7 phosphate buffer and 0.25 mM ABTS2–, and C) pH 7 phosphate buffer, 0.25 mM ABTS2–, and 0.11 mM BOD. Scan rate was 10 mV/s, working electrode was glassy carbon, and a Pt disk was used as the counter electrode Adapted from ref. 148. Copyright 2001 Elsevier Science B.V.

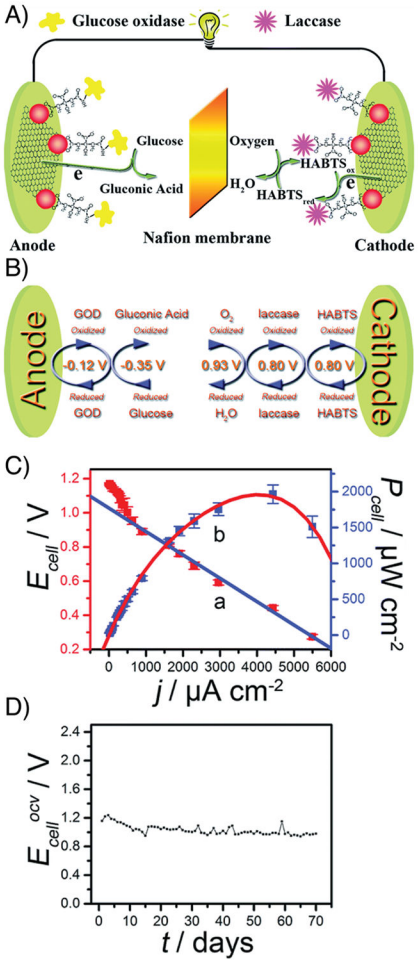


**Figure 27.**

A) General schematic of the mediated fuel cell system using $ABTS^{2-}$ as a mediator for $O_2$ reduction in the cathode. B) Formal redox potentials (vs. SHE) for each redox couple in the mediated fuel cell (GOD = glucose oxidase and HABTS = protonated $ABTS^{2-}$). C) Power curve of the assembled fuel cell. D) Open-circuit potential measurements of the cell over 70 days of operation. Adapted from ref. 152. Copyright 2015, The Royal Society of Chemistry.

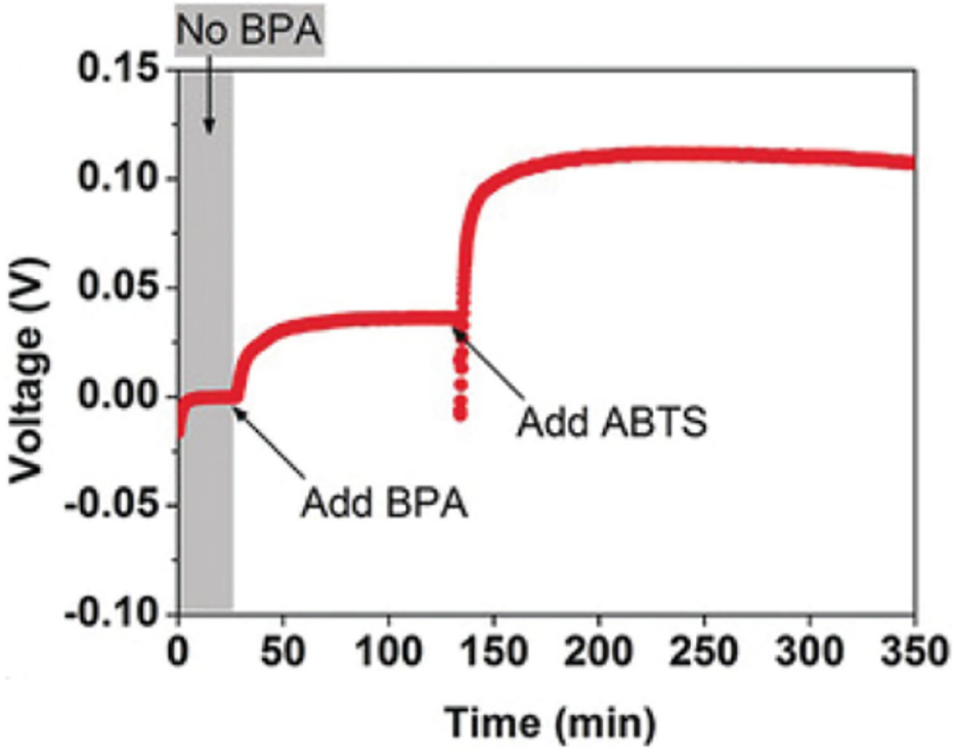


**Figure 28.**

Change in cell potential after addition of bisphenol A (BPA) and $ABTS^{2-}$ using immobilized laccase enzyme on both anode and cathode. Adapted from ref. 153. Copyright 2017, Wiley-VCH Verlag GmbH & Co.

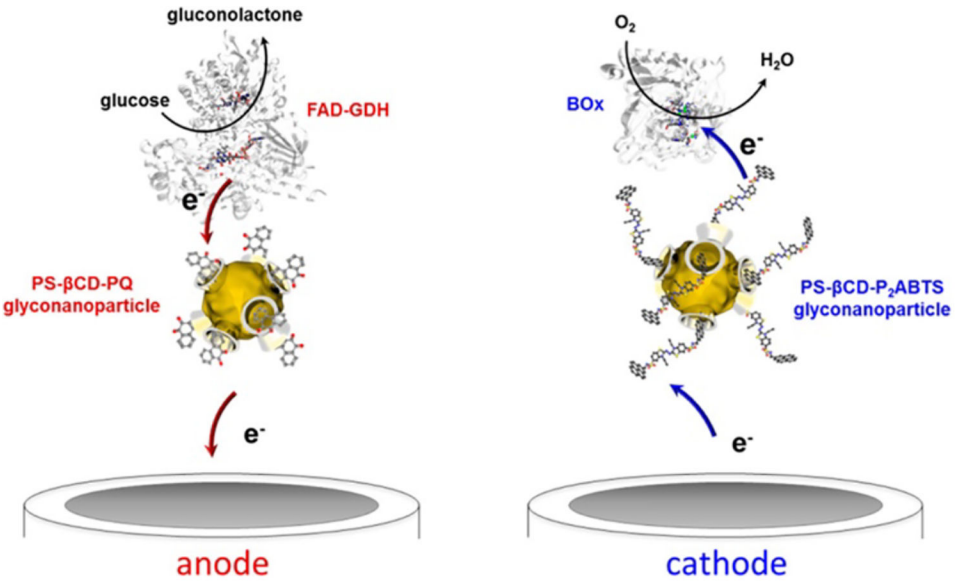


**Figure 29.**

Anode and cathode designs for “solubilized enzymatic fuel cell” using glyconanoparticle-entrapped 9,10-phenanthrenequinone and $P_2ABTS^{2-}$ mediators. The cathodic enzyme used was bilirubin oxidase (Box) and the anodic enzyme used was fungal flavin adenine dinucleotide-dependent glucose dehydrogenase (FAD-GDH). Adapted from ref. 154. Copyright 2018, American Chemical Society.

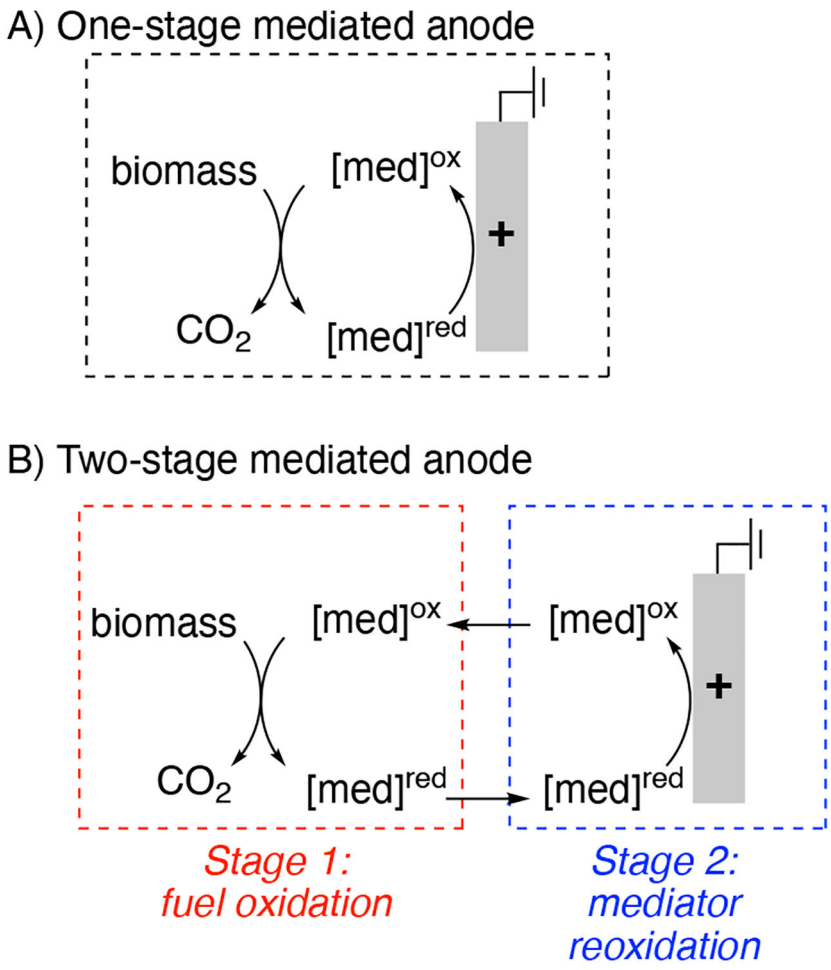


**Figure 30.**
Depiction the anode sequence for A) one-stage versus B) two-stage mediated biomass oxidation processes.

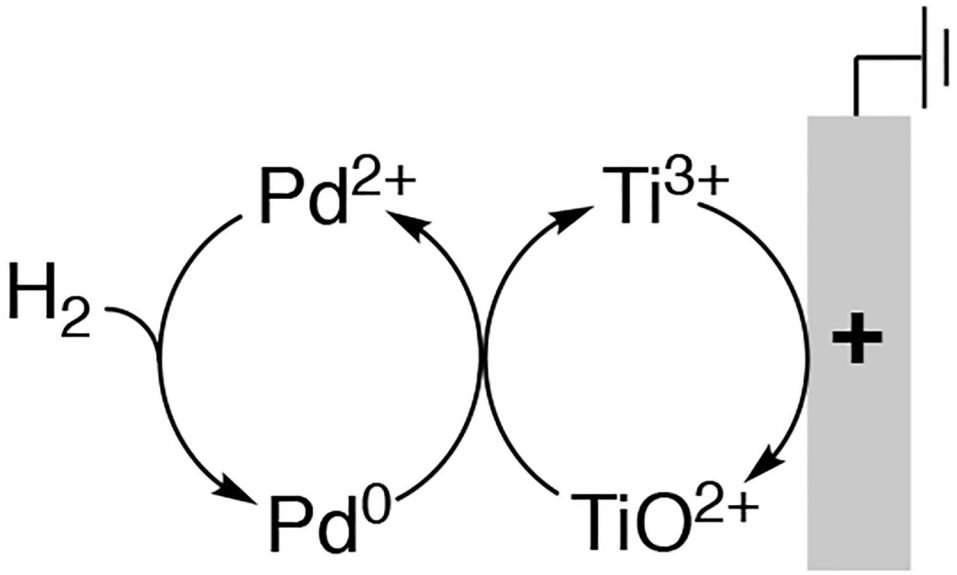


**Figure 31.**
Redox scheme for $TiO^{2+}$-mediated anode using $H_2$ fuel with a $Pd^0/Pd^{2+}$ catalyst. For relevant studies, see refs. 40 and 80.

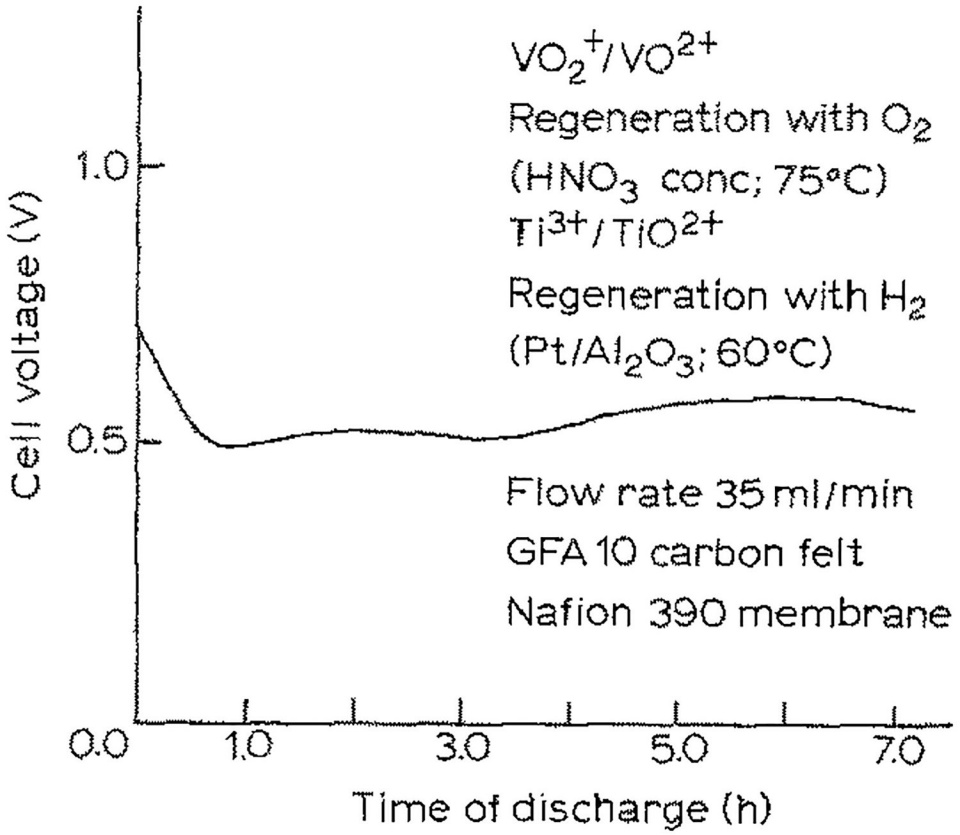


**Figure 32.**

Discharge cell voltage vs. time for double MedFC. Cathode solution is 0.2 M $VO_2^+$ in 1 M $H_2SO_4$ regenerated with $HNO_3$ and $O_2$ at 75 °C. Anode solution is 1 M $TiCl_3$ in 10% HCl regenerated with $Pt/Al_2O_3$ catalyst with $H_2$ at 60 °C ($H_2|Pt/Al_2O_3|TiO^{2+}||VO^{2+}|NO_x|O_2$). Adapted from ref. 80. Copyright 1990, Chapman and Hall Ltd.

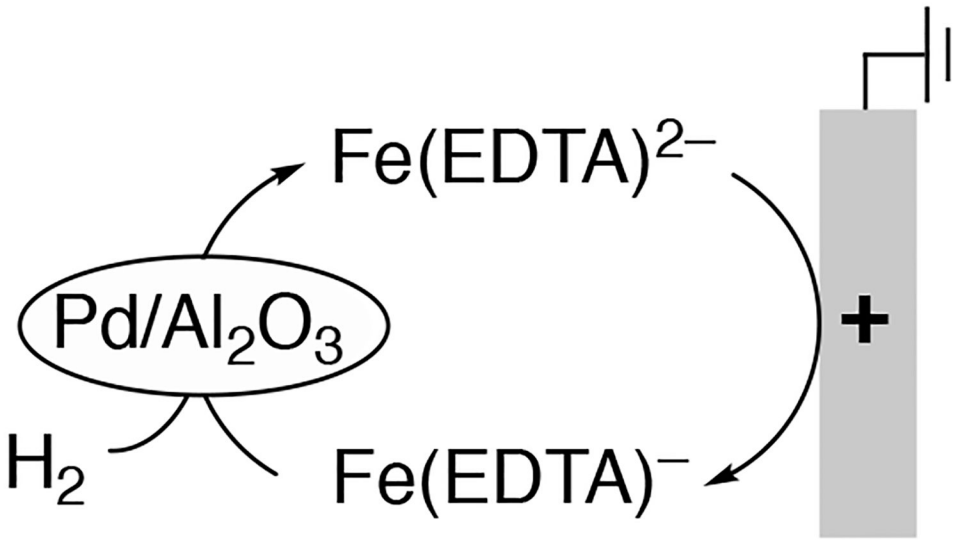


**Figure 33.**
Redox scheme of $Fe(EDTA)^{2-}$-mediated anode for $H_2$ oxidation with $Pd/Al_2O_3$ catalyst. See ref. 80.

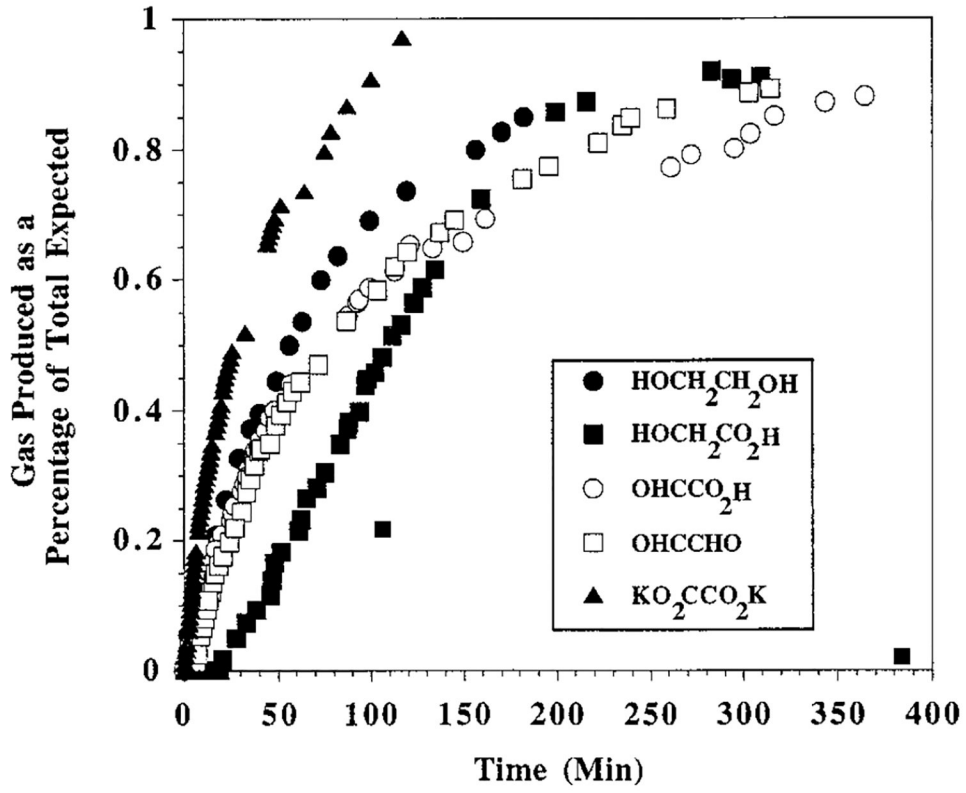


**Figure 34.**

Rate of $CO_2$ formation vs. time for the oxidation for some organic compounds catalyzed by Pt black with $Fe^{3+}$ as electron donor. Reactions were conducted at 80 °C in 3 M $H_2SO_4$. Adapted from ref. 83. Copyright 1996, Academic Press.

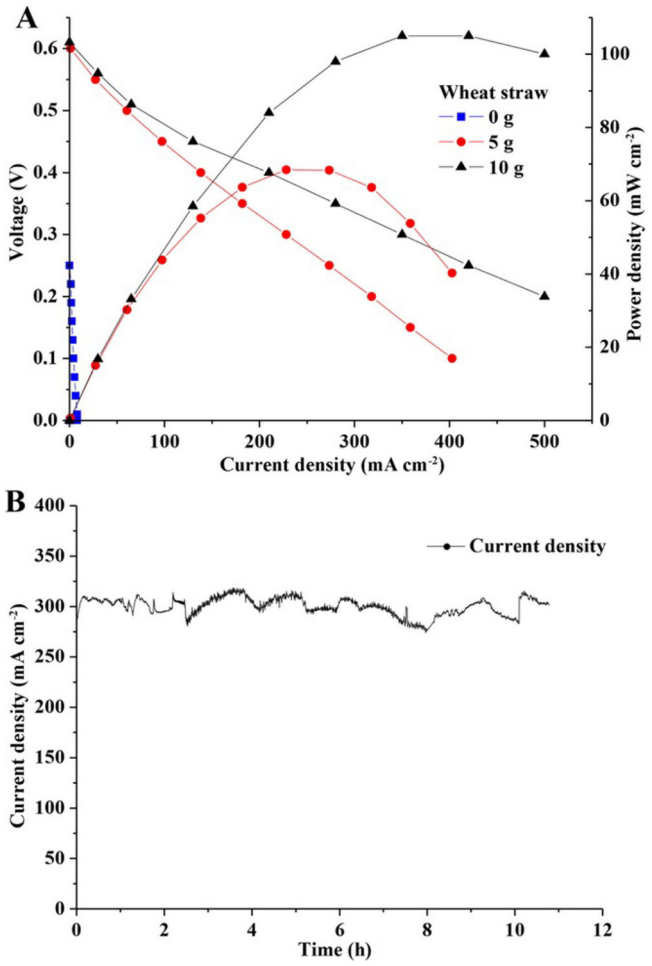


**Figure 35.**

A) Polarization curves and B) Continuous one-stage operation of a fuel cell using the $Fe^{2+}/Fe^{3+}$ redox couple as a mediator for wheat straw oxidation and a $VO_2^{+}/VO^{2+}$-mediated, $HNO_3$-catalyzed cathode for $O_2$ reduction (wheat straw|$Fe^{2+}$||$VO^{2+}$|$NO_x$|$O_2$). Adapted from ref. 85. Copyright 2017, John Wiley & Sons, Inc.

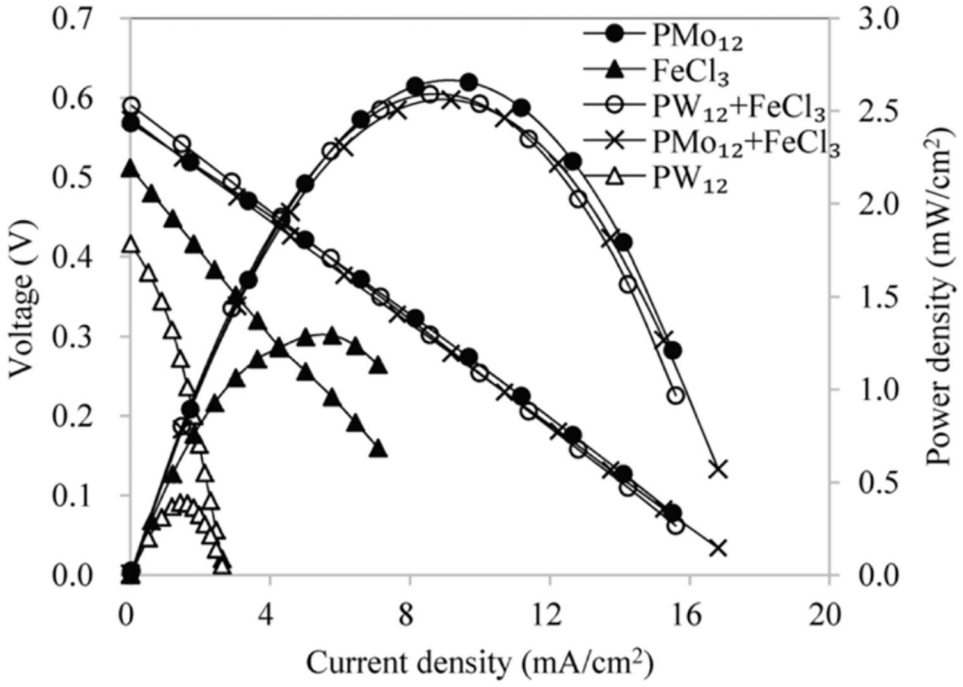


**Figure 36.**

Polarization curves for mediated fuel cell using POM or POM + $FeCl_3$ as mediator for glucose oxidation. $H_{12}P_3Mo_{18}V_7O_{85}$ was used as a cathodic mediator. The anode contained 1.0 M glucose and 1.5 M phosphoric acid and was operated at 23–25 °C. Mediator concentrations in the various experiments were as follows: 0.3 M $PMo_{12}$, 1.0 M $FeCl_3$, 0.06 M $PW_{12}$ + 1.0 M $FeCl_3$, 0.03 M $PMo_{12}$ + 1.0 M $FeCl_3$, and 0.3 M $PW_{12}$. Adapted from ref. 110.

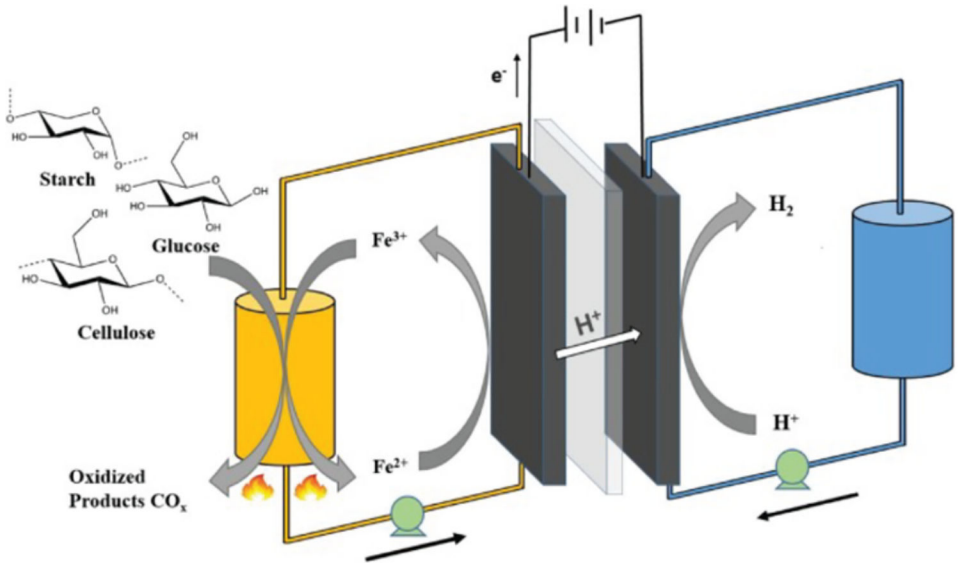


**Figure 37.**

Schematic of $H_2$ electrolysis system using $Fe^{2+}/Fe^{3+}$ mediator for the oxidation of biomass. Adapted from ref. 157. Copyright 2017, Elsevier Ltd.

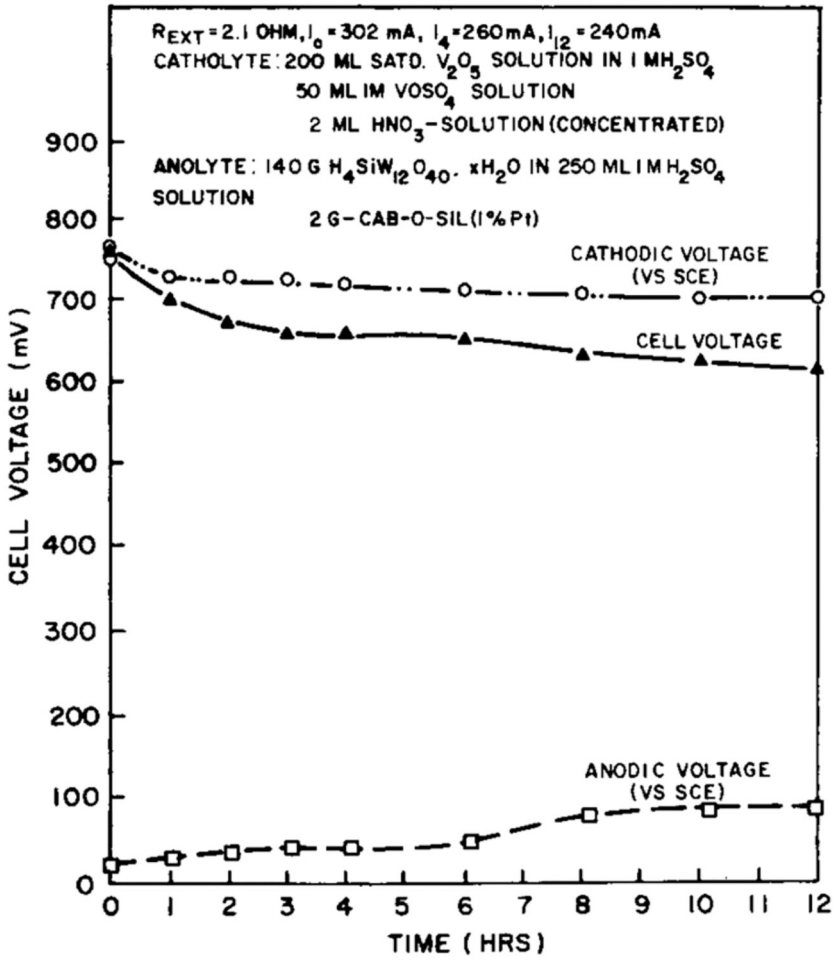


**Figure 38.**

Sustained performance curve of a doubly mediated $H_2/O_2$ fuel cell. The cathode utilized a $VO_2^+$ mediator reoxidized with $HNO_3$ in 1 M $H_2SO_4$ at 75–80 °C, and the anode contained $H_4SiW_{12}O_{40}$ reduced by $H_2$ with a Pt/silica catalyst at 25–30 °C ($H_2|Pt|H_4SiW_{12}O_{40}||VO^{2+}|NO_x|O_2$). The cell was discharged through a 2.1-ohm resistor. Flow rate was 230 mL/min. $I_0$, $I_4$, and $I_{12}$ correspond to the current at 0, 4, and 12 h. Adapted from ref. 79. Copyright 1985, Chapman and Hall Ltd.

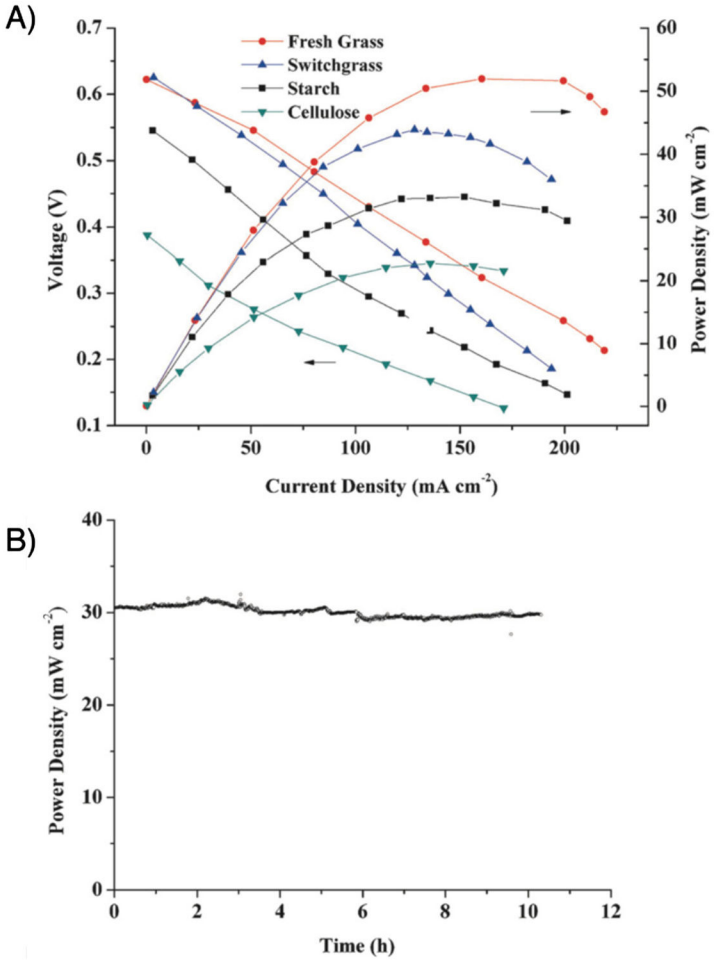


**Figure 39.**

(A) Polarization curves for a variety of biomass sources at 80 °C using 0.3 M $H_3PW_{11}MoO_{40}$ as the anodic mediator and 0.3 M $H_{12}P_3Mo_{18}V_7O_{85}$ as the cathodic mediator. (B) Power density measured over 10 h of operation using starch as biomass source. Adapted from ref. 107. Copyright 2014 WILEY-VCH Verlag GmbH & Co.

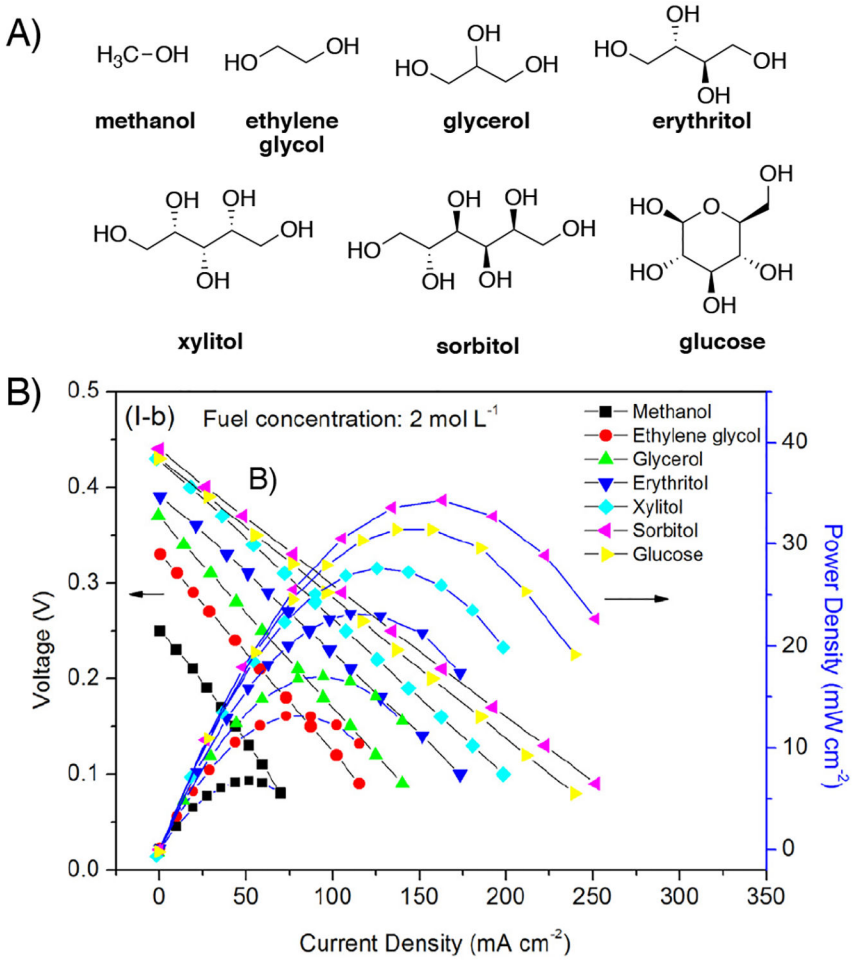


**Figure 40.**

(A) Structures of alcohols used as fuels. (B) Polarization curves obtained using anodic mediator solutions prepared by irradiation of solutions containing 2 M of the alcohol and 0.2 M $H_3PMo_{12}O_{40}$ as the mediator. Adapted from reference 108. Copyright 2016, Elsevier B.V.

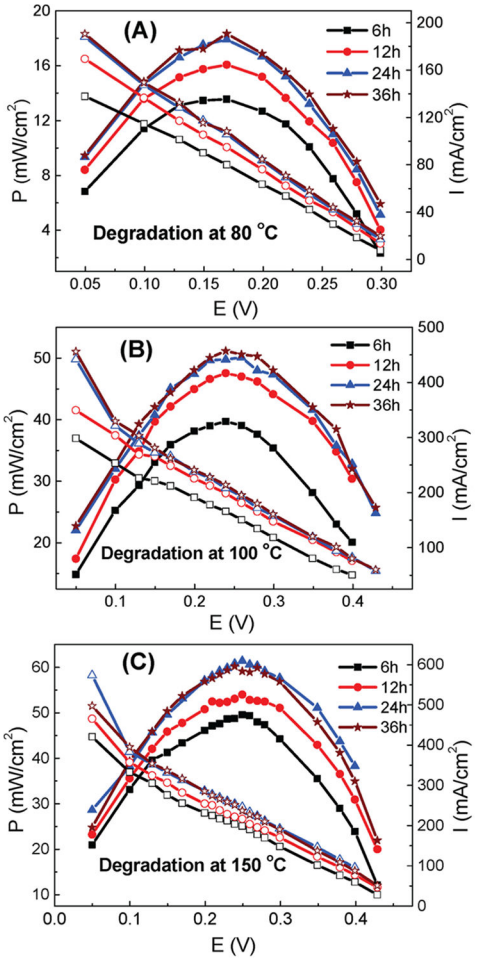


**Figure 41.**

Polarization curves for sewage sludge-powered mediated fuel cell using $H_3PMo_{12}O_{40}$ as anodic mediator and $H_{12}P_3Mo_{18}V_7O_{85}$ as cathodic mediator. Sewage sludge was treated with $H_3PMo_{12}O_{40}$ for 6, 12, 24, or 36 h at (a) 80 °C, (b) 100 °C, or (c) 150 °C prior to the fuel cell experiment. Adapted from reference 111. Copyright 2017 Elsevier Ltd.

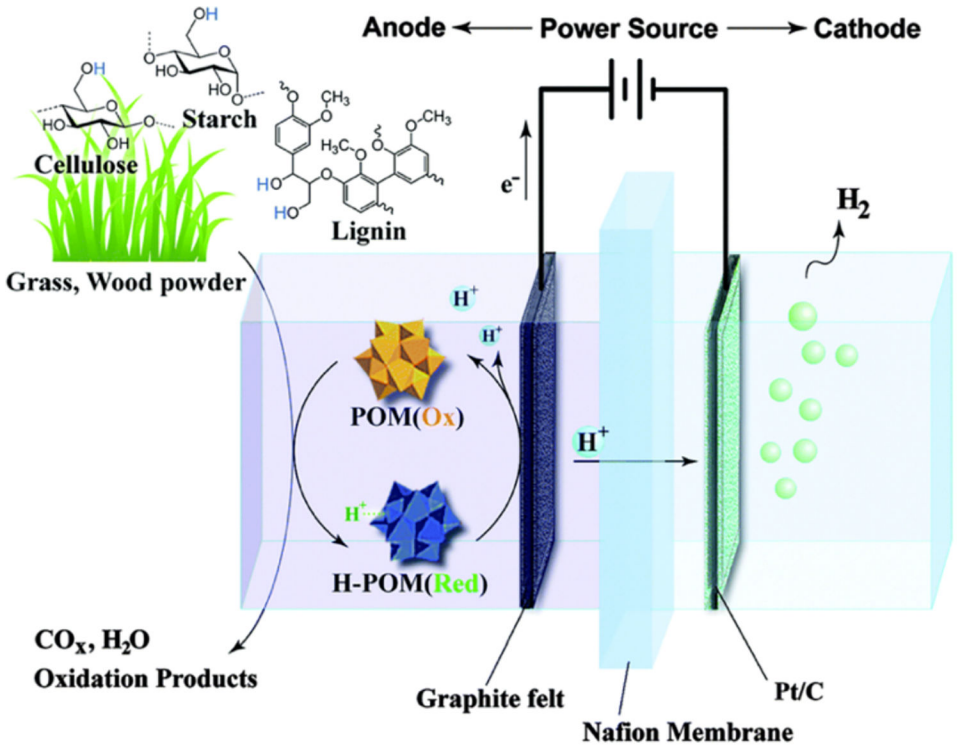


**Figure 42.**

Schematic of electrochemical $H_2$ evolution using biomass as $H_2$ source and POM-based mediators. Adapted from reference 162 with permission from The Royal Society of Chemistry. Copyright 2016 The Royal Society of Chemistry.

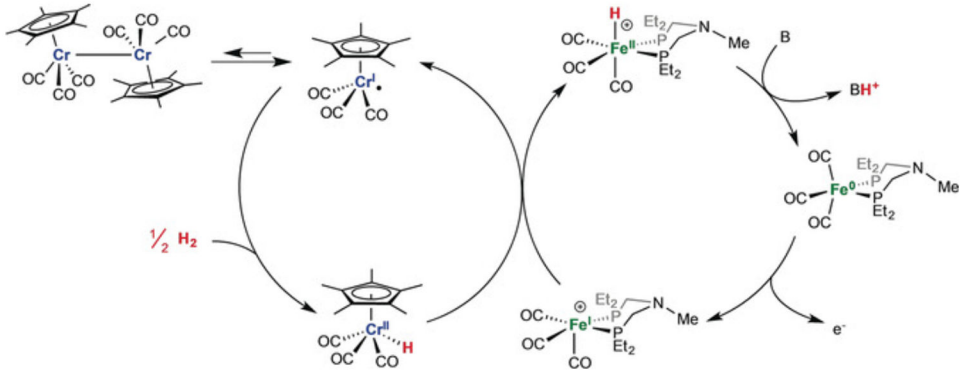


**Figure 43.**

Proposed mechanism for electrochemical $H_2$ oxidation using $Cp^*Cr(CO)_3/Fe(P_2N)$ system. Adapted from reference 165. Copyright 2018 Wiley-VCH Verlag GmbH & Co.

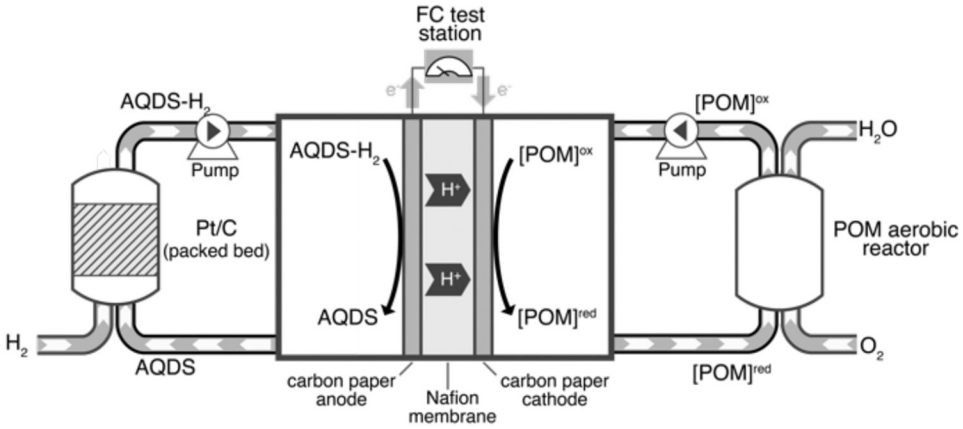


**Figure 44.**

Schematic of MedFC utilizing AQDS as an anodic mediator for $H_2$ oxidation with a Pt/C catalyst and a POM-mediated cathode. Adapted from reference 105.

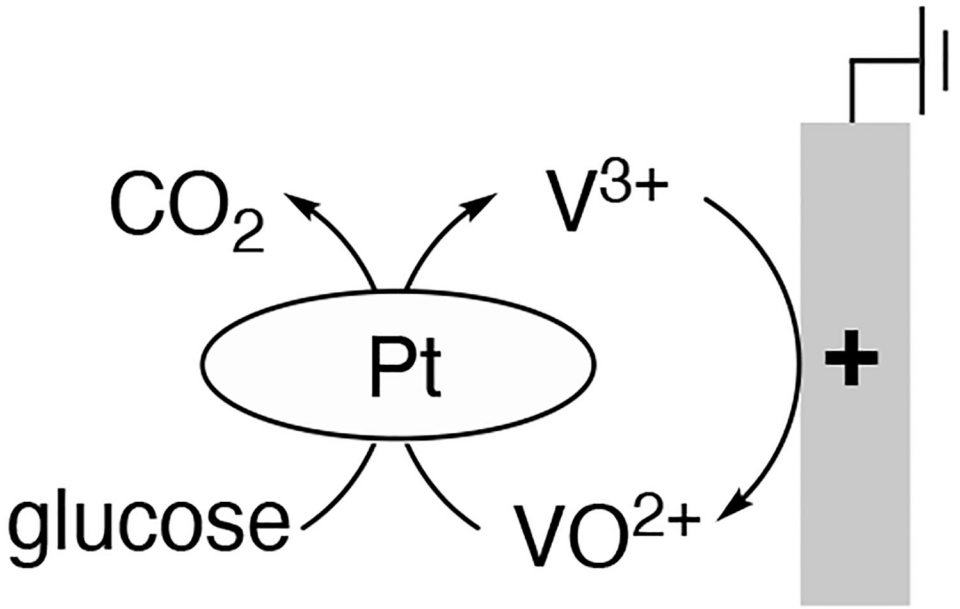


**Figure 45.**
Redox scheme for $V^{3+}$-mediated anode using glucose fuel and Pt catalyst. See refs. 169–170.

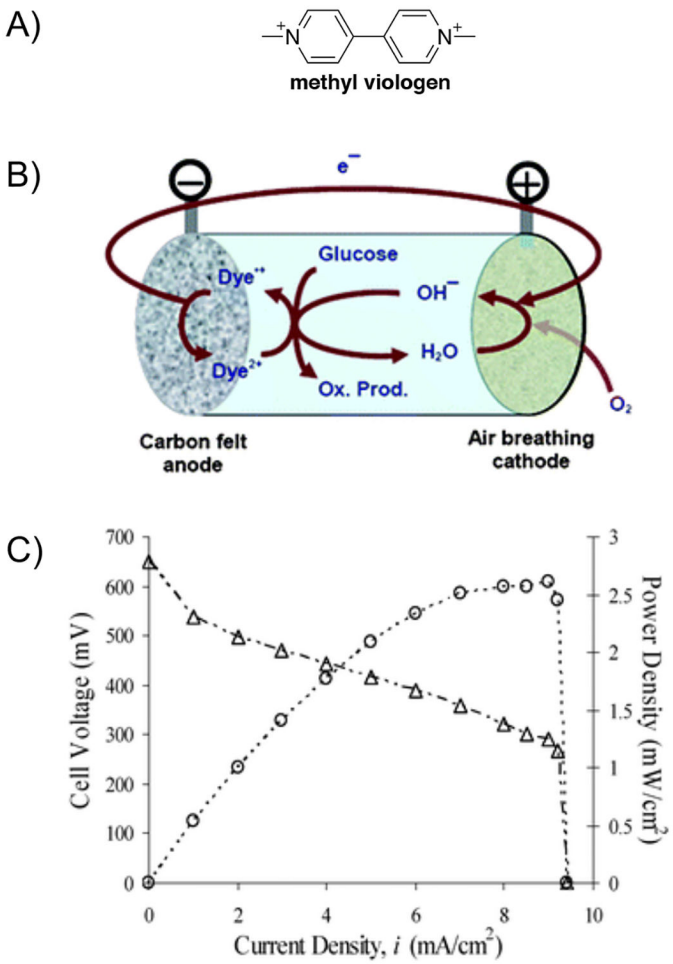


**Figure 46.**

A) Structure of methyl viologen. B) Schematic of $MV^{2+}$-mediated ("$Dye^{2+}$") fuel cell using glucose fuel and air breathing cathode. C) Polarization curve for glucose-$O_2$ fuel cells with $MV^{2+}$ as anodic mediator. Cell contained 2 M glucose and 28 mM $MV^{2+}$ in 3 M KOH solution. Adapted from ref. 172. Copyright 2009, The Royal Society of Chemistry.

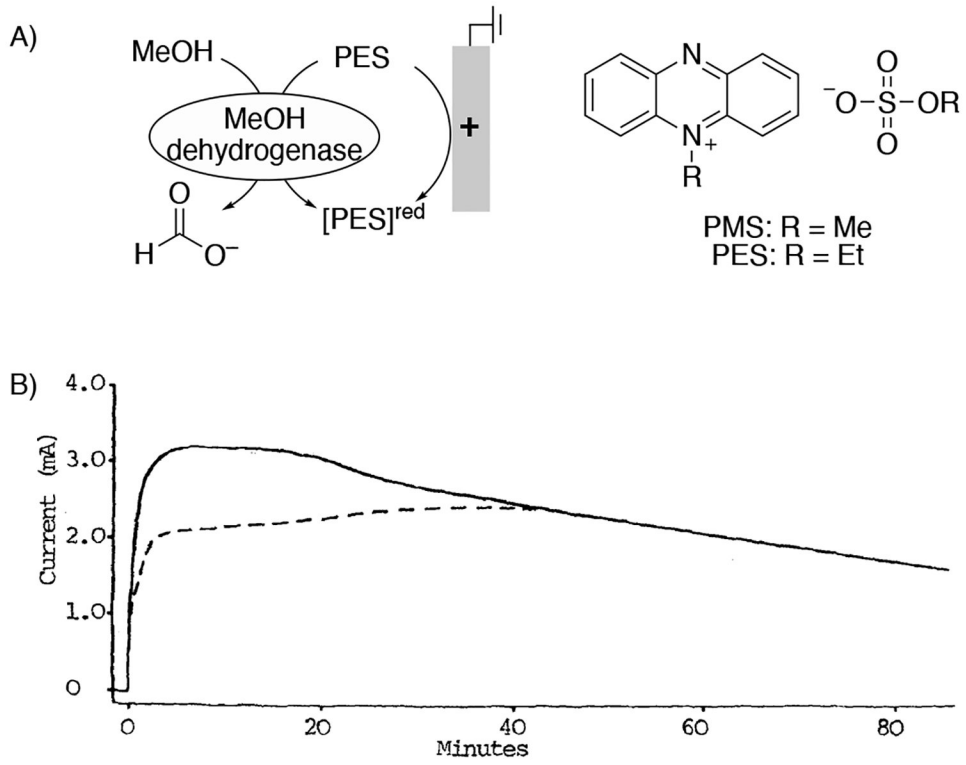


**Figure 47.**

(A) Redox scheme for PES-mediated anode using methanol as a fuel and methanol dehydrogenase enzyme as catalyst and structures of PMS and PES. For systems using this mediated anode, see refs. 184–185. (B) Current output of mediated anode fuel cell using PES as anodic mediator. Anode compartment contained 2.3 mg (dashed line) or 4.6 mg (solid line) methanol dehydrogenase, 0.35 mL of 40 mM PES in water, 3.6 mL of buffer, and 10 μL methanol. Adapted from reference 184. Copyright 1981 Science and Technology Letters.

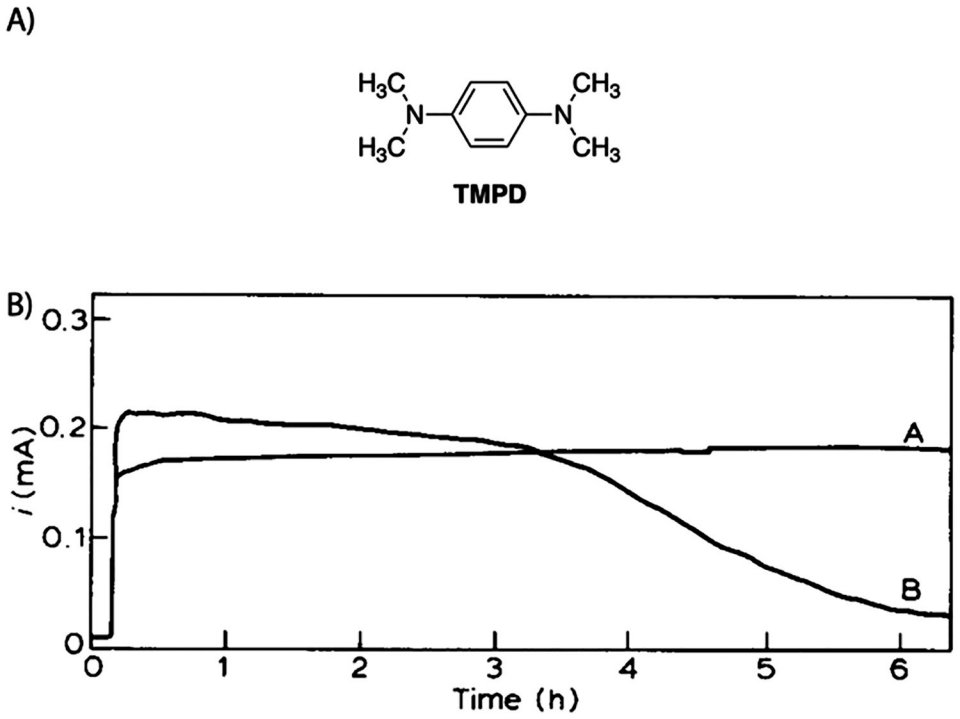


**Figure 48.**

(A) Structure of *N,N,N',N'*-tetramethyl-4-phenylenediamine (TMPD). (B) Current output of a fuel cell using A) 4.0 mM TMPD or B) 4.0 mM PES with alcohol dehydrogenase as the enzyme and methanol as fuel. Adapted from reference 186. Copyright 1983 Elsevier Inc.

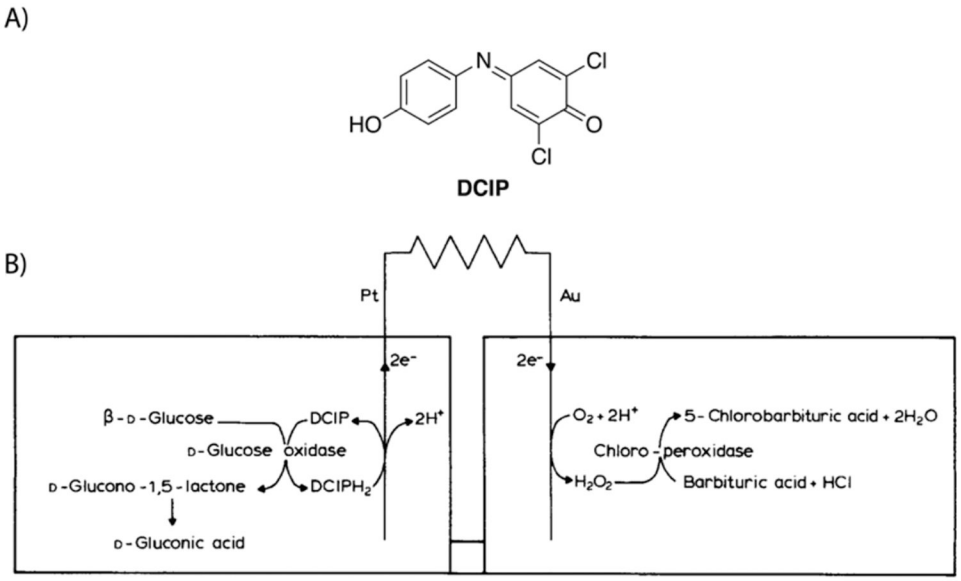


**Figure 49.**

(A) Structure of dichlorophenolindophenol (DCIP). (B) Schematic of biofuel cell used for the synthesis of 5-chlorobarbituric acid. The anode was mediated by DCIP. Adapted from reference 189. Copyright 1984 Elsevier Inc.

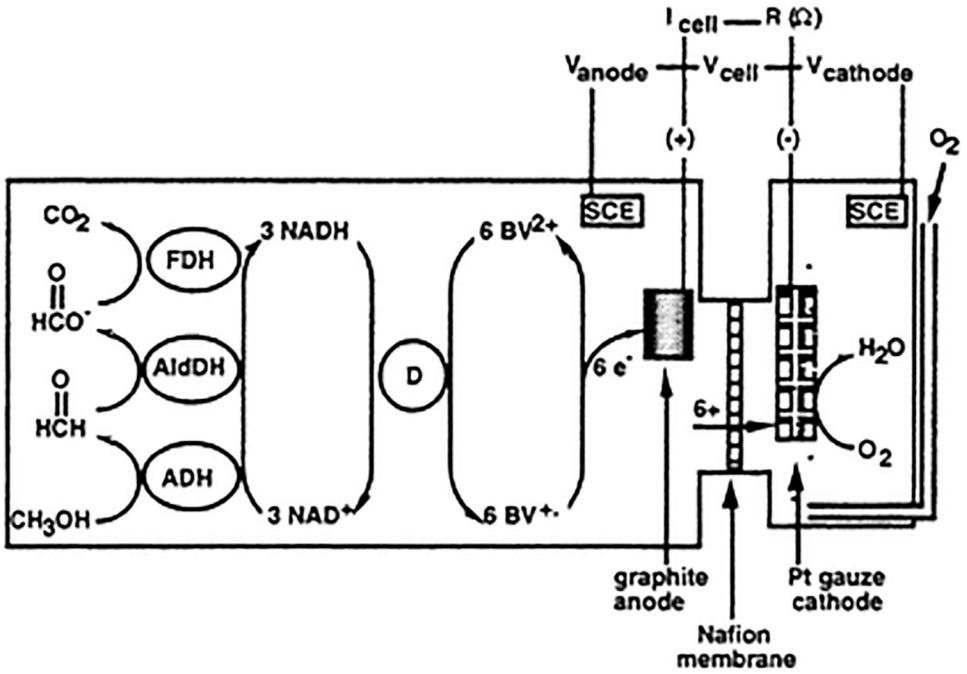


**Figure 50.**

Schematic of a methanol/oxygen biofuel cell, in which methanol is oxidized to $CO_2$ by $NAD^+$-dependent dehydrogenases ADH, AldDH, and FDH. Diaphorase (D) catalyzes the oxidation of NADH to $NAD^+$ with benzylviologen, $BV^{2+}$, as an electrochemical mediator. Adapted from reference 190. Copyright 1998 Elsevier S.A.

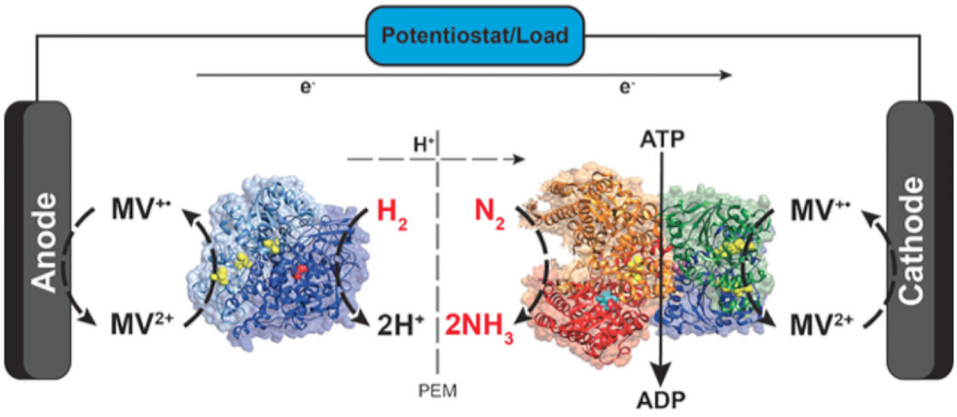


**Figure 51.**

Schematic of biofuel cell using methyl viologen as a mediator in both anode and cathode. The cell produces $NH_3$ from $N_2$ reduction in the cathode compartment. Adapted from ref. 193. Copyright 2017, John Wiley & Sons, Inc.

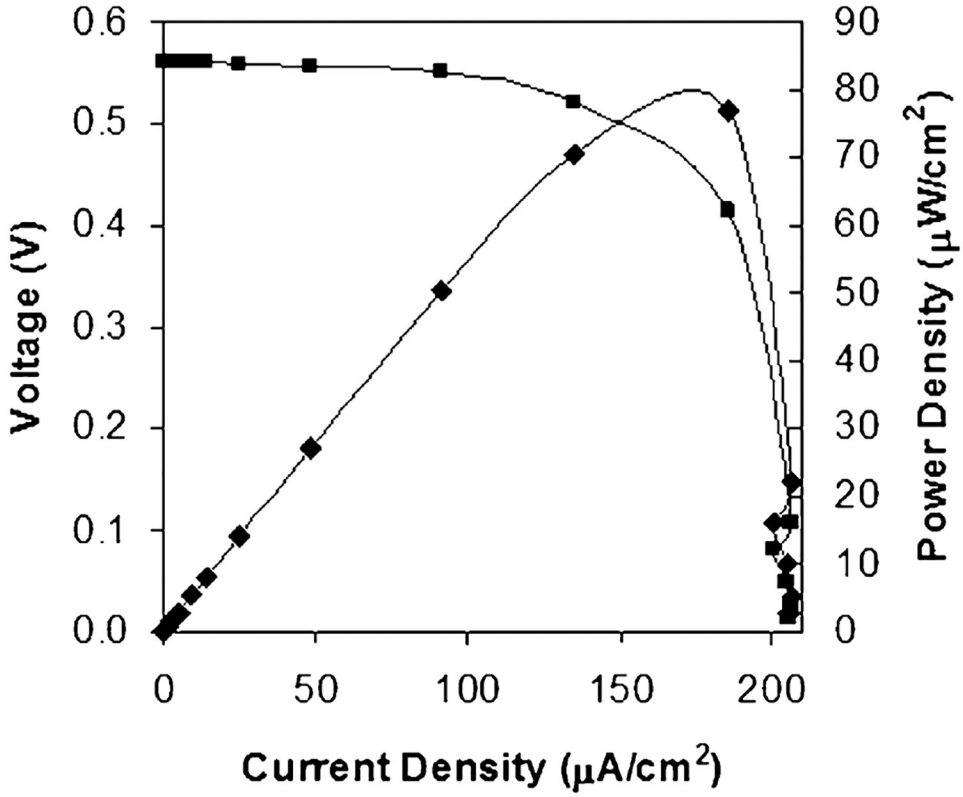


**Figure 52.**

Polarization curve of glucose/$O_2$ biofuel cells using benzoquinone as an anodic mediator with a CNT-$GO_x$ bioanode. Adapted from reference 195. Copyright 2009 Wiley Periodicals, Inc.

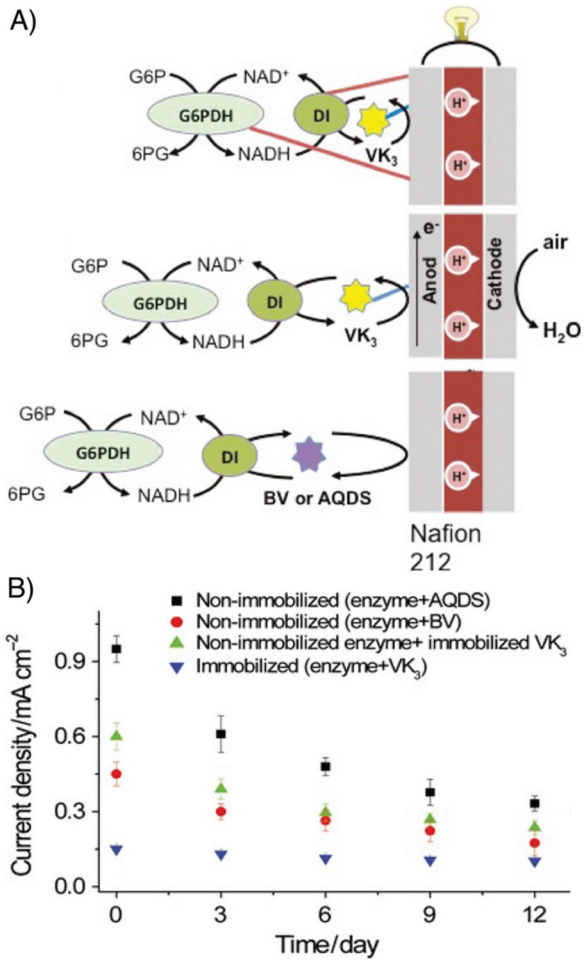


**Figure 53.**

A) Schematic diagrams of enzymatic fuel cell anodes with glucose 6-phosphate as the fuel. The four formulations included (a) immobilized enzymes with immobilized vitamin K3 mediator, (b) soluble enzymes with immobilized vitamin K3 mediator, and (c and d) soluble enzymes with free benzyl viologen (BV) or free AQDS mediators. G6P = glucose 6-phosphate, G6PDH = glucose 6-phosphate dehydrogenase, DI = diaphorase. B) Current vs. time plots for the four $O_2$/glucose 6-phosphate fuel cell strategies. Cell was discharged through a 150-ohm resistor. Fresh G6P substrate was added every 3 days. The electrolyte contained 5 mM mediator, 20mM G6P, 8mM $NAD^+$, 0.1 M pH 7.3 HEPES buffer, 10mM $MgCl_2$, 0.5mM $MnCl_2$, 0.1 M NaCl, 2 U/mL G6PDH, and 2.7 U/mL diaphorase. Adapted from reference 196.

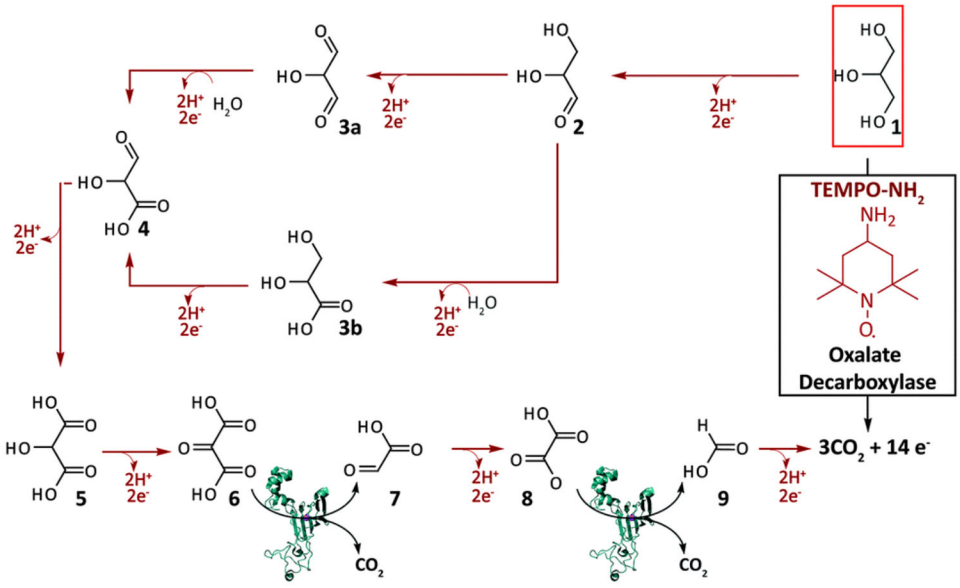


**Figure 54.**

Electro-oxidation cascade pathway for the complete oxidation of glycerol to $CO_2$ catalyzed by TEMPO-$NH_2$ and oxalate decarboxylase. The red arrows indicate the oxidations by TEMPO-$NH_2$. Adapted from reference 198. Copyright 2015 The Royal Society of Chemistry.

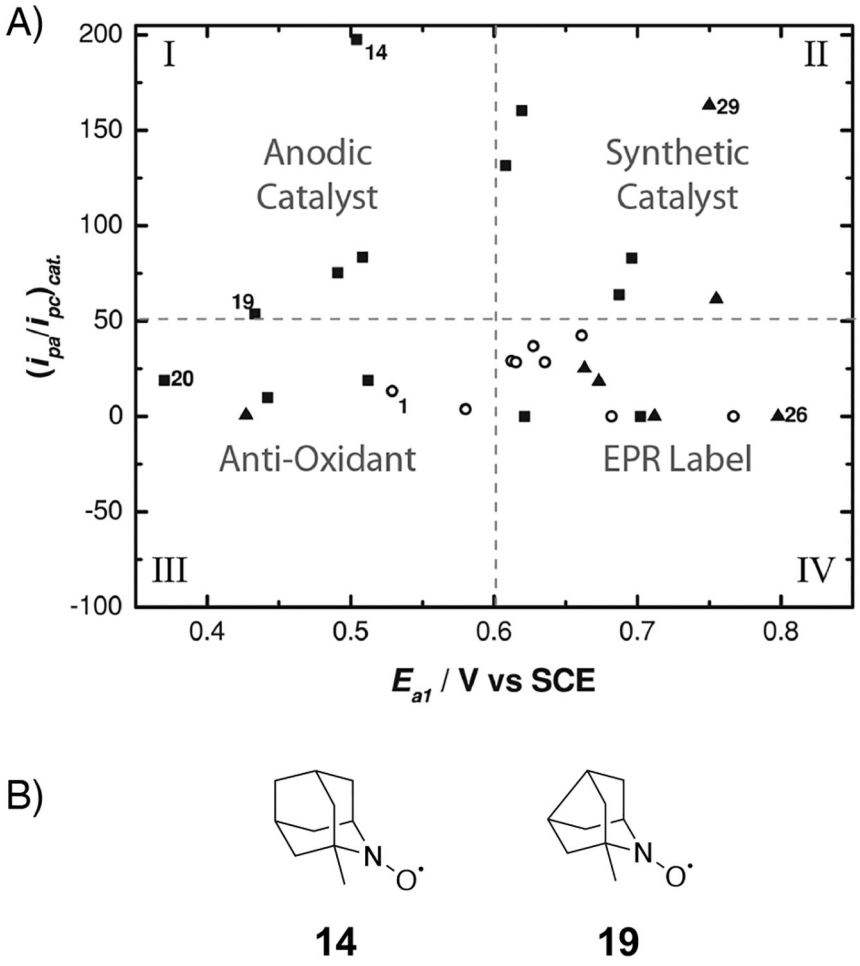


**Figure 55.**

A) Plot of catalytic activity ($i_{pa}/i_{pc}$)cat vs. $E_{a1}$ (nitroxyl/oxoammonium redox potential) separated into four quadrants based on catalyst characteristics. Adapted from reference 200. Copyright 2015, American Chemical Society. B) Structure of two optimal nitroxyl derivatives in the “Anodic Catalyst” quadrant.

**Table 1.**

Reported systems using Br mediators for $O_2$ reduction

| Anode | | | Cathode | | |
|---|---|---|---|---|---|
| ***fuel*** | ***catalyst*** | ***mediator*** | ***mediator*** | ***catalyst*** | ***ref.*** |
| C | – | $Sn^{4+}/Sn^{2+}$ | **$Br^-/Br_2$** | $NO_x$ | 70 |
| $H_2$ | Pd black | $TiO^{2+}/Ti^{3+}$ | | | 40 |
| $H_2$ | Pt | – | | | 73 |

**Table 2.**

Reported fuel cell systems using V-based mediators for $O_2$ reduction.

| **Anode** | | | **Cathode** | | |
|---|---|---|---|---|---|
| ***fuel*** | ***catalyst*** | ***mediator*** | ***mediator*** | ***catalyst*** | ***ref*** |
| $H_2$ | Pt | – | **$VO^{2+}/VO_2^+$** | HCl | 75 |
| – | – | $V^{2+}/V^{3+}$ | | $NO_x$ | 79 |
| $H_2$ | Pt | $Ti^{3+}/TiO^{2+}$ | | | 80 |
| $CH_4$, ethylene glycol, coal | Pt | $Fe^{2+}/Fe^{3+}$ | | | 82–84 |
| biomass | – | $Fe^{2+}/Fe^{3+}$ | | | 85, 86 |
| sugars | Pt | $V^{3+}/VO^{2+}$ | | Pt | 81 |
| $H_2$ | Pt | $H_4SiW_{12}O_{40}$ | | POM | 76–78 |
| | Pt | – | **V-containing POM** | | 63, 95–102,104 |
| | Pt/C | AQ | | | 105 |
| sugars | POM | $Fe^{2+}/Fe^{3+}$ | | | 110 |
| biomass | POM | | | | 107, 111, 112 |
| alcohols | | | | | 108 |
| lignin | | | | | 113 |
| coal | | | | | 109 |

**Table 3.**

Performance comparison of a reported conventional PEM fuel cell, previously reported mediated cathode fuel cell systems, and results from Davies and coworkers.[63]

| System | Cathode material | Cathode reaction | Liquid Electrolyte | OCP (V) | Cell voltage @ 0.2 A/cm$^2$ (V) | Cell voltage @ 1 A/cm$^2$ (V) | Max power (W/cm$^2$) | Ref. |
|---|---|---|---|---|---|---|---|---|
| Conventional PEMFC | Pt/C | $O_2 + 4\ e^- + 4\ H^+ \rightarrow 2\ H_2O$ | None | 0.96 | 0.81 | 0.67 | ≥ 0.83 | 23 |
| Mediated cathode ($HNO_3$) | N-doped carbon | $NO_3^- + 2\ e^- + 2\ H^+ \rightarrow NO_2^- + H_2O$ | 5 M $HNO_3$ | 1.04 | 0.95 | 0.46 | 0.51 | 129 |
| Mediated cathode (POM) | carbon | $VO_2^+ + e^- \rightarrow VO^{2+}$ | 0.45 M POM[a] | 0.83 | 0.68 | 0.46 | 0.51 | 96 |
| Mediated cathode (POM) | carbon | $VO_2^+ + e^- \rightarrow VO^{2+}$ | 0.3 M HV3 @ 0.05 $V^{IV}$ | 0.99 | 0.9 | 0.72 | 1 | 63 |
| Mediated cathode (POM) | carbon | $VO_2^+ + e^- \rightarrow VO^{2+}$ | 0.3 M HV3 @ 0.65 $V^{IV}$ | 0.78 | 0.72 | 0.5 | 0.58 | 63 |
| Mediated cathode (POM) | carbon | $VO_2^+ + e^- \rightarrow VO^{2+}$ | 0.3 M HV3 @ steady state[b] | 0.81 | 0.73 | – | 0.36 | 63, 102 |
| Mediated cathode (POM) | carbon | $VO_2^+ + e^- \rightarrow VO^{2+}$ | 0.3 M NaV4 @ steady state[b] | 0.80 | 0.75 | 0.53 | 0.58 | 63, 102 |

[a] POM identity was not disclosed

[b] Steady-state data was calculated from regeneration rates and cell data

**Table 4.**

Performance of various cathode chemistries on fuel cell performance using lignin as fuel.

| Oxidant[a] | OCP (mV) | Maximum Power Density (mW/cm$^2$) |
|---|---|---|
| $O_2$ @ Pt/C | 350 | 0.96 |
| $O_2$ + 0.1 M $H_3PMo_{12}O_{40}$ | 690 | 5 |
| 0.2 M $KMnO_4$ | 900 | 45.1 |
| $O_2$ + 0.1 M $K_5PV_2Mo_{10}O_{40}$ | 330 | 0.41 |

[a]: 1 atm $O_2$

**Table 5.**

Reported systems using iron-based mediators for $O_2$ reduction.

| Anode | | | Cathode | | |
|---|---|---|---|---|---|
| ***fuel*** | ***catalyst*** | ***mediator*** | ***mediator*** | ***catalyst*** | ***ref*** |
| Zn | – | – | **$Fe^{2+}/Fe^{3+}$** | charcoal | 114 |
| $H_2$ | Pt/C | – | | Fe(pc) | 61 |
| | | | **$K_3Fe(CN)_6$** | Mn complex | 118 |
| | | | **Fc species** | Fe complex | 119–123 |

**Table 6.**

Reported systems using $NO_x$ species as mediators for $O_2$ reduction.

| Anode | | | Cathode | | |
|---|---|---|---|---|---|
| ***Fuel*** | ***catalyst*** | ***mediator*** | ***mediator*** | ***catalyst*** | ***ref*** |
| MeOH or $HO(CH_2)_2OH$ | Pt | – | **$HNO_3$** | | 124–127 |
| $H_2$ | Pt/C | – | | | 128–129 |

**Table 7.**

Mediated anode systems utilizing chemical catalysts. In all cases, the oxidant used is $O_2$.

| Anode | | | Cathode | | |
|---|---|---|---|---|---|
| ***fuel*** | ***catalyst*** | ***mediator*** | ***mediator*** | ***catalyst*** | ***ref*** |
| $H_2$ | Pd | **$Ti^{3+}/TiO^{2+}$** | $Br^-/Br_2$ | $NO_x$ | 40 |
| | $Pt/Al_2O_3$ | | $VO^{2+}/VO_2^+$ | | 80 |
| | $Pd/Al_2O_3$ | **$Fe(EDTA)^{2-}/Fe(EDTA)^-$** | | | 80 |
| | $Pt/Al_2O_3$ | **$Mo^{3+}/Mo^{4+}$** | | | 79 |
| | | **$H_4SiW_{12}O_{40}$** | | | 79 |
| | | | | POM | 63 |
| | Pt/C | **AQ** | POM | | 105 |
| alcohols, sugars or lignin | – | | – | – | 166–168 |
| sugars | POM | **$Fe^{2+}/Fe^{3+}$** | POM | | 110 |
| methane, alcohols | Pt | | $VO^{2+}/VO_2^+$ | $NO_x$ | 82–83 |
| biomass | – | | | | 84–86 |
| sugars | Pt | **$V^{3+}/VO^{2+}$** | | Pt | 81, 169 |
| sugars | – | **viologen** | – | Co | 171–175, 177 |
| biomass | **POM** | | – | Pt/C | 113, 159 |
| alcohols | | | POM | | 107 |
| coal | | | | | 109 |
| biomass | | | | | 111, 112 |

**Table 8.**

Enzymatic fuel cells using at least one soluble mediator in the anode or cathode.

| Anode | | | Cathode | | | |
|---|---|---|---|---|---|---|
| ***fuel*** | ***catalyst*** | ***mediator*** | ***mediator*** | ***catalyst*** | ***oxidant*** | ***ref*** |
| $H_2$ | Pt | – | **$ABTS^{2-}$** | laccase | $O_2$ | 146 |
| | *Desulfovibrio vulgaris* | viologen | | bilirubin oxidase | | 149 |
| glucose | glucose oxidase | **$Fc(CH_2OH)$** | | bilirubin oxidase or laccase | | 147–151 |
| glucose | glucose oxidase/AuNP-graphene | – | | laccase/AuNP-graphene | | 152 |
| BPA | laccase | – | | laccase | | 153 |
| glucose | glucose dehydrogenase | **PS-βCD-PQ** | **PS-βCD-$P_2$ABTS** | bilirubin oxidase | | 154 |
| MeOH | methanol dehydrogenase | **PMS or PES** | – | Pt | | 184–185 |
| MeOH | quinoprotein alcohol dehydrogenase | **TMPD** | | | | 186 |
| glucose | glucose oxidase | | Os polymer | laccase | | 188 |
| MeOH | multi-enzyme cascade | **$BV^{2+}$ +NADH** | – | Pt | | 190 |
| glucose | glucose oxidase | **DCIP** | | | | 189 |
| | | **quinone** | | | | 195 |
| glucose-6-phosphate | G6PDH and diaphorase | **quinone + NADH** | | | | 196 |
| MeOH | alcohol dehydrogenase | **TMPD** | – | | $KMnO_4$ | 187 |
| $H_2$ | NiFe hydrogenase | **$MV^{2+}$** | **$MV^{2+}$** | MoFe Nitrogenase | $N_2$ | 193 |